Research Paper

GEOSPHERE

GEOSPHERE, v. 19, no. 1

https://doi.org/10.1130/GES02556.1

14 figures; 2 plates; 1 table; 1 set of supplemental files

CORRESPONDENCE: nmidttun@umich.edu

CITATION: Midttun, N., Niemi, N.A., and Gallina, B., 2023, Stratigraphy of the Eocene–Oligocene Titus Canyon Formation, Death Valley, California (USA), and Eocene extensional tectonism in the Basin and Range: Geosphere, v. 19, no. 1, p. 258–290, https://doi.org/10.1130/GES02556.1.

Science Editor: Andrea Hampel
Associate Editor: Jeffrey Lee

Received 3 June 2022
Revision received 22 August 2022
Accepted 20 September 2022

Published online 22 December 2022

Stratigraphy of the Eocene–Oligocene Titus Canyon Formation, Death Valley, California (USA), and Eocene extensional tectonism in the Basin and Range

Nikolas Midttun, Nathan A. Niemi, and Bianca Gallina

Department of Earth and Environmental Sciences, University of Michigan, Ann Arbor, Michigan 48109, USA

ABSTRACT

Geologic mapping, measured sections, and geochronologic data elucidate the tectono-stratigraphic development of the Titus Canyon extensional basin in Death Valley, California (USA), and provide new constraints on the age of the Titus Canyon Formation, one of the earliest syn-extensional deposits in the central Basin and Range. Detrital zircon maximum depositional ages (MDAs) and compiled $^{40}Ar/^{39}Ar$ ages indicate that the Titus Canyon Formation spans 40(?)–30 Ma, consistent with an inferred Duchesnean age for a unique assemblage of mammalian fossils in the lower part of the formation. The Titus Canyon Formation preserves a shift in depositional environment from fluvial to lacustrine at ca. 35 Ma, which along with a change in detrital zircon provenance may reflect both the onset of local extensional tectonism and climatic changes at the Eocene–Oligocene boundary. Our data establish the Titus Canyon basin as the southernmost basin in a system of late Eocene extensional basins that formed along the axis of the Sevier orogenic belt. The distribution of lacustrine deposits in these Eocene basins defines the extent of a low-relief orogenic plateau (Nevadaplano) that occupied eastern Nevada at least through Eocene time. As such, the age and character of Titus Canyon Formation implies that the Nevadaplano may have extended into the central Basin and Range, ~200 km farther south than previously recognized. Development of the Titus Canyon extensional basin precedes local Farallon slab removal by ~20 m.y., implying that other mechanisms, such as plate boundary stress changes due to decreased convergence rates in Eocene time, are a more likely trigger for early extension in the central Basin and Range.

INTRODUCTION

During the Cenozoic, the Basin and Range extensional province of western North America (Fig. 1) underwent distributed continental extension driven by a combination of external stresses (i.e., changing plate boundary stresses) and internal stresses (i.e., topographically induced gravitational potential energy gradients and buoyancy forces) (e.g., Sonder and Jones, 1999). Our ability to separate the relative influence of these geodynamic drivers relies on estimates of the initial state of topography and lithospheric structure prior to extension (e.g., Jones et al., 1996; Molnar et al., 2015; Levandowski et al., 2017; Ghosh et al., 2019; Zhou and Liu, 2019; Lund Snee and Zoback, 2020). Internal stresses are thought to have been a major driver of pre-Miocene extension in the Basin and Range, when significant gravitational potential energy gradients may have existed along the margins of the Nevadaplano, an inferred region of over-thickened crust constructed across western North America during the Cretaceous Sevier orogeny. External stress changes caused by plate boundary reorganization may also have played a role in continuing extension after initial orogenic collapse. Separating the roles of external stress changes and internal driving stresses on extension in the Basin and Range depends on knowing the location and rate of extension across the Basin and Range throughout the Cenozoic.

Early extension in the Basin and Range is thought to have started with a Cretaceous and Paleogene phase of relatively small magnitude syn-convergent upper-crustal extension, followed by a later phase of larger-magnitude extensional collapse (Dickinson, 2002). Late Cretaceous and early Paleogene low-magnitude, syn-convergent extension is primarily inferred from a sparse stratigraphic record (e.g., Potter et al., 1995; Dubiel et al., 1996; Druschke et al., 2009; Lund Snee et al., 2016), and to a lesser degree from thermochronologic and geochronologic evidence (e.g., Wells et al., 1990; Applegate and Hodges, 1995; Camilleri and Chamberlain, 1997; Sullivan and Snoke, 2007). The record of Eocene to Miocene extension is both more widespread and indicative of larger magnitude extension that likely resulted in significant crustal thinning and topographic collapse, as recorded in thermochronologic data from metamorphic core complexes (e.g., Holm and Dokka, 1991; Lee, 1995; Foster and Raza, 2002; Vogl et al., 2012; Evans et al., 2015; Lee et al., 2017) and stratigraphic sequences deposited in hanging-wall sedimentary basins (Satarugsa and Johnson, 2000; Wagner and Johnson, 2006; Smith et al., 2017; Canada et al., 2020).

The importance of internal stresses in localizing early extension in the Basin and Range is reasoned from the narrow north-south–oriented belt of Cordilleran metamorphic core complexes that lie to the west of the Sevier fold-thrust belt (Fig. 1; e.g., Coney and Harms, 1984). Localization of extension along this north-south belt is inferred to have been driven by enhanced topographic and buoyancy stresses in a continental lithosphere that

Nikolas Midttun https://orcid.org/0000-0001-7729-8851

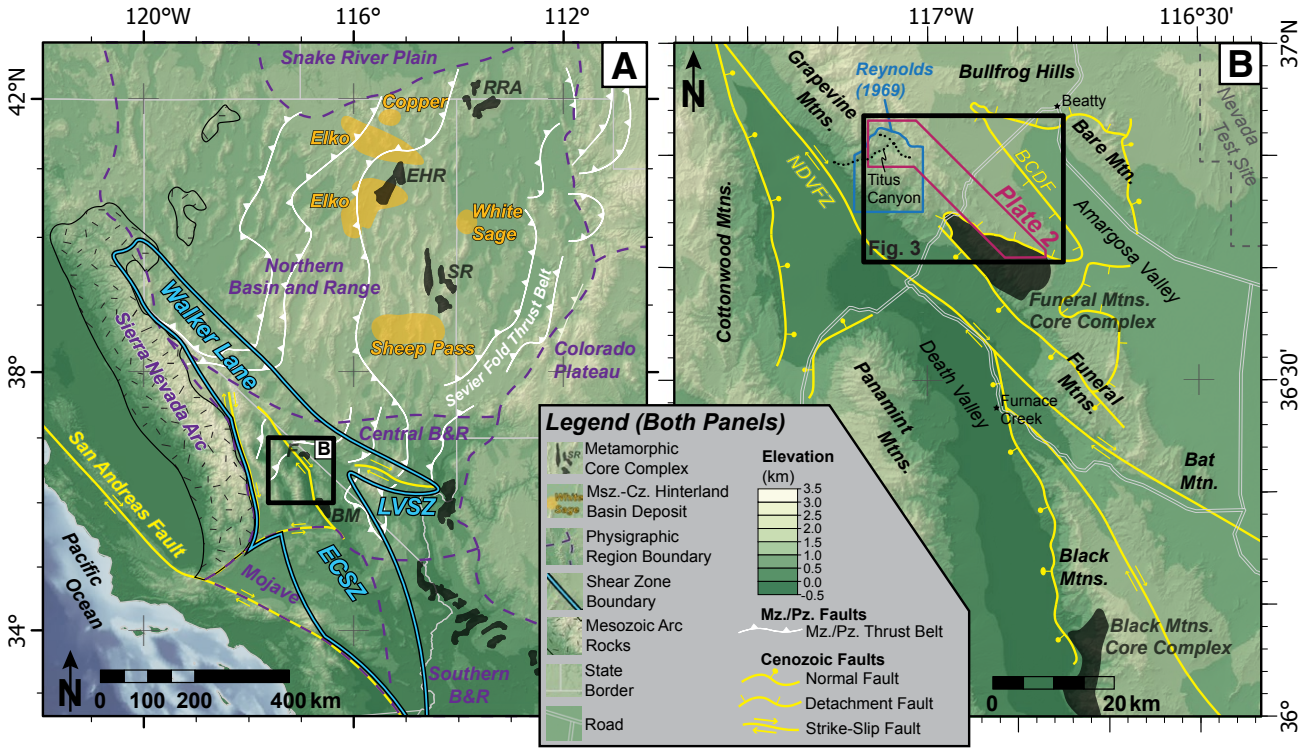

Figure 1. Shaded elevation maps of western North America and the Grapevine and Funeral Mountains of northern Death Valley. Elevation data are from the National Oceanic and Atmospheric Administration's Earth TOPOgraphy dataset (ETOPO) and the Shuttle Radar Topography Mission (SRTM). Panel A: Shaded relief map of western North America showing physiographic regions, major thrust belts, metamorphic core complexes, the Sierra Nevada arc, the San Andreas fault, major shear zones, and the extent of panel B. Panel B: Shaded relief map of northern Death Valley with key place names, Cenozoic faults, highways, the extent of the map in Reynolds (1969), the extent of the geologic map on Plate 2, and the extent of Figure 3. Abbreviations: RRA—Raft River–Albion metamorphic core complex, EHR—East Humboldt–Ruby metamorphic core complex; SR—Snake Range metamorphic core complex; F—Funeral Mountains metamorphic core complex; B&R—Basin and Range; BM—Black Mountains metamorphic core complex; ECSZ—Eastern California shear zone; LVSZ—Las Vegas shear zone; NDVFZ—Northern Death Valley fault zone; BCDF—Boundary Canyon detachment fault.

was over-thickened by late Cretaceous shortening during the Sevier orogeny (Coney and Harms, 1984; Sonder et al., 1987; Jones et al., 1998). The presence of thickened crust in the Cordillera prior to extension is supported by multiple lines of evidence, including palinspastic reconstructions of extension (e.g., Coney and Harms, 1984; Bahadori et al., 2018), stable isotope proxy estimates of paleotopography (e.g., Chamberlain et al., 2012; Lechler et al., 2013; Cassel et al., 2014; Snell et al., 2014), and petrologic estimates of crustal thickness (Best et al., 2009; Chapman et al., 2015).

Despite compelling evidence of crustal thickening in the Sevier hinterland, the lag between the attainment of maximum crustal thickness and subsequent extensional collapse and crustal thinning (ca. 60 Ma; Chapman et al., 2015) suggests that the onset of extension may also require an external forcing. Two main mechanisms are proposed to have initiated early Basin and Range extension: the first is the time-transgressive, north-south removal of the Farallon slab and subsequent heating and weakening of the over-thickened crust (e.g., McQuarrie and Oskin, 2010); the second is a reduction in plate convergence rates resulting in plate boundary stress changes (e.g., Schellart et al., 2010). A particular challenge in disentangling the roles of these two external drivers is that a wealth of information regarding early Basin and Range extension is derived from studies in the northern Basin and Range (e.g., Potter et al., 1995; Druschke et al., 2009; Cassel et al., 2014; Lund Snee et al., 2016; Smith et al., 2017; Cassel et al., 2018; Long, 2018; Canada et al., 2019; Canada et al., 2020), where Eocene removal of the Farallon slab is contemporaneous with the ca. 40 Ma change in the rate of plate

convergence and initiation of trench retreat along the plate boundary (Jurdy, 1984; Humphreys, 1995; McQuarrie and Oskin, 2010; Schellart et al., 2010). Farther south, in the central Basin and Range, Farallon slab removal occurred in the middle Miocene, at ca. 15 Ma, significantly later than the Eocene reduction in plate convergence, thus presenting a potential opportunity to examine the extensional response of the Basin and Range to slab removal and plate boundary reorganization separately. To leverage such an opportunity, however, requires the preservation of thermochronologic or stratigraphic evidence of Eocene extensional tectonism.

The Titus Canyon Formation, in eastern Death Valley (Fig. 1), is recognized as one of the earliest syn-extensional basin deposits in the central Basin and Range (Reynolds, 1969; Saylor, 1991; Snow and Lux, 1999; Fridrich and Thompson, 2011; Niemi, 2012). Previous detailed studies of the Titus Canyon Formation primarily focused on mapping its extent (Reynolds, 1969; Niemi, 2012) and describing its lithostratigraphy (Stock and Bode, 1935; Saylor, 1991; Gutenkunst, 2006), collectively providing limited geochronology and biostratigraphy to constrain the depositional age of the formation and thus the evolution of the Titus Canyon basin. We present ten new measured sections (Plate 1) and a detailed geologic map (Plate 2) of the Titus Canyon Formation in eastern Death Valley National Park. The stratigraphic sections and geologic mapping are accompanied by newly determined stratigraphic positions of paleontologic sites, detrital zircon U-Pb analyses used to inform both basin provenance and provide maximum depositional age (MDA) constraints, and compiled and recalculated $^{40}Ar/^{39}Ar$ geochronologic age data. We develop both an age model for the Titus Canyon Formation and a basin evolution model for the Titus Canyon basin in response to tectonic drivers. These models yield revisions to both the internal stratigraphy and stratigraphic continuity of the Titus Canyon Formation, as well as a reassessment of regional correlations of early Cenozoic stratigraphy in the Death Valley region. The age model and basin evolution model are considered in the context of Farallon slab removal and Eocene plate boundary reorganization to connect the development of the Titus Canyon basin to the initiation of extension across the entire Basin and Range province.

PALEOGENE STRATIGRAPHY OF THE DEATH VALLEY REGION—CORRELATIONS AND CONTROVERSIES

Paleogene strata in northern Death Valley that may record the earliest phases of extensional tectonism in the western Basin and Range are thin, discontinuous, and difficult to date. These challenges have inhibited the development of lithostratigraphic and chronostratigraphic models of these strata, resulting in a lack of consensus around regional correlation and temporal range of Paleogene rocks (Fig. 2; e.g., Snow and Lux, 1999; Fridrich and Thompson, 2011). We outline below several of the controversies surrounding these strata to illustrate the challenges associated with correlating strata across the highly extended Death Valley region.

Cenozoic strata in the Death Valley region were deposited in rapidly evolving extensional basins, resulting in significant lateral variability, time-transgressive deposition, and complex interplay between deposition and active faulting (e.g., Çemen et al., 1999; Snow and Lux, 1999; Snyder and Hodges, 2000; Niemi, 2002; Fridrich and Thompson, 2011). Early efforts to map and define stratigraphic units within Death Valley were restricted to isolated study areas, resulting in nomenclature that varied from mountain range to mountain range for units that may in fact be lithologically or temporally correlative. Snow and Lux (1999) presented a tectono-stratigraphic framework that coherently placed these individual formations into allostratigraphic packages that they correlated across the entire Death Valley region, and in doing so defined three distinct episodes of basin development (Fig. 2). They termed these three phases the pre-extensional, syn-extensional, and post-extensional basin development stages, and although the phases are time-transgressive across the Death Valley region, the phases are identified by the development of regional unconformities, variations in depositional rates and styles, and variations in volcanic input. This tectono-stratigraphic framework was further expanded by Fridrich and Thompson (2011), who correlated seven tectono-stratigraphic assemblages across the Death Valley region (five of these seven assemblages that are geographically relevant to northern Death Valley are shown on Fig. 2). The oldest tectono-stratigraphic package, referred to as the Titus Canyon Assemblage (Fridrich and Thompson, 2011) or the Grapevine Sequence (Snow and Lux, 1999), contains two early-extensional units, the Titus Canyon Formation and the Ubehebe Formation; however, the depositional age, formational boundaries, and stratigraphic relationships between these two units remain unresolved (cf. Snow and Lux, 1999; Fridrich and Thompson, 2011).

Previous Work Describing the Titus Canyon Formation

The Titus Canyon Formation was first defined by Stock and Bode (1935), who were excavating fossil land mammal remains in the southern Grapevine Mountains (Fig. 1), including a Titanothere skull (Stock, 1936). Stock and Bode performed preliminary stratigraphic measurements and descriptions of the fossiliferous beds and defined the Titus Canyon Formation as an ~1000-m-thick sequence of brightly colored conglomerates, sandstones, limestones, and tuffs, but they did not provide detailed mapping of the areal extent of the unit or of its relationship to adjacent geologic units. The Titus Canyon Formation was originally assigned an Oligocene age based on the mammalian fossils found within it (Stock and Bode, 1935; Mason, 1988). Reynolds (1969) significantly refined the stratigraphy of the Titus Canyon Formation with the detailed geologic mapping in Titanothere and Titus canyons (Fig. 3) and also defined a type section for the formation in upper Titus Canyon (Fig. 3). Reynolds (1969) internally divided the Titus Canyon Formation into four units, from stratigraphically lowest to highest: (1) the sedimentary breccia facies; (2) the variegated facies; (3) the brown conglomerate facies; and (4) the green conglomerate facies, and provided an interpretation of the Titus Canyon basin as an extensional basin.

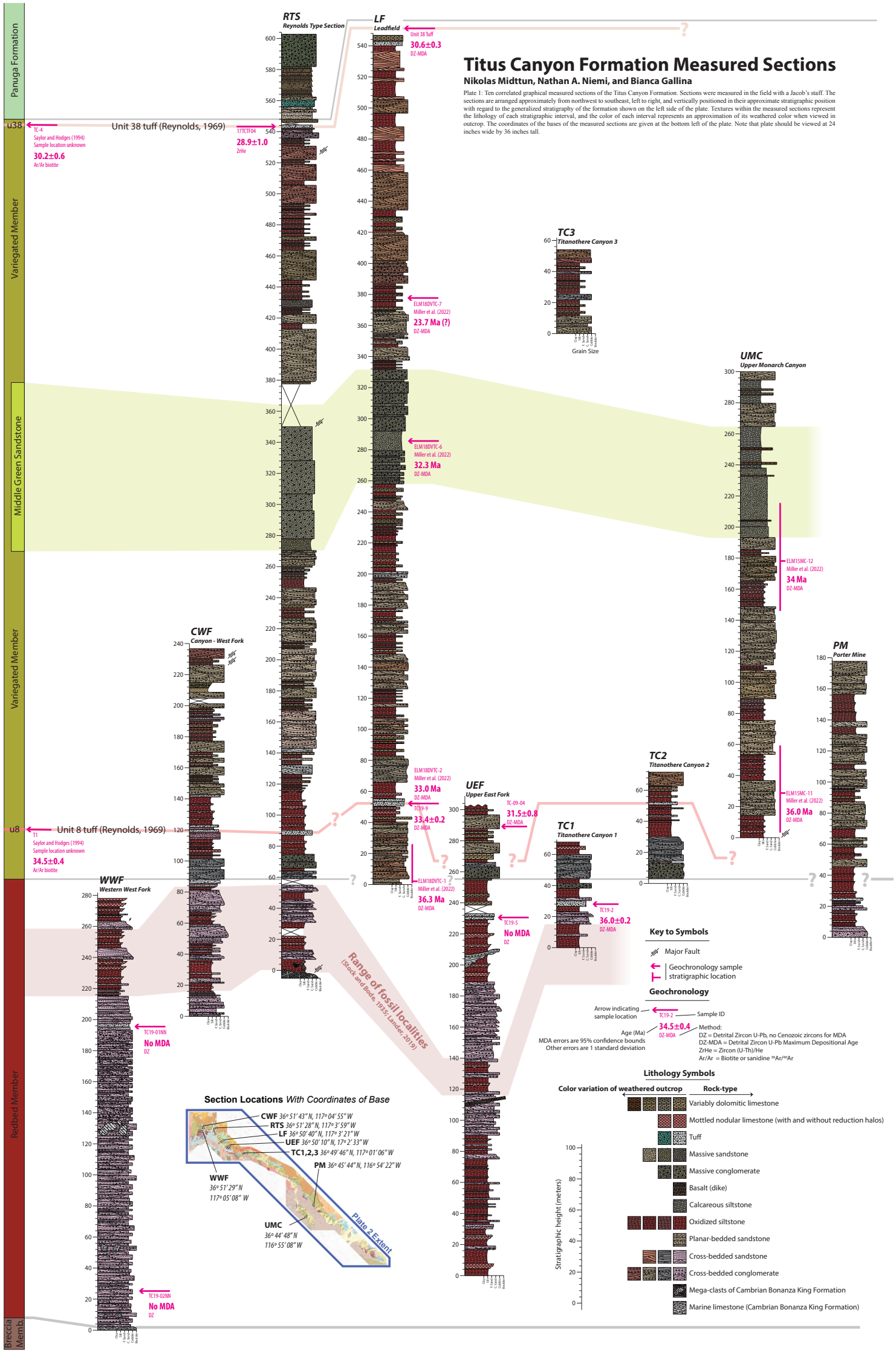

Plate 1. Ten correlated graphical measured sections of the Titus Canyon Formation. Plate should be viewed at 24 inches wide by 36 inches tall. To view Plate 1 at full size, please visit https://doi.org/10.1130/GEOS.S.21291084.

Plate 2. Geologic map of the southern Grapevine Mountains and northern Funeral Mountains, with an emphasis on Cenozoic stratigraphy. Plate is intended to be viewed at 50 inches wide and 40 inches tall. To view Plate 2 at full size, please visit https://doi.org/10.1130/GEOS.S.21291084. Geologic map database can be interactively viewed and downloaded at https://arcg.is/1rriKn.

Plate 2:
Cenozoic Rocks of the Southern Grapevine and Northern Funeral Mountains
Death Valley, California

Nikolas Midttun, Nathan A. Niemi, Bianca Gallina

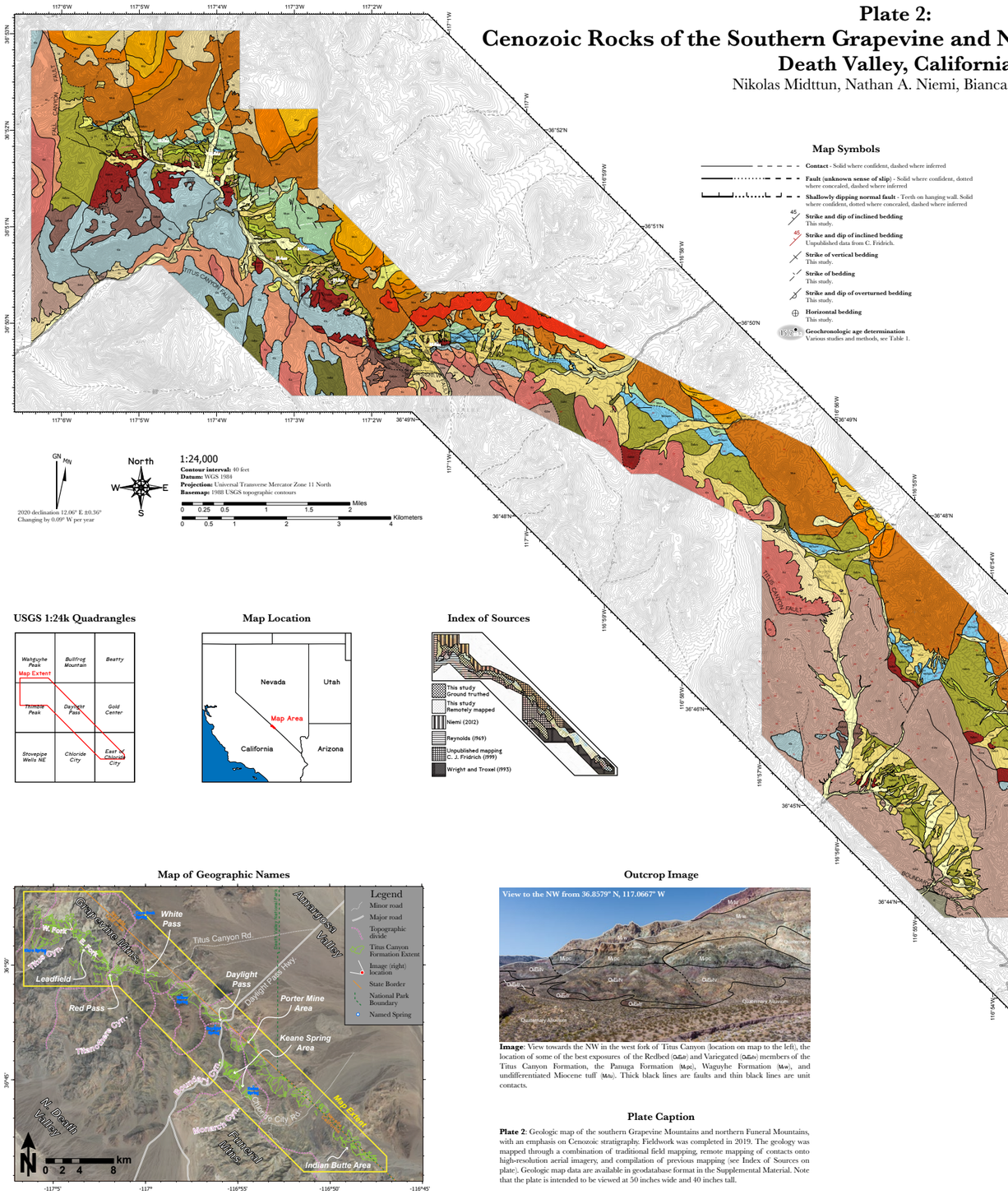

Map Symbols

- **Contact** - Solid where confident, dashed where inferred
- **Fault (unknown sense of slip)** - Solid where confident, dotted where concealed, dashed where inferred
- **Shallowly dipping normal fault** - Teeth on hanging wall. Solid where confident, dotted where concealed, dashed where inferred
- **Strike and dip of inclined bedding** This study.
- **Strike and dip of inclined bedding** Unpublished data from C. Fridrich.
- **Strike of vertical bedding** This study.
- **Strike of bedding** This study.
- **Strike and dip of overturned bedding** This study.
- **Horizontal bedding** This study.
- **Geochronologic age determination** Various studies and methods, see Table 1.

Correlation of Map Units

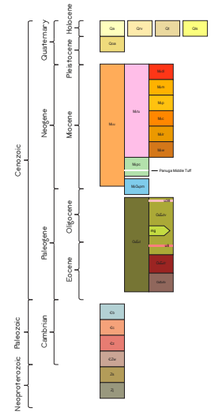

Description of Map Units

- **Qls** Quaternary Landslide Deposit (Holocene) - Landslide debris including semi-coherent blocks of bedrock that have moved downslope
- **Qrv** Quaternary Rock Veneer (Holocene) - Thin deposits of monolithologic regolith blanketing low gradient slopes
- **Qt** Quaternary Talus (Holocene) - Angular cliff fragments resulting from rock fall collected at the base of steep slopes
- **Qa** Quaternary Alluvium (Holocene) - Unlithified sediment in active channels; grain size ranges from sand to boulder
- **Qoa** Quaternary Old Alluvium (Holocene and Pleistocene) - Weakly lithified sands and cobbles in elevated terraces
- **Mu** Tertiary Undifferentiated (Miocene) - Tertiary sedimentary and volcanic deposits, undifferentiated
- **Mtu** Tertiary Tuff Undifferentiated (Miocene) - Tertiary volcanic deposits, undifferentiated
- **Mdt** Donovan Mountain Latite (Miocene) - Dark gray and reddish brown welded and unwelded tuff with minor breccia intervals
- **Mtt** Timber Mountain Group (Miocene) - Brown, pale red, and light gray partially welded to densley welded tuffs
- **Mpt** Paintbrush Group (Miocene) - Crystal-poor gray to reddish brown welded and unwelded tuff
- **Mct** Crater Flat Group (Miocene) - Red pumiceous tuff and white tuffaceous siltstone to pinkish gray welded tuff
- **Mlr** Lithic Ridge Tuff (Miocene) - Non-welded ash flow tuff weathering bluish and pinkish gray
- **Mwf** Wahguyhe Formation (Miocene) - White to pale yellow shales, sandstones, conglomerates, and highly altered tuffs
- **Mpc** Panuga Formation (Miocene) - Thick green conglomerates interbedded with coarse sandstone, contains three distinctive crystaline tuffs including the Panuga Middle Tuff. $^{40}Ar/^{39}Ar$ age: 15.7±0.2 Ma (sanidine).
- **Mcp** Rocks of Porter Mine (Miocene and Oligocene) - Bluish gray and greenish gray tuffaceous conglomerate, sandstone, and mudstone. May correlate with the Ubehebe Formation. $^{40}Ar/^{39}Ar$ ages: 19.5±0.3 Ma (biotite), 23.6±0.1 Ma (sanidine), 28.2±0.2 Ma (biotite).
- **Tct** Titus Canyon Formation (Oligocene and Eocene) - Brightly colored red siltstones, green-gray conglomerates, purple sandstones, and yellow limestones.
  - **Tctm** Variegated member - Interbedded greenish and yellowish gray conglomerates, red siltstone, and yellow-gray limestones forming low rounded hills. Includes three marker units, the Unit 38 (u38) and Unit 8 (u8) tuffs, and the middle green sandstone (mg), a massive gray-green sandstone exhibiting distinctive spheroidal weathering. $^{40}Ar/^{39}Ar$ ages: 30.2±0.6 Ma (u38, biotite), 34.5±0.4 Ma (u8, biotite).
  - **Tctr** Redbed member - Predominantly recessive brick red calcareous siltstone interlingered with grayish purple cross-bedded sandstone and conglomerate
  - **Tctbr** Basal Breccia member - Massive to weakly stratified matrix-supported breccia and conglomerate with a wide range of clast sizes ranging from 1 cm pebbles to boulders 2 meters in diameter. Clasts are primarily composed of Paleozoic limestone, quartzite, and chert
- **Cbk** Bonanza King Formation (Cambrian) - Light to dark gray banded dolostone
- **Cc** Carrara Formation (Cambrian) - Green-gray siltstone interbedded with calcareous sandstones and limestones including bioclastic debris
- **Cz** Zabriskie Quartzite Formation (Cambrian) - Purplish red to grayish pink massively bedded quartzite with well rounded grains
- **Ewc** Wood Canyon Formation (Cambrian and Neoproterozoic) - Interbedded greenish gray siltstone and quartzite, light gray dolostone, and limestone
- **Ns** Stirling Quartzite Formation (Neoproterozoic) - Greenish gray siltstone, fine pink and yellow quartzite, laminated dolostone and limestone
- **Nj** Johnnie Formation (Neoproterozoic) - Brown to purple shale, interbedded dolomite and quartzite with pebble conglomerate

USGS 1:24k Quadrangles

Map Location

Index of Sources

Map of Geographic Names

Outcrop Image

Image: View towards the NW in the west fork of Titus Canyon (location on map to the left), the location of some of the best exposures of the Redbed (QTctr) and Variegated (QTctv) members of the Titus Canyon Formation, the Panuga Formation (Mpc), Waguyhe Formation (Mw), and undifferentiated Miocene tuff (Mtu). Thick black lines are faults and thin black lines are unit contacts.

Plate Caption

Plate 2: Geologic map of the southern Grapevine Mountains and northern Funeral Mountains, with an emphasis on Cenozoic stratigraphy. Fieldwork was completed in 2019. The geology was mapped through a combination of traditional field mapping, remote mapping of contacts onto high-resolution aerial imagery, and compilation of previous mapping (see Index of Sources on plate). Geologic map data are available in geodatabase format in the Supplemental Material. Note that the plate is intended to be viewed at 50 inches wide and 40 inches tall.

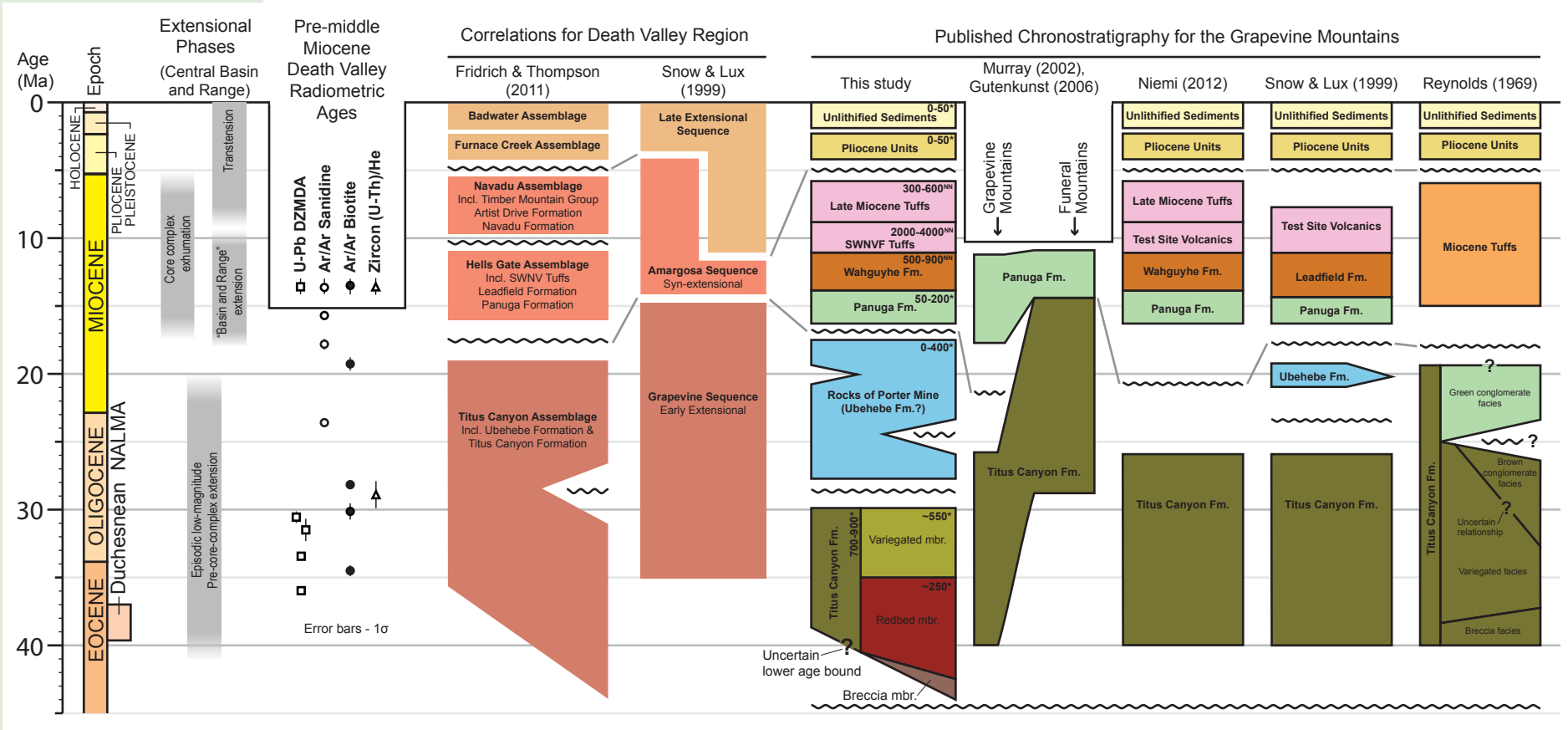

Figure 2. Stratigraphic correlation chart for the past 45 m.y. showing extensional phases in the central Basin and Range, pre-middle Miocene radiometric ages, Death Valley stratigraphic assemblages, and stratigraphy of the Grapevine and Funeral Mountains (study area). Post-middle Miocene radiometric ages (e.g., Bindeman et al., 2006) were excluded from this chart for visual clarity. All geochronologic ages plotted on this figure are listed in Table 1. Numbers in upper-right corner of units in This Study column are compiled and measured stratigraphic thicknesses (meters) where NN—Niemi (2012); *—this study. NALMA—North American Land Mammal Age; DZMDA—detrital zircon maximum depositional ages; SWNVF—Southwest Nevada volcanic field.

Controversies on the Age and Definition of the Titus Canyon Formation

The stratigraphic definition of the Titus Canyon Formation by Reynolds (1969) was revisited with the expanded availability of geochronologic age control (Snow and Lux, 1999). In particular, $^{40}Ar/^{39}Ar$ ages bracketing an angular unconformity between the green conglomerate facies and the underlying variegated facies revealed a 15 m.y. hiatus in deposition, with an Oligocene depositional age for the variegated facies and a middle Miocene age for the green conglomerate facies (Saylor and Hodges, 1994; Snow and Lux, 1999). This discovery led to a revised stratigraphic definition of the Titus Canyon Formation that reassigned the green conglomerate facies to the Miocene Panuga Formation (Snow and Lux, 1999).

Geochronologic analyses throughout the Death Valley region led to the revised definition and regional correlation of multiple other early Cenozoic deposits. Early Cenozoic sedimentary strata from Bat Mountain (Fig. 1), in the southern Funeral Mountains (Fig. 1; McAllister, 1971; Çemen et al., 1982, 1985; Çemen and Wright, 1990) and the Cottonwood Mountains (Fig. 1; McAllister, 1952; Snow, 1990; Snow and White, 1990; Snow, 1993) were demonstrated to share latest Oligocene to early Miocene depositional ages, on the basis of intercalated tuffs (Çemen et al., 1999; Snow and Lux, 1999). These

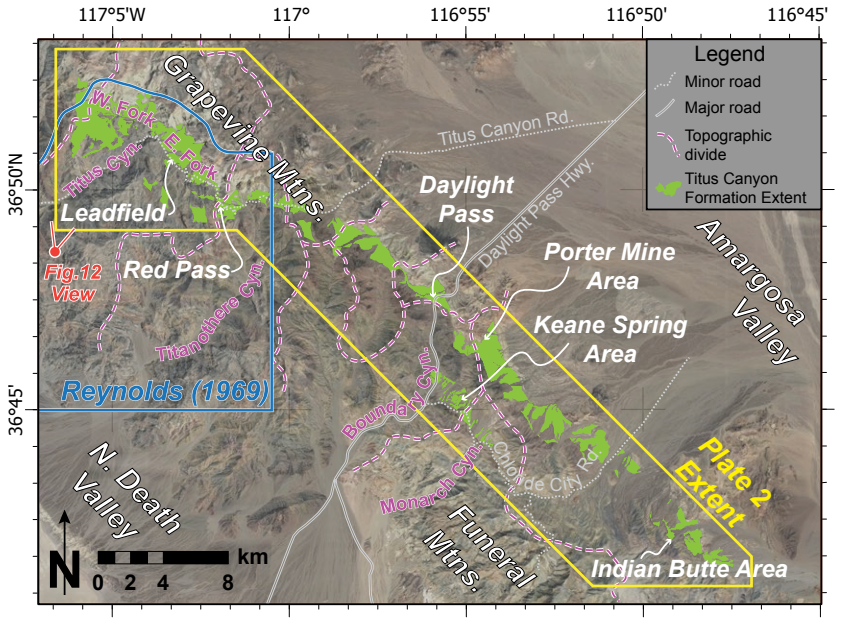

Figure 3. Aerial imagery of the study area in the southern Grapevine and northern Funeral Mountains showing place names, roads, topographic divides, the extent of the Titus Canyon Formation, the extent of the geologic map of Reynolds (1969), and the extent of the geologic map in Plate 2. Imagery is © 2021 Google Earth and Maxar Technologies.

strata were defined as the Ubehebe Formation and consist of a fining-upwards sequence of conglomerates, sandstones, marls, and tuffs exposed in the Cottonwood and southern Funeral Mountains (Fig. 1; Çemen et al., 1982; Çemen et al., 1999; Snow and Lux, 1999). In both the Cottonwood Mountains and the Funeral Mountains (Fig. 1), the Ubehebe Formation is deposited directly on the sub-Tertiary unconformity (i.e., the regional unconformity across the Basin and Range defined by the deposition of Cenozoic strata on deformed Paleozoic or Mesozoic strata), and it is separated by a distinct angular unconformity from the overlying Panuga Formation (Snow and Lux, 1999).

In the southern Grapevine Mountains (Fig. 1), where the Titus Canyon Formation is defined, no strata demonstrably equivalent in age to the Ubehebe Formation have been previously recognized (Reynolds, 1969; Niemi, 2012). Snow and Lux (1999) considered the possibility that the Titus Canyon Formation might be an older, time-transgressive equivalent to the Ubehebe Formation, since Ubehebe Formation strata were not definitively observed stratigraphically above the Titus Canyon Formation anywhere, and the two units share some lithologic similarities. They concluded, however, that the Titus Canyon Formation is most likely distinct in age from, and thus not correlative with, the Ubehebe Formation. This conclusion hinged on reports that the Titus Canyon Formation is overlain by 20–24 Ma strata, equivalent in age to the Ubehebe Formation, at two isolated and relatively small, exposures (Reynolds, 1974; Wright and Troxel, 1993).

Strata broadly similar in lithology to the Titus Canyon and Ubehebe Formations have subsequently been reported along the eastern flank of Funeral Mountains (Fig. 1; Murray, 2002; Gutenkunst, 2006; Ridgway et al., 2011). Sections along the eastern Funeral Mountains were correlated by Gutenkunst (2006) to the Titus Canyon Formation on the basis of their similar lithofacies. However, geochronologic analyses from these sections ranged from latest Oligocene to early Miocene (Gutenkunst, 2006), which would suggest temporal equivalence to the Ubehebe Formation, not the Titus Canyon Formation. The continuum of exposures of early Cenozoic strata from the Grapevine Mountains southward along the eastern margin of the Funeral Mountains to Bat Mountain, at the southern end of the Funeral Mountains (Fig. 1), led Fridrich and Thompson (2011) to challenge the distinction of Snow and Lux (1999) and to propose that the Titus Canyon and Ubehebe Formations reflect a single, time-transgressive continuum of deposition. Support for this interpretation, in part, arises from a lack of definitive absolute age control that differentiates the depositional age of the Titus Canyon Formation from the Ubehebe Formation.

Resolving the Early Extensional and Basin Development History of the Death Valley Region

The challenge of resolving and understanding the early extensional history of the Death Valley region arises from two specific issues. First is the lack of absolute age control on the deposition of the Titus Canyon Formation, as discussed above. The age of the Titus Canyon Formation is primarily derived from paleontologic evidence and has been reported as Eocene to Oligocene (Stock and Bode, 1935; Mason, 1988; Lander, 2019), presenting difficulties in comparing the age of the Titus Canyon Formation to other lithologic units. The second issue is a lack of detailed mapping of the extent, continuity, and regional correlation of the Titus Canyon Formation, which had the added effect of preventing extrapolation of the limited biostratigraphic and geochronologic age constraints that do exist for the formation. Geologic maps at 1:48,000 scale in the Grapevine and Funeral Mountains (Cornwall and Kleinhampl, 1964; Wright and Troxel, 1993; Niemi, 2012) expanded the recognized areal extent of the Titus Canyon Formation beyond Titus Canyon to a

northwest-southeast strip along the eastern Grapevine and Funeral Mountains (Fig. 3). However, these maps omit the internal stratigraphy of the Titus Canyon Formation as defined by Reynolds (1969), and, in areas particularly relevant to discriminating the Titus Canyon and Ubehebe Formations, pre-date the recognition of these two formations (e.g., Cornwall and Kleinhampl, 1964; Wright and Troxel, 1993).

Below, we present detailed measured sections (Plate 1) and geologic mapping (Plate 2) in the southern Grapevine Mountains and northern and central Funeral Mountains (Fig. 1) that inform the above-described controversies. The internal stratigraphy of the Titus Canyon Formation is mapped throughout the study region, with recognition of the possibility that the Ubehebe Formation can be differentiated from the Titus Canyon Formation. Robust geochronologic age constraints (Table 1) are provided for the type section of the Titus Canyon Formation and are integrated with previously unpublished age constraints from other sections to develop a coherent early Cenozoic chronostratigraphy for eastern Death Valley and resolve the age, stratigraphic definition of, and regional tectonic significance of, the Titus Canyon Formation.

METHODS

To refine the internal stratigraphy and determine an age model for the Titus Canyon Formation, we measured stratigraphic sections, undertook large-scale field mapping, and completed zircon

TABLE 1. SUMMARY OF GEOCHRONOLOGY SAMPLES

Sample	Latitude (°N)	Longitude (°W)	Age (Ma)	Age error	Age method	Grains	Source	Analytical data	Location certainty	Stratigraphic position
Unit 38 Tuff	36.84675	117.04754	30.6 ± 0.3	± 1σ	U/Pb zircon MDA	106	This study	Table S1	GPS	Unit 38 Tuff, Variegated member, Titus Canyon Formation
TC-09-04	36.84037	117.04137	31.5 ± 0.8	± 1σ	U/Pb zircon MDA	87	This study	Table S1	GPS	Variegated member, Titus Canyon Formation
TC19-9	36.84424	117.05414	33.4 ± 0.2	± 1σ	U/Pb zircon MDA	105	This study	Table S1	GPS	Unit 8 Tuff, Variegated member, Titus Canyon Formation
TC19-2	36.82998	117.01923	36.0 ± 0.2	± 1σ	U/Pb zircon MDA	105	This study	Table S1	GPS	Variegated member, Titus Canyon Formation
TC19-5	36.83873	117.03860	N.D.**	N.A.	U/Pb zircon	110	This study	Table S1	GPS	Redbed member, Titus Canyon Formation
TC19-01NN	36.85915	117.09045	N.D.**	N.A.	U/Pb zircon	103	This study	Table S1	GPS	Redbed member, Titus Canyon Formation
TC19-02NN	36.86059	117.08305	N.D.**	N.A.	U/Pb zircon	110	This study	Table S1	GPS	Redbed member, Titus Canyon Formation
17TCTF04	36.86301	117.06580	28.9 ± 1.0	± 1 S.E.	(U-Th)/He zircon	3	This study	Table S2	GPS	Unit 38 Tuff, Variegated member, Titus Canyon Formation
17TCTF01	36.83907	117.03937	15.2 ± 1.4#	± 1 S.E.	(U-Th)/He zircon	3	This study	Table S2	GPS	Unit 8 Tuff, Variegated member, Titus Canyon Formation
17TCTF03	36.85942	117.06672	25.7 ± 4.0#	± 1 S.E.	(U-Th)/He zircon	3	This study	Table S2	GPS	Unit 8 Tuff, Variegated member, Titus Canyon Formation
17CH03	36.73715	116.85796	24.4 ± 2.1	± 1 S.E.	(U-Th)/He zircon	3	This study	Table S2	GPS	Rocks of Porter Mine (Ubehebe Formation)
FM-2_16.5 Biotite2	36.69517	116.79875	19.3 ± 0.5	± 1σ	Ar/Ar biotite	N.A.	Murray (2002), Gutenkunst (2006)	Table S3, Fig. S1	Estimated*	Rocks of Porter Mine (Ubehebe Formation)
FM-3_102.5 Sanidine1	36.69304	116.79596	23.6 ± 0.1	± 1σ	Ar/Ar sanidine	N.A.	Murray (2002), Gutenkunst (2006)	Table S3, Fig. S1	Estimated*	Rocks of Porter Mine (Ubehebe Formation)
FM-3_2.1 Biotite1	36.69159	116.79298	28.2 ± 0.2	± 1σ	Ar/Ar biotite	N.A.	Murray (2002), Gutenkunst (2006)	Table S3, Fig. S1	Estimated*	Rocks of Porter Mine (Ubehebe Formation)
TC-4	N.L.	N.L.	30.2 ± 0.6	± 1σ	Ar/Ar biotite	N.A.	Saylor and Hodges (1994)	N.A.††	N.L.	Unit 38 Tuff, Variegated member, Titus Canyon Formation
T1	N.L.	N.L.	34.5 ± 0.4	± 1σ	Ar/Ar biotite	N.A.	Saylor and Hodges (1994)	N.A.††	N.L.	Unit 8 Tuff, Variegated member, Titus Canyon Formation
592-GV1 K1	36.8650	117.0778	15.7 ± 0.2	± 1σ	Ar/Ar sanidine	N.A.	Snow and Lux (1999)	Table S3	Estimated§	Panuga Formation
ELM18DVTC-1	36.843966	117.05466	36.3	N.D.	U/Pb zircon MDA	113	Miller et al. (2022)	Miller et al. (2022)	N.A.	Titus Canyon Formation
ELM18DVTC-2	36.844193	117.05427	33.0	N.D.	U/Pb zircon MDA	100	Miller et al. (2022)	Miller et al. (2022)	N.A.	Titus Canyon Formation
ELM18DVTC-6	36.84493	117.05031	32.3	N.D.	U/Pb zircon MDA	84	Miller et al. (2022)	Miller et al. (2022)	N.A.	Titus Canyon Formation
ELM18DVTC-7	36.844348	117.04692	23.7	N.D.	U/Pb zircon MDA	116	Miller et al. (2022)	Miller et al. (2022)	N.A.	Titus Canyon Formation
ELM15MC-11	36.739036	116.90889	36.0	N.D.	U/Pb zircon MDA	64	Miller et al. (2022)	Miller et al. (2022)	N.A.	Titus Canyon Formation
ELM15MC-12	36.741279	116.90561	34	N.D.	U/Pb zircon MDA	90	Miller et al. (2022)	Miller et al. (2022)	N.A.	Titus Canyon Formation

*Location uncertainty 200 meters. Position of sample within a measured stratigraphic section is known, but location of measured section is uncertain.
§Sample coordinates reported in Snow and Lux (1999) are incorrect. Coordinates given here are estimated from bearing, distance, and stratigraphic position described in Snow and Lux (1999).
#Age inconsistent with stratigraphic constraints.
**No Cenozoic zircons for maximum depositional age (MDA).
††Original complete analytical data no longer available (K. Hodges, personal commun., 2020).
N.D.—not determined. N.A.—not applicable. N.L.—no sample location given in Saylor and Hodges (1994). S.E.—standard error.

U-Pb geochronology. These efforts resulted in ten detailed measured stratigraphic sections (Plate 1), a 1:24,000 scale geologic map (Plate 2), and maximum depositional ages (MDAs) for the Titus Canyon Formation. These data were correlated with published and unpublished $^{40}Ar/^{39}Ar$ age determinations to develop a new basin evolution and regional stratigraphic model for the early-extensional sequences in Death Valley.

Geologic Mapping and Measured Sections

Geologic mapping included field and remote components. Fieldwork was conducted over two field seasons in 2019. We measured and described the internal stratigraphy of the Titus Canyon Formation using a Jacob's staff at ten locations, comprising a total of 2600 m of strata. During geologic mapping in the field, the locations of faults and contacts were recorded directly onto high-resolution, orthorectified aerial imagery using a GPS-enabled tablet running Esri Collector for ArcGIS. Field mapping was principally focused on detailed analysis of Eocene to early Miocene stratigraphic units, with older and younger units mapped remotely (see index map on Plate 2). The locations and contacts of Proterozoic and Paleozoic units were principally derived from previous 1:48,000 and 1:100,000 geologic maps (Cornwall and Kleinhampl, 1964; Reynolds, 1969; Wright and Troxel, 1993; Carr et al., 1996; Niemi, 2012). Geologic contacts on those maps, which were originally on topographic base maps, were digitally refined to 1:24,000 scale by tracing color changes visible on high-resolution aerial imagery. In addition to ground truthing, some contacts between early Cenozoic sedimentary strata (including the Titus Canyon Formation) and overlying Miocene units were mapped by referencing the geologic mapping of Niemi (2012) and unpublished mapping by C. Fridrich (1999, personal commun.) and tracing contacts onto high-resolution aerial imagery. All field and remote mapping was compiled on a 1:24,000 U.S. Geological Survey topographic map base composed of digital line graphs (DLGs; 1980–1990 vintage), which were simplified for visual clarity (Plate 2).

We precisely located Caltech and the Los Angeles County Museum paleontological localities excavated in the 1930s (Stock and Bode, 1935; Mason, 1988; Lander, 2019) by visually matching distinctive outcrops visible in original glass slide images of excavations to their modern exposures. We have purposefully obfuscated the exact geographic locations of fossil localities to protect the sites, although the stratigraphic position of such sites in reported measured sections (Plate 1) is representative of their observed positions within the Titus Canyon Formation.

Geochronology

New geochronologic analyses were undertaken by multiple methods; these new data were combined with previously unpublished $^{40}Ar/^{39}Ar$ ages to obtain an age model for deposition of the Titus Canyon Formation. All ages are summarized in Table 1.

Detrital Zircon U-Pb Geochronology

Seven samples of tuffs and tuffaceous sandstones were collected from a range of stratigraphic levels within the Titus Canyon Formation for geochronologic analysis (Fig. 4 and Table 1). Selected samples appeared tuffaceous as assessed in the field with a hand lens. Zircon separates were produced at the University of Michigan following standard mineral separation techniques for rock crushing, sieving, and heavy liquids separation. U-Pb geochronology on detrital zircons (analytical data are available in Table S1[1]) was performed using laser ablation–inductively coupled plasma mass spectrometry (LA-ICPMS) at the University of Arizona LaserChron Center following the analytical methods of Gehrels et al. (2008).

[1]Supplemental Material. Table S1: Analytical data for Titus Canyon detrital zircon U-Pb analyses. Table S2: Analytical data for Titus Canyon zircon (U-Th)/He analyses. Table S3: Analytical data for $^{40}Ar/^{39}Ar$ ages of Gutenkunst (2006). Figure S1: Recalculated $^{40}Ar/^{39}Ar$ analytical plots for data originally from Gutenkunst (2006). Please visit https://doi.org/10.1130/GEOS.S.21291075 to access the supplemental material, and contact editing@geosociety.org with any questions.

Maximum Depositional Age Analysis from U-Pb Detrital Zircon Geochronology

Maximum depositional ages were calculated from the zircon U-Pb ages for detrital zircon samples that contained Cenozoic zircons (four out of seven samples). There are a variety of published methods for MDA determination (e.g., Dickinson and Gehrels, 2009; Coutts et al., 2019), many of which are recognized to bias MDA estimates to young values when seeking the youngest zircon age or population (e.g., Coutts et al., 2019; Vermeesch, 2021). We present MDAs based on the Maximum Likelihood Age (MLA) algorithm, which is designed to minimize MDA bias (Galbraith and Laslett, 1993; Vermeesch, 2021). Application of the MLA method (Fig. 5) yielded consistent age determinations for a single tuffaceous unit dated by U-Pb detrital zircon MDA, $^{40}Ar/^{39}Ar$, and zircon (U-Th)/He methods (Unit 38 tuff; Table 1), and consistent U-Pb detrital zircon MDA and $^{40}Ar/^{39}Ar$ ages determined on samples from two localities that were inferred to be the same geologic unit based on field mapping and stratigraphic relationships.

All Cenozoic zircon U-Pb ages from each detrital zircon sample were included in each MLA analysis, with the exception of a single 24 Ma zircon grain from the Unit 38 Tuff. This age was excluded because it could be demonstrated independently that the age disagreed with stratigraphic constraints on the depositional age of the unit sampled. Additionally, the measured U concentration from this grain (6675 ppm) was a factor of 6 higher than for any other grain analyzed, suggesting that the young age may be the result of diffusional lead loss due to radiation damage (Lee et al., 1997).

Zircon (U-Th)/He Thermochronology

Four tuffaceous sandstones were dated with the (U-Th)/He method at the University of Michigan Thermochronology lab following the standard methods of Niemi and Clark (2018). Three grains were analyzed per sample and reported uncertainties are ± 1 standard error of the mean age of each sample. Ages are summarized in Table 1, and full analytical data are in Table S2 (see footnote 1).

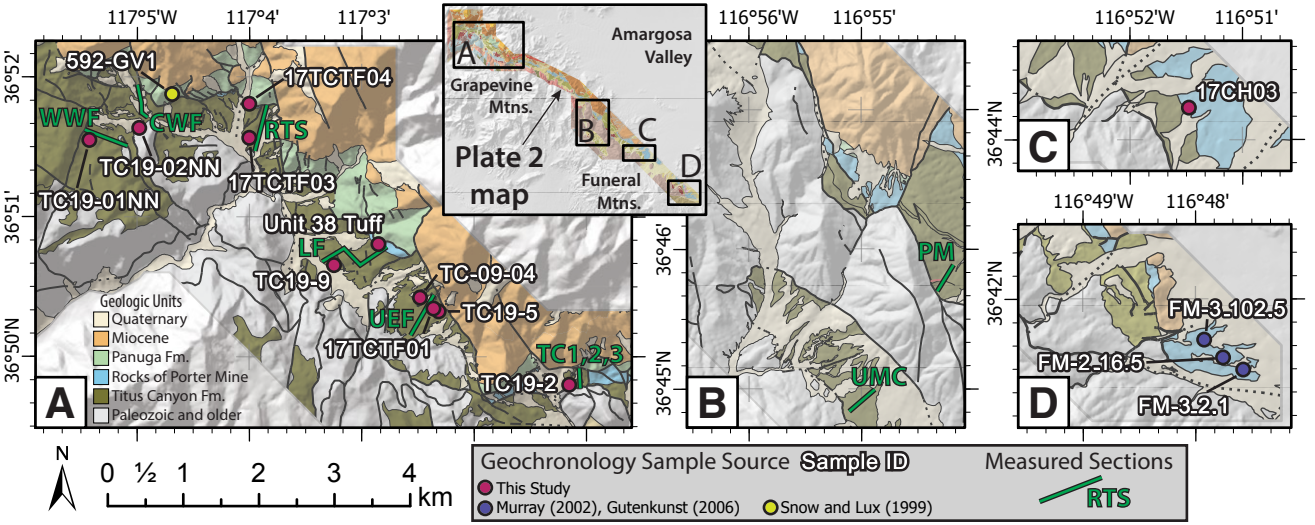

Figure 4. Location maps of measured sections (green and black; Plate 1) and geochronology samples (various colors with black outlines; Table 1). Geologic base map is simplified from Plate 2 with hillshade overlay. Abbreviated measured section names from Plate 1: WWF—Western West Fork; CWF—Canyon West Fork; RTS—Reynolds Type Section; LF—Leadfield; UEF—Upper East Fork; TC1,2,3—Titanothere Canyon 1, 2, and 3; UMC—Upper Monarch Canyon; PM—Porter Mine. Latitude-longitude coordinates for of the base of each measured section are on Plate 1.

$^{40}Ar/^{39}Ar$ Geochronology

No new $^{40}Ar/^{39}Ar$ analyses were performed for this study; however, six previously analyzed $^{40}Ar/^{39}Ar$ ages from tuffs within the Titus Canyon Formation and other Cenozoic strata in eastern Death Valley were recalculated and updated to the K decay constant of Renne et al. (2010, 2011) and the MMhb-1 monitor mineral age of Spell and McDougall (2003). Three unpublished $^{40}Ar/^{39}Ar$ ages from Cenozoic strata in the eastern Funeral Mountains (Gutenkunst, 2006) were recalculated from original analytical data using IsoplotR (Vermeesch, 2018) to determine plateau, isochron, weighted, and integrated ages (Fig. S1 and Table S3, see footnote 1). Two additional unpublished $^{40}Ar/^{39}Ar$ ages collected from the Titus Canyon Formation (Saylor and Hodges, 1994) were recalculated using the ArAR program (Mercer and Hodges, 2016). Original analytical data are not available for the samples from Saylor and Hodges (K. Hodges, personal commun., 2020). A single published $^{40}Ar/^{39}Ar$ age from the Panuga Formation in the southern Grapevine Mountains (Snow and Lux, 1999) was recalculated using ArAR (Mercer and Hodges, 2016). All $^{40}Ar/^{39}Ar$ ages are summarized in Table 1.

The accuracy of the geographic and stratigraphic positions of the $^{40}Ar/^{39}Ar$ samples is variable (location uncertainties are summarized in Table 1). Three sample locations from Gutenkunst (2006) were reported as stratigraphic position within a measured stratigraphic section from the eastern Funeral Mountains (section FM of Murray, 2002). The location of the FM measured section is approximated from a small-scale figure; so we employed field observations of the orientation and younging direction of strata in the field area of Murray (2002) to assess the location of the measured section and to estimate the geographic position of the samples in the field (Fig. 4). The two sample locations from Saylor and Hodges (1994) are unknown, but their approximate location within the stratigraphy was reported. An $^{40}Ar/^{39}Ar$ age from the Panuga Formation in the southern Grapevine Mountains (Fig. 1) is well defined stratigraphically (Snow and Lux, 1999). The written description of the sample locality within the Panuga Formation is consistent with the known distribution of this formation (Snow and Lux, 1999); however, reported geographic coordinates for this sample are inconsistent with both the written description and the distribution of the Panuga Formation. We therefore estimated the sample coordinates from the written description (Sample 592-GV1 K1; Fig. 4 and Table 1).

REVISED STRATIGRAPHY AND AGE OF PALEOGENE STRATA IN EASTERN DEATH VALLEY

Our mapping supports the division of Paleogene strata in eastern Death Valley into the 40(?)–30 Ma Titus Canyon Formation, and the ca. 28–19 Ma Rocks of Porter Mine, units that can be differentiated based on their lithologic content, differing volcanic content, distinct depositional

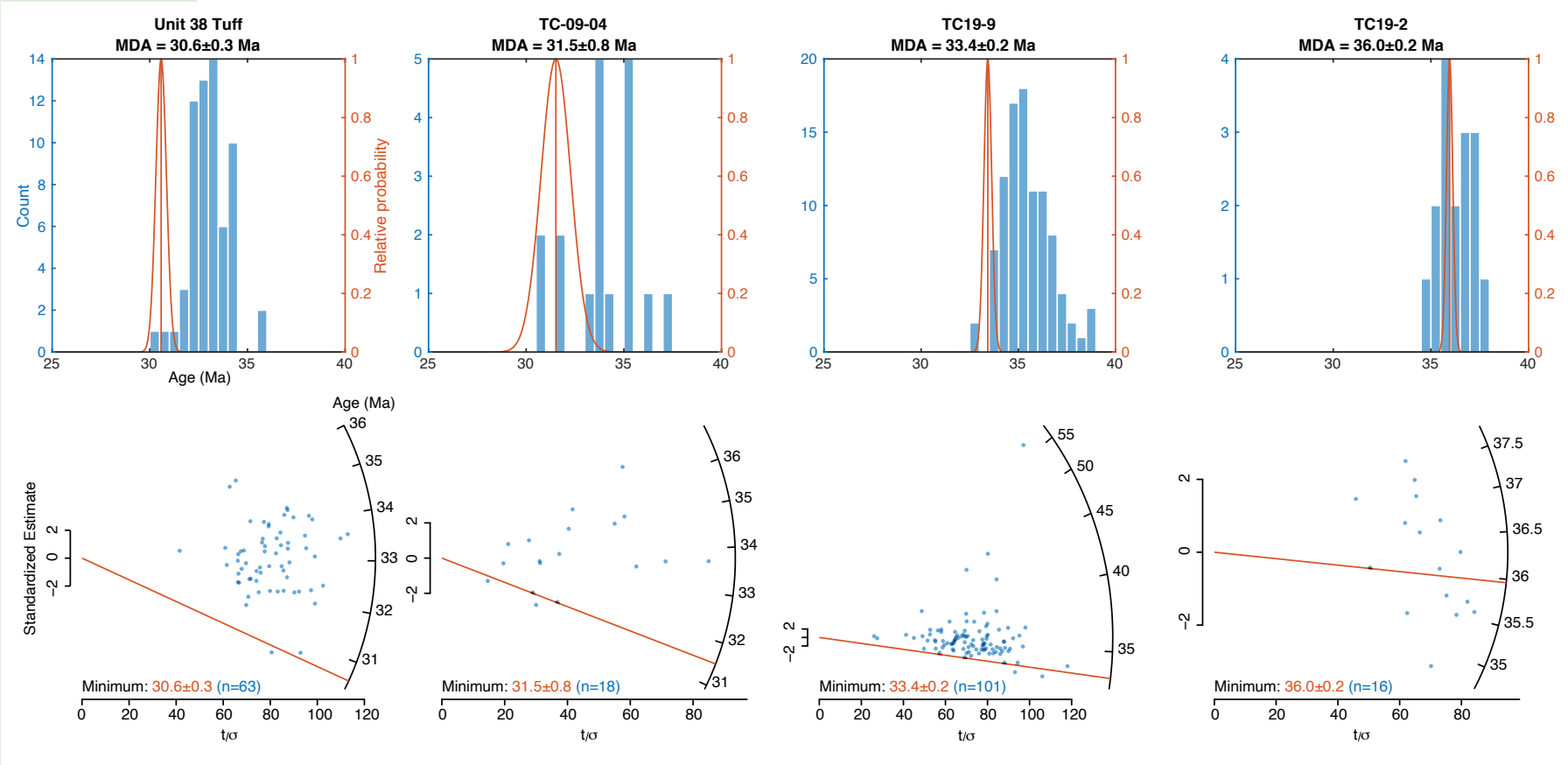

Figure 5. Detrital zircon U-Pb age distributions, radial plots, and estimated maximum depositional ages (MDA) based on the Maximum Likelihood Estimation (MLE) algorithm of Vermeesch (2021) for four samples that contained Cenozoic zircons. Lower panels show radial plots (Galbraith and Laslett, 1993; Vermeesch, 2021) along with an orange line indicating the estimated MDA. The maximum likelihood MDA is reported with ± 1σ errors. The upper plots show histograms of individual grain ages (blue) overlaid with the normal probability distribution (orange) of the MDA age based on the MLE analysis. Each sample uses all of its Cenozoic grains for the MDA calculation (n given in radial plots) with the exception of the Unit 38 Tuff which has a single 24 Ma outlier removed. The 24 Ma grain had 6675 ppm U—6 × the U concentration of the other grains in the sample—and contradicted independent stratigraphic constraints on the age of the Unit 38 Tuff.

timing based on radiometric ages, and consistent superposed stratigraphic relationship throughout the map area. Based on its distinctive lithology and our revised geochronology, the Rocks of Porter Mine may correlate with the Ubehebe Formation of Snow and Lux (1999). We describe both units below, with emphasis on the characteristics that distinguish them, both in the field and in terms of depositional age.

Titus Canyon Formation

Our geologic mapping identifies exposures of the Titus Canyon Formation in a 35-km-long strip along the northeastern margin of the southern Grapevine and northern Funeral Mountains (Fig. 3 and Plate 2). The thickness of the formation varies from 500 m to ~1 km, with an overall trend of thickening to the northwest (Plate 2). Compared to previous studies (Stock and Bode, 1935; Cornwall and Kleinhampl, 1964; Wright and Troxel, 1993), our mapping extends the recognized distribution of the Titus Canyon Formation farther to the southeast. A small number of exposures originally mapped as the Titus Canyon Formation ~10 km northwest of the area mapped on Plate 2 (Stock and Bode, 1935; Saylor, 1991) have been previously refined as correlating with younger stratigraphic units (Niemi, 2012).

The depositional base of the Titus Canyon Formation is best exposed in the West Fork of Titus Canyon (in the vicinity of 36.8551°N, 117.0852°W), where the formation is deposited on the Cambrian Bonanza King Formation. Toward the southeast end of the mapping area near Indian Butte (Fig. 3, ~36.7015°N, 116.8117°W), the nature of the base of the Titus Canyon Formation becomes obscured by poor exposure and pervasive faulting but appears to lie primarily on the Cambrian Zabriskie Quartzite or Neoproterozoic to Cambrian Wood Canyon Formation (Plate 2). In many locations, especially near the southeastern extent of the map, extensive postdepositional normal faulting (Fig. 6) has put the Titus Canyon Formation in fault contact with underlying Paleozoic bedrock, making it difficult to determine the nature of the depositional base of the formation. Preserved exposures of the Titus Canyon Formation all lie in the hanging wall of the late Miocene Boundary Canyon detachment fault (Plate 2; Wright and Troxel, 1993).

Revised Lithostratigraphy of the Titus Canyon Formation

Here, we redefine the internal stratigraphy of the Titus Canyon Formation from the previous descriptions provided by Reynolds (1969) and Snow and Lux (1999). Reynolds uses the term "facies" in the names of all his mapped sub-formation units (e.g., brown conglomerate facies). Our mapping indicates that the divisions between our proposed map units are laterally extensive and well defined; so we divide the stratigraphy of the Titus Canyon Formation into members, listed here from oldest to youngest: (1) the Basal breccia member (largely unmodified from Reynolds' sedimentary breccia facies); (2) the Redbed member (rocks that were originally included in the lower part of the variegated facies of Reynolds); and (3) the Variegated member (the remainder of the variegated facies of Reynolds after removing the Redbed member). We include the brown conglomerate facies of Reynolds in the Variegated member.

Basal breccia member. The lowest unit of the Titus Canyon Formation, the Basal breccia member, includes rocks previously called the sedimentary

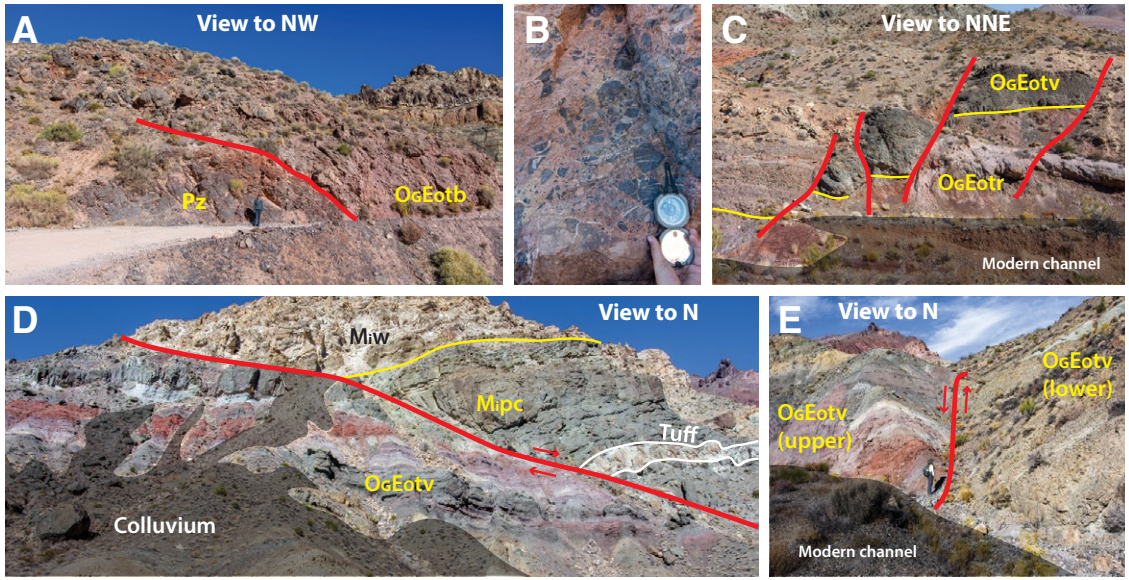

Figure 6. Field photos of different expressions of normal faulting in the study area. (A) Shallowly dipping normal fault exposed ~0.5 km east of Red Pass on Titus Canyon road (Fig. 3) separating the Breccia member of the Titus Canyon Formation (OGEOtb) from Paleozoic rocks (Pz) below. (B) Typical matrix supported angular to subangular breccia of the Basal breccia member of the Titus Canyon Formation. The Titus Canyon Formation is faulted along much of its basal contact; so some exposures of limestone breccia near the base of the formation may be products of fault-zone brecciation as opposed to sedimentary deposition. (C) Characteristic small offset, closely spaced, and steeply dipping normal faults that pervade the study area, here seen offsetting the contact between the Variegated (OGEOtv) and Redbed (OGEOtr) members of the Titus Canyon Formation. (D) A major shallowly dipping normal fault placing Miocene Panuga Formation (Mipc) and Wahguyhe Formation (Miw) onto the upper Variegated member of the Titus Canyon Formation (OGEOtv) in the upper west fork of Titus Canyon (Fig. 3). (E) Moderate offset steeply dipping normal fault in the upper west fork of Titus Canyon with an opposite dip direction (~NE) to the majority of faults (~SW) in the study area.

breccia facies by Reynolds (1969). The member is relatively thin (~0–30 m) and discontinuous, even where it is best exposed in the west fork of Titus Canyon and along the Titus Canyon Road southeast of Red Pass (Fig. 3). The base of the member is marked by the first occurrence of angular fragments of Bonanza King Formation (Fig. 6B), which are typically deposited onto intact Bonanza King Formation. The member consists of massive or weakly stratified matrix-supported breccia and conglomerate with pebble- to boulder-sized (up to 2-m-diameter) clasts composed of primarily Paleozoic limestone, quartzite, and chert.

Redbed member. We define the Redbed member of the Titus Canyon Formation as a succession of recessive brick-red calcareous siltstones to mudstones interfingered with resistant packages of grayish-purple sandstone and matrix-supported sandy conglomerate (Figs. 7B and 7D). This member approximately represents the lower third of the variegated facies defined by Reynolds (1969). The Redbed member comprises 250 m of strata at its thickest exposures, though many locations have as little as 50 m of section that may be truncated by faults (Plate 1). The Redbed member is present across the entire map area, identifiable by its distinct combination of purplish-gray conglomerate and sandstone with brick-red siltstone. The Redbed member fines upward overall, with its base consisting of predominantly purplish-gray cross-bedded sandy conglomerate that transitions upsection to recessive brick-red siltstone, which quickly become the dominant lithology toward the top of the member (Fig. 7A). While the transition from dominantly purple-gray conglomerate to brick-red siltstone occurs at ~150 m above the base of the member in the west fork of Titus Canyon (Fig. 3), elsewhere the transition varies in stratigraphic position within the member, and we therefore did not interpret the transition as a mappable unit contact. The red recessive exposures of the member are characterized by massive or weakly stratified brick-red siltstone containing sparse secondary calcite veins, sparse light greenish-gray oxidation halos, and sparse knobby calcareous concretions. In some places, the recessive red siltstone is organized into 1–5-m-thick bedding packages that become slightly more resistant and calcareous up section before truncating at a planar surface and repeating (Fig. 7D). Intervals of resistant grayish-purple conglomerate contain well-rounded pebble- to cobble-sized clasts composed primarily of quartzite with some limestone and chert. Quartzite clasts are highly polished and have percussion marks. Conglomerate lenses generally fine upwards into grayish-purple sandstone consisting of fine to coarse sub-angular grains in planar beds or sets of 10–20-cm-tall cross-beds (Figs. 7C and 7D). The purple sandstone and conglomerate intervals weather into resistant, smooth, rounded outcrops, while the recessive brick-red siltstone forms steep slopes mantled with loose weathered material (Figs. 7A and 7B). All the Duchesnean fossil localities (Stock and Bode, 1935; Lander, 2019)

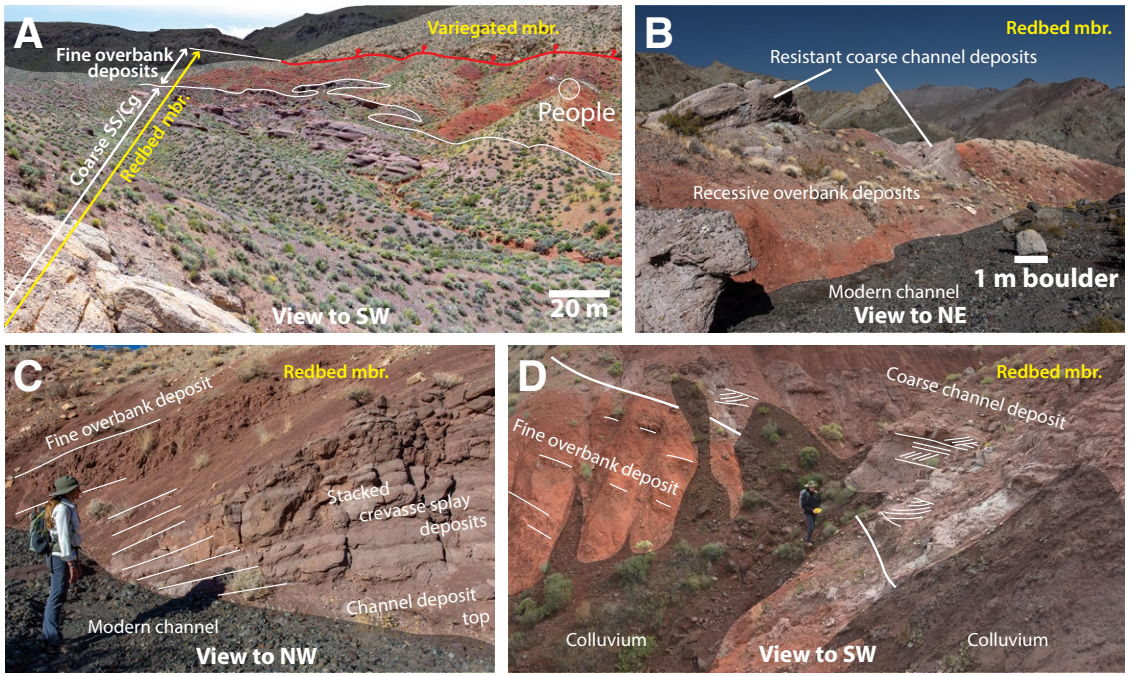

Figure 7. Field photos of the Redbed member of the Titus Canyon Formation in the west fork of Titus Canyon (Fig. 3). (A) View of the transition between thick clast-supported quartzite conglomerates (bottom left) into overlying fine-grained brick-red siltstones (upper right). The Variegated member is visible at the top of the image across a fault. (B) Exposure of the fining-upward purplish-gray cross-bedded pebbly sandstone channel bodies cutting through brick-red overbank deposits that characterize the upper Redbed member. (C) Repeated ~20-cm-thick sandstone beds that thin and fine upwards into overlying red siltstone overbank deposits. These may represent episodic crevasse splay events from a nearby channel. (D) Typical exposure of resistant purple cross-bedded sandstone channel body above recessive brick-red siltstone overbank deposits. Visible on the left of the panel is a typical rhythmic sequence of slightly more resistant and calcareous beds within an overall recessive red siltstone. Abbreviations: SS—sandstone; Cg—conglomerate.

that we were able to locate lie within the brick-red siltstone beds of the Redbed member (Plate 1).

Variegated member. We redefine the Variegated member of the Titus Canyon Formation from the description of Reynolds (1969) as a sequence of colorful siltstones, sandstones, conglomerates, and limestones containing three marker units, including a distinctive green sandstone and conglomerate referred to as the middle green sandstone, and two tuffs (units 8 and 38 of Reynolds, 1969; Plate 1). The Variegated member is no more than 500 m thick and comprises repeating sequences (10–20 m thick) of moderately resistant pale greenish- or yellowish-gray sandy conglomerate separated by 5–10-m-thick recessive packages of interbedded red calcareous siltstone and yellow limestone (Fig. 8A and Plate 1). The member outcrops as rounded hills that reflect differences in the erodibility of the conglomerate and siltstone intervals (Fig. 8A). The sandy conglomerate intervals (Fig. 8C) are typically matrix-supported, massive to cross-bedded, and contain 0.5–30-cm-diameter clasts of limestone, quartzite, and distinctive small black chert pebbles 0.5–3 cm in diameter. Conglomerates are separated by red calcareous siltstone intervals that contain common reduction halos (Fig. 8D) and 0.5–1.5-m-thick gray or red micritic limestones that in some places show thin bedding-parallel sparry laminae (Fig. 8E) and commonly weather to a distinctive pale yellow (Fig. 8E). The micritic limestone beds are mostly devoid of allochems with the exception of a few oncolite beds in Titanothere Canyon and near Indian Butte (Fig. 3); these beds contain abundant oncoids (Fig. 8G; Titanothere Canyon outcrop, 36.8298°N, 117.0128°W; Indian Butte outcrop, 36.7025°N, 116.8088°W). Limestone-rich intervals have been previously used as marker intervals in the Titus Canyon Formation, though their lateral continuity is not clear between different sections. The tracing of a single limestone bed over significant distances is made difficult by their relatively thin lenticular nature and the pervasive faulting in the area. As such, we cannot demonstrate the continuity of an "algal limestone" marker bed (Stock and Bode, 1935; Reynolds, 1969; Saylor, 1991) as a distinctive, traceable unit throughout the Titus Canyon Formation. Overall, the Variegated member does not display upsection changes in grain size and has a relatively consistent grain-size distribution. While the member is lithologically uniform through its entire thickness, with the exception of the Middle green sandstone marker unit, discussed below, sandy conglomerate intervals within the Variegated member do take on a redder oxide-stained appearance upsection (Plate 1).

Middle green sandstone. The rhythmic bedding of the Variegated member is interrupted near its middle, where a distinctive sequence of greenish sandstones and conglomerates form a 50–60-m-thick marker unit originally identified by Stock and Bode (1935) as the "middle sandstone and conglomerate." We dub this interval the middle green sandstone, a marker unit that can be found at most

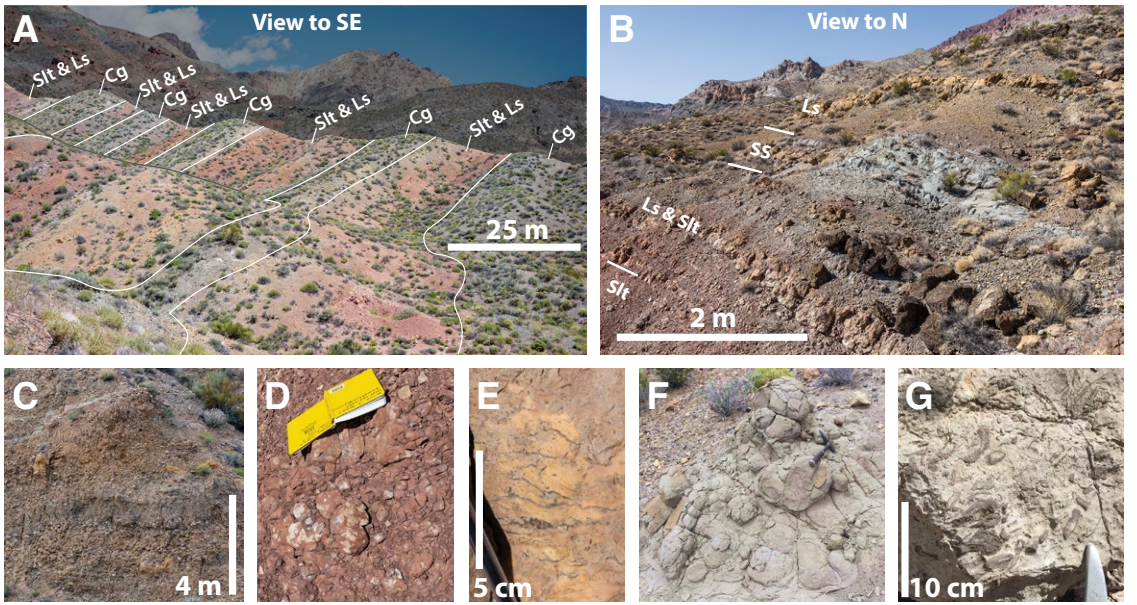

Figure 8. Field photos of the Variegated member of the Titus Canyon Formation. (A) View to the southeast from east of Leadfield (Fig. 3) showing characteristic hills and saddles held up by alternating packages of resistant yellowish-greenish gray conglomerate (C) and recessive mottled reddish siltstone with yellow limestone interbeds (D and E). (B) The Variegated member becomes more limestone rich upsection, with thicker reddish-yellow recessive intervals between conglomerate channel bodies. A sequence of limestones and sandstones is shown in this image from below the middle green sandstone marker bed (not in view) near Leadfield (Fig. 3). (C) Thick exposure of weakly bedded to massive yellowish-gray conglomerate typical of the lower half of the Variegated member. Clasts range from granule up to 20 cm diameter. (D) Characteristic texture found within recessive red siltstones in the Variegated member, including reduction halos and mottled to massive bedding. (E) Limestone from a recessive interval of the Variegated member showing yellowish weathering color (fresh rock is gray) and distinctive fabric of bedding-parallel sparry laminae. (F) Distinctive spheroidal weathering texture of the middle green sandstone marker unit. (G) Example of oncoids found in 1–2-m-thick limestone beds of the Variegated member. Image taken near Indian Butte (Fig. 3). Abbreviations: Ls—limestone; Slt—siltstone; Cg—conglomerate.

localities throughout the map area, and which exhibits somewhat variable lithology but always includes a massive, recessive bluish gray-green, well-sorted medium sandstone near its base; the sandstone weathers into distinctive spheroidal outcrops (Fig. 8F). Many exposures of this marker unit also include resistant greenish-gray, matrix-supported sandy conglomerate, and rarely recessive bluish green-gray mudstone and thin brown limestones. The conglomerates that accompany the middle green sandstone interval contain a similar clast composition to those in the rest of the Variegated member, but with a greener sandy matrix. The red siltstone intervals immediately above and below the middle green sandstone contain some of the most well-developed micrite limestone beds in the entire formation (Fig. 8B and Plate 1).

Marker tuffs. Within the Variegated member, we have mapped two additional marker beds previously identified by Reynolds (1969): the unit 8 tuff near the bottom of the member and the unit 38 tuff, which is near the top of the member. The unit 8 and unit 38 tuffs are tuffaceous sandstones with a slightly off-white color and fine powdery appearance. They appear rich in ash but in some places exhibit cross-bedding and a sandy composition that suggest they might be reworked, a possibility supported by the significant width of the Cenozoic age peaks in their detrital zircon spectra (Fig. 9).

Age Constraints from the Titus Canyon Formation

We report new geochronologic age information for the Titus Canyon Formation and develop an age model for the formation, based on a variety of geochronologic approaches, and we discuss this age model with respect to recognized paleontologic age constraints.

Maximum depositional age analysis from U-Pb detrital zircon geochronology. Of four Titus Canyon Formation samples from the vicinity of Titus and Titanothere canyons in the southern Grapevine Mountains (Fig. 3) that contained Cenozoic zircons, three came from the Variegated member, and a fourth came from the top of the Redbed member (Fig. 9 and Table 1). Samples from stratigraphically lower in the Redbed member contained primarily Mesozoic zircons (Fig. 9). Maximum depositional ages, based on MLA analysis (Fig. 5), and reported in stratigraphic order, are 36.0 ± 0.2 Ma from near the top of the Redbed member, and 33.4 ± 0.2 Ma, 31.5 ± 0.8 Ma, and 30.6 ± 0.3 Ma from the Variegated member (Figs. 2 and 9; Table 1). Miller et al. (2022) reported six detrital zircon MDA determinations for samples collected from the Titus Canyon Formation near Leadfield and Monarch Canyon (Fig. 3); from oldest to youngest, these are 36.3 Ma, 36.0 Ma, 34 Ma, 33.0 Ma, 32.3 Ma, and 23.7 Ma (Table 1, Fig. 9).

^{40}Ar/^{39}Ar geochronology. Of the six published and unpublished ^{40}Ar/^{39}Ar ages previously determined on tuffs in the southern Grapevine and northern Funeral Mountains (Saylor and Hodges, 1994; Snow and Lux, 1999; Murray, 2002; Gutenkunst, 2006), two ages are from strata that we have mapped as the Variegated member of the Titus Canyon Formation (Table 1). One is a sample most likely collected from the unit 38 tuff, which yielded a sanidine ^{40}Ar/^{39}Ar age of 30.4 ± 0.6 Ma (Saylor and Hodges, 1994) consistent with the zircon MDA that we determined for the same unit (30.6 ± 0.3 Ma). The second is a sample from near the base of the Variegated member which yielded a biotite ^{40}Ar/^{39}Ar age of 34.5 ± 0.4 Ma (Saylor and Hodges, 1994). This age is similar to the 33.4 ± 0.2 Ma MDA from the base of the Variegated member near Leadfield (Fig. 3).

Zircon (U-Th)/He geochronology. The zircon (U-Th)/He method can be used to determine eruptive ages of tuffs and other volcanic rocks (e.g., Niemi, 2012); however, due to the relatively low closure temperature of helium in zircon (~180 °C), this method is susceptible to resetting in cases where samples have been modestly buried or reheated. We measured four zircon (U-Th)/He ages on samples from the southern Grapevine Mountains (Fig. 4 and Table 1), three of which were collected from the Titus Canyon Formation in Titus Canyon (Fig. 3). Of these three samples, one from the unit 38 tuff near the top of the Variegated member yielded an age (28.9 ± 1.0 Ma) that overlapped within error with other radiometric age determinations for the unit 38 tuff. Two ages determined on the unit 8 tuff, near the base of the Variegated member, yielded ages younger than the stratigraphically higher unit 38 tuff, in one case by 15 m.y. We hypothesize that middle Miocene emplacement of at least six major ignimbrite sheets across the region (Plate 2; Niemi, 2012) may have variably reset underlying zircon (U-Th)/He ages in the Titus Canyon area by inducing hydrothermal circulation (e.g., Abbey et al., 2018). We therefore note when zircon (U-Th)/He ages agree with other geo- and thermochronometers, but we do not find that this method produces consistently reliable eruption ages in the Titus Canyon region.

Paleontologic constraints on the age of the Titus Canyon Formation. Paleontologic evidence has been used to assign ages ranging from Eocene to Oligocene to the Titus Canyon Formation (Stock and Bode, 1935; Stock, 1936; Lander, 2019), with more recent studies coalescing around agreement on a Duchesnean North American Land Mammal age (middle to late Eocene, 37–40 Ma; e.g., Mason, 1988). A recent reassessment of fossils from the Titus Canyon Formation resulted in the identification of nine new local faunas, eight of which are found in the southern Grapevine Mountains in Titus and Titanothere canyons, all of which are inferred to be late Duchesnean in age (Lander, 2019).

Depositional age of the Titus Canyon Formation. The age of the base of the Titus Canyon Formation remains unresolved, as does the age of the Basal breccia member. The age of the Redbed member is partially constrained by both paleontologic and geochronologic data. Geochronologically, the 36.0 ± 0.2 Ma MDA from a sandstone near the top of the Redbed member, and the 34.5 ± 0.4 Ma ^{40}Ar/^{39}Ar from the base of the Variegated member tightly bracket the age of the top of the Redbed member at ca. 35 Ma. This age places the ca. 34 Ma Eocene–Oligocene boundary and climate transition (e.g., Liu et al., 2009; Fan et al., 2018) at or just above the Redbed–Variegated member contact. A Duchesnean age for fossils in the Titus Canyon Formation is consistent with the geochronologic constraints, as all the fossil localities are found within the Redbed member below the stratigraphic level of the 36.0 ± 0.2 Ma MDA constraint. We find the correlation between the Titus Canyon local fauna and the Upper Porvenir local fauna that yields an age of ca. 37–38 Ma at the stratigraphic

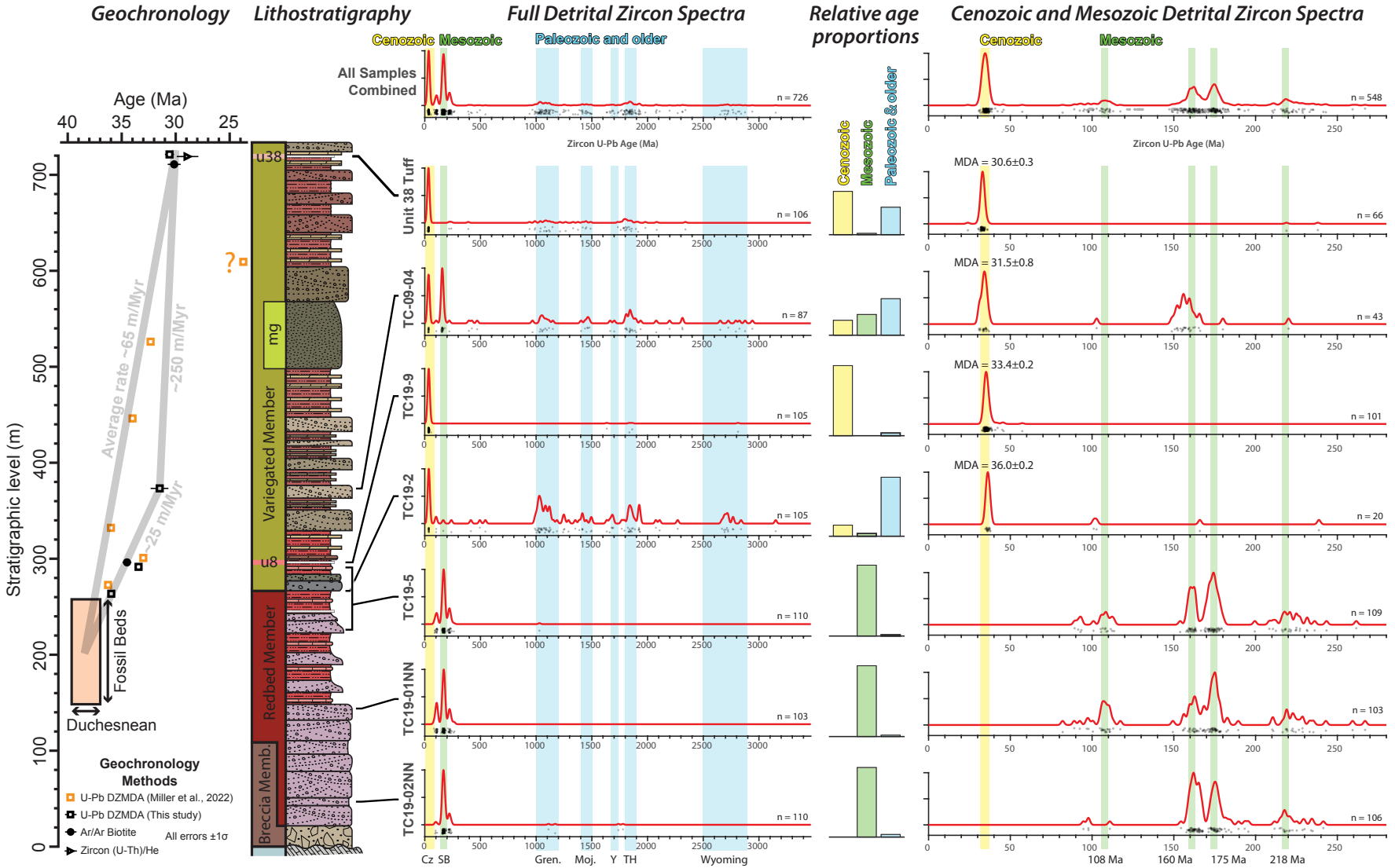

Figure 9. A plot of depositional age constraints versus stratigraphic level, a simplified lithostratigraphic column, and detrital zircon spectra for seven samples in the Titus Canyon Formation. Geochronology: Plot showing potential variation in deposition rates through time based on geochronology within the Titus Canyon Formation. Lithostratigraphy: Generalized stratigraphic column of the Titus Canyon Formation compiled from the measured sections shown in Plate 1. Leader lines indicate the approximate positions within the stratigraphy where samples were collected. Full Detrital Zircon Spectra: Each transparent dot represents a single zircon U-Pb age, and the red curves above the dots are kernel density estimates (made in MATLAB, bandwidth of 10 m.y.) for the distribution of zircon ages. Vertical bars indicate characteristic source peaks in the spectra. Relative age proportions: A bar graph showing the proportion of grains in a sample that are Cenozoic, Mesozoic, and Paleozoic and older. Each graph is normalized to the number of grains in the sample. Cenozoic and Mesozoic Detrital Zircon Spectra: Zoomed in spectra to highlight details in the distribution of 280 Ma and younger zircons (bandwidth of 1 m.y.). Maximum depositional age determinations are annotated onto the youngest Cenozoic grain cluster when present. Abbreviations: CZ—Cenozoic; SB—Sierra Nevada Batholith; Gren.—Grenville orogen; Moj.—Mojave basement; Y—Yavapai basement; TH—Trans Hudsonian orogen; Wyoming—Wyoming craton.

position of the fossil localities within the Titus Canyon Formation to be reasonable, given other existing age constraints. In the western West Fork and Upper East Fork sections (Fig. 3 and Plate 1), 100–200 m of strata of the Redbed member underlie the stratigraphic position of the fossil localities. No Cenozoic zircons were recovered from samples collected from these strata. Given the ages of the fossils in the Titus Canyon Formation, and an estimated rate of deposition for the Redbed member (Fig. 9), it would be surprising if the base of the Redbed member were older than middle Eocene. However, determining the age of the lower portions of the Redbed member may require approaches with limited reliance on absolute age dating, such as magnetostratigraphy, and the coarse conglomeratic nature of these deposits may prove challenging in that regard.

The age of the Variegated member is well constrained by our data and spans from ca. 35 Ma at the base of the member, as described above, to ca. 30 Ma at the top, as recorded by multiple age measurements on the unit 38 tuff near the top of this member (Plate 1). No more than a few meters of Variegated member strata overlie the unit 38 tuff at any measured section, suggesting that this age is representative of the preserved top of the Titus Canyon Formation. Overall, the six MDAs from Miller et al. (2022) agree with our age model, with the lone exception of their sample ELM18DVTC-7, which produced a 23.7 Ma MDA despite lying distinctly below the confidently dated ca. 30 Ma unit 38 tuff (Fig. 9 and Plate 1). We observed no obvious structural or depositional structure that could explain such an age discrepancy, and further investigation will be necessary to reconcile these two ages.

In summary, the Titus Canyon Formation is middle Eocene to early Oligocene in age, contains a fossil record of Duchesnean land mammals, and encompasses the Eocene–Oligocene boundary.

Provenance of the Titus Canyon Formation

In addition to their use in determining maximum depositional ages, detrital zircon U-Pb ages also provide information about provenance (e.g., Thomas, 2011). In samples from the Titus Canyon Formation, three distinct populations of zircon U-Pb ages are identifiable (Fig. 9). The oldest population of grains range from 3.1 Ga to 400 Ma, forming significant peaks at ca. 2.7 Ga, 1.9–1.8 Ga, 1.5–1.4 Ga, and 1.1–1.0 Ga (blue shaded peaks on Fig. 9). An intermediate age population forms a distinctive triple peak distribution of 105 Ma, 170 Ma, and 220 Ma (the prominent 170 Ma peak is shaded green on Fig. 9). The youngest zircon age population is Cenozoic and forms a cluster ranging from 40 Ma to 30 Ma (yellow shaded peak on Fig. 9). Broadly speaking, these three populations represent derivation from the Neoproterozoic and Paleozoic miogeocline (e.g., Gehrels et al., 1995), the Sierran arc (e.g., Lechler and Niemi, 2011), and Cenozoic volcanic centers of the Basin and Range (e.g., McQuarrie and Oskin, 2010).

The relative proportion of each of these three populations changes as a function of stratigraphic position in the Titus Canyon Formation (Fig. 9). The lowest three samples, all collected from the Redbed member, include almost entirely Mesozoic zircons, with no Cenozoic zircons and very few Paleozoic and Precambrian zircons. Samples from the Variegated member have a more variable detrital zircon age population distribution. Sierran zircons are the subordinate population in all samples from the Variegated member, while the major populations are characterized by either a Paleozoic and older miogeoclinal source or a Cenozoic volcanic source, presumably depending on whether the sample was dominated by fluvial erosion and transport or volcanic airfall deposition. The detrital zircon spectra of Miller et al. (2022) show a similar provenance pattern, with the upper half of the Titus Canyon Formation showing more Cenozoic volcanic zircons, fewer Mesozoic Sierran arc zircons, and more Paleozoic or older zircons than the lower half of the formation.

Rocks of Porter Mine

In the vicinity of the type section of the Titus Canyon Formation, near Leadfield (Fig. 3), the Variegated member of the Titus Canyon Formation is overlain in angular unconformity by distinctive green conglomerates of the middle Miocene Panuga Formation (Reynolds, 1969; Snow and Lux, 1999; Niemi, 2012). Both of these units can be traced southward along the eastern side of the Grapevine Mountains, where they remain juxtaposed across an unconformity. However, south of Daylight Pass (Fig. 3), which approximately separates the Grapevine Mountains from the Funeral Mountains, the two units continue to be distinguishable but are separated by an intervening package of strata that is not readily ascribed to either of these two units (Plate 2). Where exposures of this intervening sequence of strata have been previously mapped, they have been variably assigned to the Panuga Formation (or Green conglomerate facies) (Murray, 2002; Gutenkunst, 2006), the Titus Canyon Formation (Saylor, 1991; Gutenkunst, 2006) or referred to as Miocene Tuffaceous Sandstone and Volcanic Breccia (Wright and Troxel, 1993). We describe the lithostratigraphy and geochronologic age control on these strata below and demonstrate that these strata are lithologically and temporally distinct from the Titus Canyon Formation. We informally name these strata the Rocks of Porter Mine, for exposures south of Daylight Pass near Porter Mine (Fig. 3; 36.7741°N, 116.9129°W), and we discuss correlation of these strata with a succession of late Oligocene to early Miocene rocks that are regionally widespread in the Death Valley region and collectively termed the Ubehebe Formation (Snow and Lux, 1999; Fridrich and Thompson, 2011).

Lithostratigraphy

An intact section of the Rocks of Porter Mine previously mapped as Titus Canyon Formation (Saylor, 1991) is found in the Funeral Mountains, ~2 km southeast of Daylight Pass, ~1 km west of the abandoned Porter Mine (Fig. 3; Plate 2; 36.7741°N, 116.9129°W). These exposures can be traced southeastward to exposures near Indian Butte (Fig. 3 and Plate 2; 36.6941°N, 116.8011°W) that were previously mapped as either Titus Canyon Formation or Panuga Formation (Saylor, 1991; Gutenkunst, 2006).

The Rocks of Porter Mine consist of bluish-green and gray conglomerates with pebble- to cobble-sized clasts, coarse sandstones, and tuffaceous sandstones that fine upwards into yellowish-beige to white sandstones, brown resistant limestones, recessive pale mudstone, and thick airfall tuffs (Fig. 10). At the southeastern extent of the mapping area (Plate 2), the lowest part of the Rocks of Porter Mine consists of 1–4-m-thick greenish-gray sandy conglomerates interbedded with 1–4-m-thick beds of mudstone and coarse sandstones (Figs. 10D and 6G) that in some places take on a striking dark-green coloration. The unit fines upwards into less colorful beige, brown, and pale-yellow fissile shales, and 10-cm- to 1-m-thick fossiliferous limestones, some of which contain small gastropods (Figs. 10E and 10F). Fossil fish have also been reported from strata equivalent to those that we describe here (Nyborg et al., 2017).

Northwest of Daylight Pass in the Grapevine Mountains, exposures of the Rocks of Porter Mine are incomplete, with the best exposure being a fault-bounded wedge in upper Titanothere Canyon directly below Red Pass (Fig. 3; 36.8302°N, 117.0251°W). Here, sandstone, conglomerate, and mudstone beds (Fig. 10D) take on a light blue-green color, similar to the lowest part of the Indian Butte stratigraphy. Below Red Pass, the Rocks of Porter Mine also contain an undated, highly resistant welded tuff with pumice fragments (Figs. 10A, 10B, and 10C; 36.8299°N, 117.0259°W). Overall, the Rocks of Porter Mine thicken to the southeast, a trend opposite that of the underlying Titus Canyon Formation. The Rocks of Porter Mine also display a greater degree of lateral variability in thickness than the Titus Canyon Formation, possibly indicating deposition in small wedge-shaped basins bounded by syn-depositional normal faults (e.g., Fridrich and Thompson, 2011).

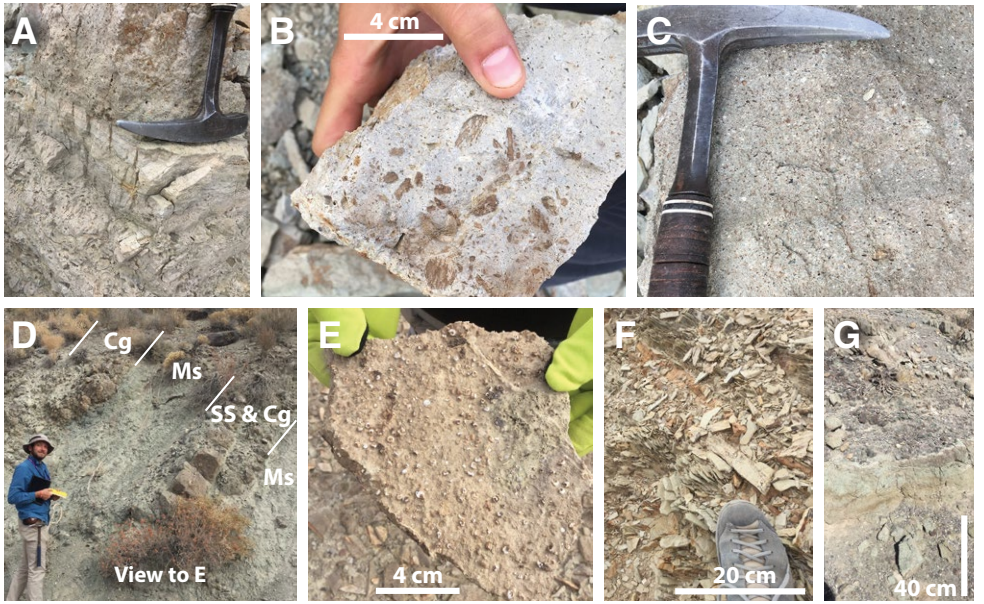

Figure 10. Field photos of the Rocks of Porter Mine. (A) Welded tuff exposed just east of Red Pass (Fig. 3) exhibiting flow banding. Photo taken at 36.8298°N, 117.0259°W. (B) Examples of brown pumice clasts from the tuff shown in A. (C) Close-up photo of greenish-gray lapilli and weak horizontal fabric in the tuff shown in A. D, E, F, and G: Various examples of the sedimentary structures and rock types associated with the Ubehebe Formation, including: (D) Resistant greenish to bluish-gray sandstones (SS) and pebbly conglomerates (Cg) interbedded with recessive pale-green mudstone (Ms). (E) 1–3-cm-thick tan-brown limestone bed showing small 3–5-mm-diameter gastropod fossils. (F) Fissile ~0.5-cm-thick laminae of tan to pale orange shale. (G) Thickly bedded massive turquoise, green, pale brown, and gray coarse sandstone and pebble conglomerate typical of Rocks of Porter Mine exposures in the study area.

Depositional Age of the Rocks of Porter Mine from $^{40}Ar/^{39}Ar$ Analyses

Based on our field observations and mapping, the Rocks of Porter Mine include several $^{40}Ar/^{39}Ar$ age analyses that were previously reported as age constraints for the Titus Canyon or Panuga Formations but which instead represent the depositional age of the Rocks of Porter Mine (Table 1). Gutenkunst (2006) analyzed three $^{40}Ar/^{39}Ar$ ages from a measured section through the Rocks of Porter Mine near Indian Butte (Fig. 3 and Plate 2); we recalculated these ages to be 28.2 ± 0.2 Ma, 23.6 ± 0.1 Ma, and 19.3 ± 0.5 Ma (Fig. 4 and Table 1). A single sample from an exposure of the Rocks of Porter Mine near Chloride Cliff road (Fig. 3) produced a zircon (U-Th)/He age of 24.4 ± 2.1 Ma, which is consistent with ages from Gutenkunst (2006), but is subject to the caveats regarding potential resetting of zircon (U-Th)/He ages described in the Methods section (Table 1). In summary, recalculated $^{40}Ar/^{39}Ar$ ages from tuffs that we map as within the Rocks of Porter Mine span the interval 28.2 ± 0.2 Ma to 19.3 ± 0.5 Ma, indicating that these strata are approximately late Oligocene to early middle Miocene in age.

Regional Correlation of the Rocks of Porter Mine

The late Oligocene to early middle Miocene depositional age range for the Rocks of Porter Mine is consistent with the depositional age range of other packages of strata previously correlated with the regionally widespread Ubehebe Formation. These include strata at Bat Mountain, at the southernmost end of the Funeral Mountains (25–20 Ma; Fridrich and Thompson, 2011; Fridrich et al., 2012) and in the Cottonwood Mountains (24–19 Ma; Snow and Lux,

1999). In addition to a similar age of deposition, the Rocks of Porter Mine share the fining-upward stratigraphy and volcanic-rich nature of other known exposures of the Ubehebe Formation, traits that differentiate this formation from the Titus Canyon Formation. Based on the depositional age determinations for the Rocks of Porter Mine, their distinct lithology, and similarities to other strata ascribed to the Ubehebe Formation, we tentatively correlate the Rocks of Porter Mine with the Ubehebe Formation of Snow and Lux (1999), pending identification and description of a type-section for this unit and targeted sampling for more comprehensive geochronologic constraints on the depositional age range of this unit.

TECTONO-STRATIGRAPHY AND FORMATION OF THE TITUS CANYON FORMATION

The Titus Canyon Formation records deposition from the Duchesnean (37–40 Ma) to the early Oligocene (30 Ma) (Fig. 9). Our differentiation of the Titus Canyon Formation from the Rocks of Porter Mine affords us an opportunity to revisit the evolution of the Titus Canyon basin and argue that its extent is limited to exposures in the northern Funeral and southern Grapevine Mountains. Depositional patterns in continental extensional basins are primarily controlled by the structural production of accommodation space and the climatically modulated supply of sediment (Carroll and Bohacs, 1999; Gawthorpe and Leeder, 2000), with a balance between basins that overfilled with sediment and host throughgoing drainages (i.e., exorheic), or underfilled and hydrologically closed (i.e., endorheic). The relative proportion of fluvial to lacustrine strata in a basin can serve as a proxy for overfilled and underfilled conditions, respectively (e.g., Geurts et al., 2020), and provides a useful framework for dividing the depositional history of the Titus Canyon basin into two phases. The following interpretations build on extensive previous sedimentologic and stratigraphic work in this region (Stock and Bode, 1935; Reynolds, 1969; Saylor, 1991; Murray, 2002; Gutenkunst, 2006; Ridgway et al., 2011; Niemi, 2012; Miller et al., 2022). Our goal is to summarize and correlate these works and place their observations within a common tectonostratigraphic and geochronologic framework, as many of the previous studies were conducted in small, disconnected study areas without robust geochronology.

Extensional Basin Initiation and Fluvial Phase (Redbed Member)

The Titus Canyon basin initiated as an incipient extensional basin no later than 37 Ma, and early deposition of the Basal breccia and Redbed members continued until ca. 35 Ma. The overall fining-upwards stratigraphy of the Basal breccia and Redbed members of the Titus Canyon Formation records a progression from proximal rock avalanche breccias and coarse fanglomerate deposits to distal overbank deposits and conglomeratic channel bodies (Reynolds, 1969; Murray, 2002; Gutenkunst, 2006; Ridgway et al., 2011). This progression is recognized in other early extensional basin sequences and arises from coarse scarp-derived deposits eventually yielding to a basin-floor fluvial system as the basin area expands (Gawthorpe and Leeder, 2000). The dominance of fluvial over lacustrine deposition during this early phase of basin formation implies an overfilled basin condition, and thus an exorheic hydrology with throughgoing drainages. Estimates of depositional rates of ~25 m/m.y., as derived from the geochronology and biostratigraphy of the Redbed member (Fig. 9) indicate a slower depositional rate than in the upper Titus Canyon Formation and a slower rate than observed in typical extensional basins (50–200 m/m.y.; Allen and Allen, 2013). Combined with the overfilled state of the basin, this implies a relatively slow tectonic subsidence rate during this period.

Provenance information from the Redbed member of the Titus Canyon Formation also sheds light on regional drainage geometries and extent at the time of Titus Canyon basin formation. Detrital zircon U-Pb provenance analysis of the Redbed member reveals consistent detrital zircon spectra throughout the unit, dominated by Mesozoic ages, with significant age peaks in the middle Jurassic (ca. 165 and 175 Ma), a broad peak of late Triassic ages, and subordinate Late Cretaceous ages (Fig. 9). These three age peaks are consistent with recognized pulses of Sierran arc magmatism (e.g., Ducea, 2001; Coleman et al., 2003; Cecil et al., 2019); however, a specific source for the observed age spectra in the Redbed member is challenging to pinpoint. The subordinate nature of the Late Cretaceous ages argues against derivation from the present-day eastern Sierra Nevada, where exposures of Late Cretaceous plutons are extensive (Chen and Moore, 1982; Coleman and Glazner, 1998).

The Titus Canyon basin was located just east of the boundary between primarily Mesozoic arc-related rocks of the Sierra Nevada to the west and Neoproterozoic through Paleozoic sedimentary strata of the Cordilleran miogeocline to the east (e.g., Jennings et al., 1977). Several ranges in the westernmost Basin and Range, including the White, Inyo, and Cottonwood mountains, expose minor Late Cretaceous and Triassic intrusive bodies and host large Jurassic batholiths, with ages that overlap the detrital zircon ages observed in the Redbed member (Chen and Moore, 1982; Snow et al., 1991; Niemi et al., 2001; Coleman et al., 2003), making them a viable source terrane for the early Titus Canyon Formation.

Conglomerate clast compositions in the Redbed member of the Titus Canyon Formation further support derivation from a westerly source (Reynolds, 1969). Although lower Paleozoic carbonate and siliciclastic strata are exposed in most of the ranges that surround Death Valley, the identification of case-hardened carbonate clasts as being derived from Pennsylvanian-aged limestone, and the identification of Permian fusulinid-bearing limestones (Reynolds, 1969), limit the source for the Redbed member conglomerate clasts to sources on the western side of modern-day Death Valley (McAllister, 1952; Niemi et al., 2001). Clasts of quartz monzonite of inferred Jurassic age, and porphyritic granite clasts, are also observed within the Redbed member. The Cottonwood Mountains, on the northwestern side of Death Valley, are a compelling source terrane for the combination of Paleozoic miogeoclinal clasts, Jurassic-aged monzonite clasts,

and upper Paleozoic fusulinid-bearing limestones (Snow and Lux, 1999; Niemi et al., 2001), as well as the Jurassic and Triassic detrital zircon spectra. Further geochronologic analysis of individual clasts is needed to link specific clasts to unique source terranes. However, despite uncertainty in the exact provenance of the Redbed member of the Titus Canyon Formation, the basin was receiving sediment from a catchment that encompassed rocks not exposed in the local bedrock of the Grapevine and Funeral mountains, and which was almost certainly derived from the west, an inference also supported by paleocurrent and sedimentary structure observations (Stock and Bode, 1935; Reynolds, 1969; Gutenkunst, 2006).

Acceleration of Extension and Fluvial-Lacustrine Phase (Variegated Member)

The Variegated member records a shift in lithologic character, provenance, and fossil content of the Titus Canyon basin. Within the Variegated, conglomeratic channel bodies and silty overbank deposits rhythmically alternate with 0.5–1.5-m-thick lacustrine micrite beds, contrasting with the coarse, proximal deposition recorded by the Redbed member (Reynolds, 1969; Murray, 2002; Gutenkunst, 2006; Ridgway et al., 2011). The appearance of lacustrine conditions above the Redbed–Variegated member contact implies a transition from entirely exorheic (fluvial) to sometimes under-filled lacustrine conditions that could have been tectonically or climactically modulated. However, the similar timing of the Redbed to Variegated member transition (approx. 36–34 Ma) to the Eocene–Oligocene climate transition (ca. 34 Ma), during which northern latitudes cooled ~5–7 °C, may support a strong climatic influence during this time (Liu et al., 2009; Fan et al., 2018). Potential climatic influence on the Titus Canyon basin is not addressed in this manuscript, but it remains an important area for future investigation.

Sediment accumulation rates and provenance data from the Variegated member, however, suggest an increase in tectonic activity within the Titus Canyon basin. Deposition rates for the Variegated member are as high as ~250 m/m.y., distinctly faster than the ~25 m/m.y. sediment accumulation rate within the Redbed member, and fast compared to compiled extensional basin rates of 50–200 m/m.y. (Fig. 9; Allen and Allen, 2013). Geologic evidence for increased rates of local tectonism as a cause for increased sediment accumulation rates are preserved within the Variegated member, which both coarsens and thickens into the Fall Canyon fault in the upper West Fork of Titus Canyon (Plate 2).

The increase in sediment accumulation rate in the Variegated member is accompanied by a shift in basin provenance signature. Detrital zircon spectra from the Variegated member record Cenozoic zircon grains, suggesting an increase in volcanic input to the basin, likely from the onset of Oligocene ignimbrite eruptions in northern and central Nevada (Coney, 1978; Best et al., 2013; Miller et al., 2022), although such a signature is not diagnostic of fluvial basin geometry or extent. More pronounced is the shift in provenance from a dominantly Mesozoic Sierran arc signature to a broad age spectrum, similar to the detrital zircon spectra of Paleozoic and Neoproterozoic miogeoclinal rocks. Three of the four detrital samples from the Variegated member yield no evidence of derivation from a Mesozoic arc source (Fig. 9), and in the one Variegated sample where Mesozoic ages are present, they are Late Jurassic to Early Cretaceous, markedly different from the mid-Jurassic and Triassic ages found in the Redbed member (Fig. 9). The greater variability in detrital zircon spectra observed within the Variegated member also reflects a departure from the Redbed member, which exhibits consistent detrital zircon signatures.

Provenance of the Variegated Member

The provenance changes we observe in the detrital zircon age spectra between the Redbed and Variegated members match previous observations of changes in clast composition in the Titus Canyon Formation (Reynolds, 1969; Murray, 2002; Miller et al., 2022). The Variegated member does not contain clasts of upper Paleozoic (Permian and Pennsylvanian) carbonates, and granitoid clasts are less common than in the Redbed member (Reynolds, 1969). Within the Variegated member, Miller et al. (2022) identify several distinctive clast compositions that together suggest an origin from the Roberts Mountain and Golconda allochthons in northern Nevada. Miller et al. (2022) link red radiolarian chert pebbles and cobbles to the Upper Paleozoic Havallah sequence in the Golconda allochthon and cobbles of black chert with pale phosphatic nodules to Devonian deep-water strata of the Roberts Mountain allochthon. Miller et al. also identify cobbles of conglomerate which themselves contain clasts of mafic volcanics, radiolarian chert, and orthoquartzite that suggest derivation from conglomerates of the Antler basin of northern and central Nevada.

While the clast assemblage identified by Miller et al. (2022) points to a provenance from northern Nevada, a significant portion of Titus Canyon sediment must be derived from more local exposures of the Neoproterozoic and Paleozoic Cordilleran Miogeocline. Highly polished and well-rounded clasts within the Titus Canyon Formation comprise distinctive formations derived from the miogeocline, including the Stirling Quartzite, Wood Canyon Formation, Zabriskie Quartzite, and Eureka Quartzite (Reynolds, 1969; Niemi, 2002). The distribution of Paleozoic quartzites across the western U.S. makes these clasts of limited utility for ascribing provenance; however, the distribution of Neoproterozoic quartzites is limited to the western portion of the central Basin and Range (Stewart, 1970). In addition to highly polished and rounded pebbles and cobbles of quartzite and chert, the Redbed member also contains angular boulders of carbonate megabreccia (1–>10 m) that are derived from paleotopographic highs composed of local bedrock (predominantly the Paleozoic Bonanza King Formation), within the Titus Canyon Basin (Reynolds, 1969).

The well-rounded nature of the conglomerate clasts within the Variegated member, especially highly polished chert and quartzite clasts, along with the observation of clasts that are distally sourced from the Golconda and Roberts Mountain allochthons, have been used to argue that the Titus Canyon Formation represents a remnant of

a larger fluvial system that transported sediment from sources in northern Nevada to the then coastal Mojave region (Miller et al. 2022). However, mature, polished, and well-rounded sedimentary clasts (especially quartzite and chert) can arise from multiple episodes of sedimentary recycling, as opposed to a singular episode of significant fluvial transport (e.g., Blatt, 1967; Horton and Schmitt, 1998). The observation that components of the Roberts Mountains/Golconda allochthon assemblage are themselves found in clasts of conglomerate within the Variegated member (Miller et al., 2022) provides further evidence of at least one generation of sedimentary recycling of the clast assemblage within the Titus Canyon Formation.

A potential source for recycled clasts is conglomerate of the Mississippian Eleana Formation, which is exposed immediately to the east of Titus Canyon at Bare Mountain and the Nevada Test Site (Fig. 1) and contains clasts of radiolarian chert, phosphatic chert, and mafic volcanics that are inferred to have been derived from erosion of the northern Antler foredeep during the Antler Orogeny (Trexler and Cashman, 1997). The Eleana Formation was deposited as a submarine fan in the southern Antler Basin foredeep (Poole and Sandberg, 1977) and contains quartzites associated with both allochthonous sources from northern Nevada and local (miogeoclinal) sources (Trexler and Cashman, 1997). Resistant clasts (cherts, quartzites, and litharenites) within the Eleana are well-rounded and polished (Trexler and Cashman, 1997). The Eleana Formation has been identified as a source of mafic volcanic and radiolarian chert clasts in other early Tertiary basins in the central Basin and Range (e.g., Goldstrand, 1992). As such, recycling of sediment from the Antler foredeep basin should be considered a possible proximal source for Titus Canyon Formation clasts that originated in the Roberts Mountains and Golconda allochthons (Miller et al., 2022).

Paleogeographic Implications of the Variegated Member

The provenance of the Titus Canyon Formation has the potential to test hypotheses of the paleotopography and drainage network integration and reorganization of the Cordillera during the Eocene to Oligocene transition from contraction to extension, a topic of considerable debate (cf. Colgan and Henry, 2009; Henry and John, 2013; Snell et al., 2014; Smith et al., 2017; Cassel et al., 2018; Long, 2018; Best et al., 2016; Lund Snee and Miller, 2022; Miller et al., 2022). However, evidence of sedimentary recycling within the clast population of the Variegated member of the Titus Canyon Formation, and the possibility of a local source for the well-rounded and polished clasts of Roberts Mountains, Golconda, and miogeoclinal affinity contradict a straightforward interpretation of the provenance of the Titus Canyon Formation (e.g., Miller et al., 2022), and thus its implications for the paleogeography of the proto-Basin and Range.

The most compelling compositional change observed between the Redbed and Variegated members is the up-section loss of Sierran-affinity granitic clasts and miogeoclinal Permian and Pennsylvanian clasts. Together, these changes broadly suggest a shift from a westerly to a northerly sediment source, a shift also observed in our detrital zircon provenance data. The Late Jurassic to Early Cretaceous ages of detrital zircons in the Variegated member, which are ages not well represented among plutons of the Sierran arc, along with the lack of Late Triassic, Middle Jurassic, and Late Cretaceous zircon ages suggest that the source area of the Variegated member cannot contain significant exposure of the most common plutonic ages of the Sierran arc (e.g., Ducea, 2001; Cecil et al., 2019). The Sylvania and Palmetto mountains, which lie ~50 km north of present-day exposures of the Titus Canyon basin, are underlain by Late Jurassic plutons that are intruded by small plutonic bodies of Late Cretaceous age. These plutonic ages are consistent with the detrital zircon spectra in the Variegated member, although geochronologic age constraints on the crystallization ages of these plutons (as opposed to cooling ages) are sparse (e.g., Maldonado et al., 1988). We note that palinspastic reconstructions of the central Basin and Range place present-day exposures of the Eleana Formation (i.e., at Bare Mountain and in the Eleana Range) to the north of the Titus Canyon Basin in Eocene time (Snow and Wernicke, 2000; Cashman and Sturmer, 2021). Together, these observations delineate a proximal region to the north of the Titus Canyon Basin that would have been a viable source for the clast population and detrital zircon spectra observed in the Variegated member.

In summary, the Titus Canyon basin initiated as an extensional basin in the late Eocene on the eastern slope of the paleo–Sierra Nevada arc. Tectonic subsidence was limited in magnitude, as evidenced by the relatively small (~1 km, Plate 1) maximum thickness of the formation. Minimal subsidence would allow the basin to remain overfilled for most of its depositional history, although it does appear to have experienced transitions from endorheic to exorheic conditions in response to tectonic or climatic forcing, as is observed in other rift systems (e.g., the Rio Grande and East African rifts; Repasch et al., 2017; Berry et al., 2019). The consistency of the detrital zircon spectra and clast composition throughout the Redbed member suggest minimal drainage reorganization or evolution during this time. The Variegated member of the Titus Canyon basin records major changes in the Titus Canyon basin, including significantly increased sediment accumulation rates and a transition to a fluvial-lacustrine sedimentary environment, as well as a transition to a more northerly provenance source. Our interpretation of the basin as extensionally controlled is compatible with the basin being an intermediate sediment sink along a longer sediment transport path (e.g., Miller et al., 2022); however, as discussed above, it is not clear that available provenance data require distal sedimentary sources.

Extent of the Titus Canyon Basin and Regional Correlations of the Titus Canyon Formation

As one of the earliest recognized pre–Basin and Range extensional units in the Death Valley region (e.g., Stock and Bode, 1935; Reynolds, 1969), the Titus Canyon Formation has been tenuously correlated with multiple poorly dated units in the central Basin and Range. A number of presumed Paleogene rock exposures in and around the Death

Valley region, including the Horse Spring Formation, the unnamed conglomerate of the Fallout and Jumbled Hills, the Rocks of Winapi Wash, and the unnamed conglomerate of Gravel Canyon, among others, have been correlated with the Titus Canyon Formation on the basis of broad lithologic similarity and similar stratigraphic position above the sub-Tertiary unconformity (Niemi, 2002, and references therein). However, these deposits have neither biostratigraphic nor absolute age control that substantiates a temporal correlation with the Titus Canyon Formation. Moreover, such lithostratigraphy-based correlations were largely proposed prior to the recognition of the complex early Cenozoic depositional history of the Death Valley region that has been delineated in the past decades (e.g., Çemen et al., 1999; Snow and Lux, 1999; Fridrich and Thompson, 2011), and that we further refine here. Descriptions of these units, gleaned primarily from stratigraphic descriptions on published geologic maps, generally bear greater similarity to the Rocks of Porter Mine (Ubehebe Formation) as defined and described here than to the Titus Canyon Formation. Frequent descriptions of fossiliferous limestones and well-developed tuff beds are particularly more diagnostic of Ubehebe-equivalent strata than of Titus Canyon. Thus, our inference is that the Titus Canyon basin was of limited spatial extent and is preserved almost exclusively within the southern Grapevine and northern Funeral Mountains, while the Ubehebe Formation may have a much broader spatial distribution across the central Basin and Range.

STRUCTURE OF THE TITUS CANYON BASIN

The Titus Canyon basin has been described as having an extensional or transtensional origin based on observations of basin-scale sedimentological architecture and facies analysis (e.g., Saylor, 1991; Gutenkunst, 2006; Fridrich and Thompson, 2011). However, a coherent structural framework for the Titus Canyon basin has not previously been defined, in part due to myriad geologic maps that partially encompass the extent of the Titus Canyon Formation (e.g., Cornwall and Kleinhampl, 1964; Reynolds, 1969; Saylor, 1991; Wright and Troxel, 1993; Niemi, 2012). In mapping the extent of the Titus Canyon Formation and synthesizing the structures that bound the formation, we find that the Titus Canyon Formation in the Grapevine Mountains is everywhere confined to the hanging wall of a complex fault system, the Fall Canyon–Titus Canyon fault system (Plate 2).

Fall Canyon Fault

The Fall Canyon fault is a steeply east-dipping normal fault that extends northward from Titus Canyon, parallel to the range crest of the Grapevine Mountains (Plate 2). The Fall Canyon fault juxtaposes upright Paleozoic strata in the upper limb of a large west-vergent fold in its footwall (the Titus Canyon anticline–Corkscrew Peak syncline, or TCA-CPS) against Cenozoic strata, including the Titus Canyon Formation and younger strata, in its hanging wall (Figs. 11 and 12). Although the lower members of the Titus Canyon Formation are not exposed along the Fall Canyon fault, in the west fork of Titus Canyon (Fig. 3), conglomeratic intervals within the Variegated member both thicken and coarsen westward toward the Fall Canyon fault. No single conglomerate is thicker than ~40 m in our measured sections, but these conglomerates merge into a single, >100-m-thick package toward the Fall Canyon fault. The thickening and coarsening of the conglomerates may represent sedimentological variability within the basin (e.g., of alluvial fans), but we interpret them as growth strata associated with the Fall Canyon fault, which would suggest that the Fall Canyon fault may have been an Eocene–Oligocene basin bounding fault to the Titus Canyon basin. The extensional nature of the basin is also evidenced by the unconformable nature of the contact between the Titus Canyon Formation and overlying strata, along with the wedge-shaped map-view pattern of Titus Canyon Formation exposures, both of which would be expected with deposition into asymmetric fault-bounded half grabens (Gawthorpe and Leeder, 2000). These observations lead us to agree with previous interpretations of the Titus Canyon basin as an extensionally subsiding, asymmetric, and west-deepening basin (Saylor, 1991; Niemi, 2002; Gutenkunst, 2006; Fridrich and Thompson, 2011). Our extensional interpretation contrasts with other interpretations of the Titus Canyon basin as a tectonically quiescent, low-relief alluvial floodplain (Miller et al., 2022).

Titus Canyon Fault

Where the trace of the Fall Canyon fault is exposed in Titus Canyon east of Leadfield (Fig. 3), it merges with the Titus Canyon fault, an enigmatic, nearly horizontal fault. The excellent exposure in Titus Canyon shows the Fall Canyon fault and Titus Canyon fault merging rather than crosscutting (Fridrich and Thompson, 2011). Additionally, the significant offset associated with the Fall Canyon fault does not continue into the footwall rocks of the Titus Canyon fault. The flat attitude of the Titus Canyon fault, and its exposure across the top of the southern Grapevine Mountains, originally led to the interpretation of this structure as a Mesozoic thrust fault (Reynolds, 1969). The recognition that this fault everywhere carries the depositional base of the Titus Canyon Formation, and that this fault is contiguous with the Fall Canyon fault, underscores the nature of this structure as a low-angle Eocene detachment fault. The Titus Canyon fault places upright lower Paleozoic strata and overlying Titus Canyon Formation in its hanging wall on upper Neoproterozoic and lower Paleozoic strata of the overturned limb of the TCA-CPS (Fig. 12; Reynolds, 1969; Fall Canyon fault zone of Lutz et al., 2021). The Titus Canyon fault has multiple structural levels that appear to localize along relatively weak shale intervals within the Cambrian Carrara Formation and Neoproterozoic Wood Canyon Formation (Plate 2). The lower Paleozoic and upper Neoproterozoic strata are significantly structurally thinned (< 1 km thick) and form the floor of the Titus Canyon basin, on which the Basal breccia member of the Titus Canyon Formation was deposited. A top-to-the-southeast sense of displacement on the Titus Canyon fault is inferred from both its

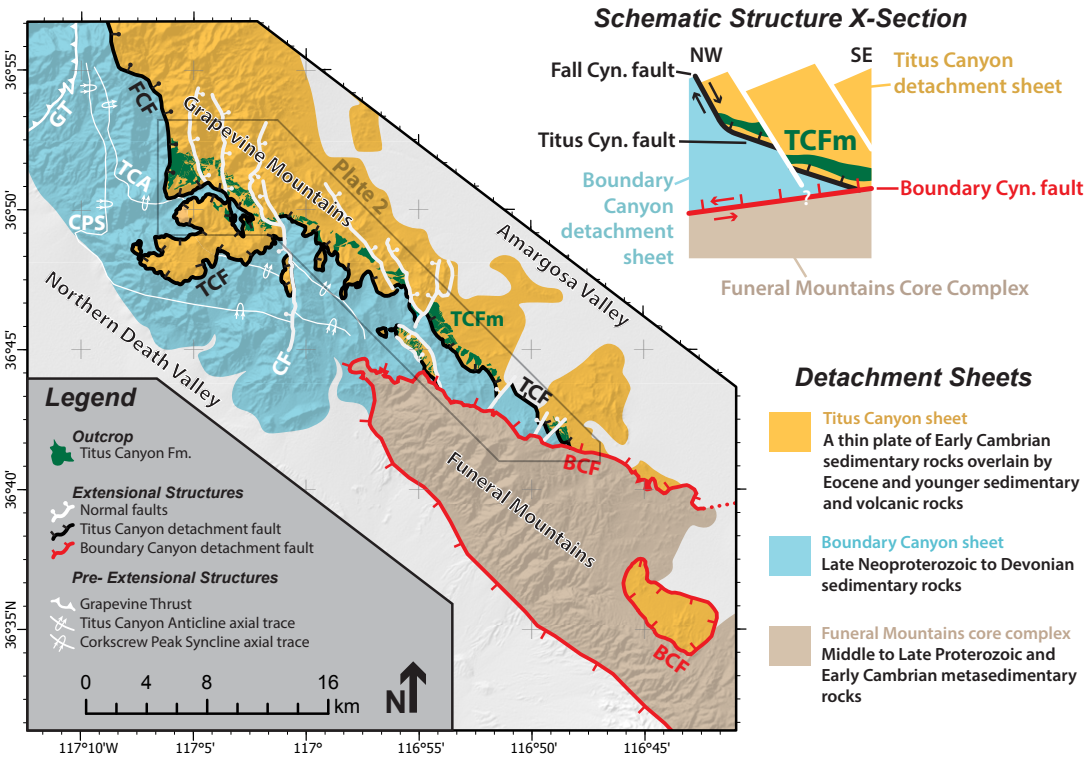

Figure 11. Simplified tectonic map of the major contractile structures, detachment faults, and detachment sheets in the southern Grapevine and northern Funeral Mountains. Features compiled from this study (Plate 2 map extent shown on figure), Reynolds (1969), Niemi (2012), Wright and Troxel (1993), and Cornwall and Kleinhampl (1964). Note that teeth are drawn on the hanging walls of all faults, and the relative dips of the structures shown in the schematic structure cross section differ from their true orientations. Abbreviations: BCF—Boundary Canyon fault; CF—Corkscrew fault; CPS—Corkscrew Peak syncline; FCF—Fall Canyon fault; GT—Grapevine thrust; TCA—Titus Canyon anticline; TCF—Titus Canyon fault; TCFm—Titus Canyon Formation.

continuity with the east-dipping Fall Canyon fault and a likely northwesterly source for the upright Paleozoic strata carried in the Titus Canyon fault hanging wall (Niemi, 2012).

Boundary Canyon Detachment

To the south, in the vicinity of Daylight Pass, all structures in the Grapevine Mountains (including the Titus Canyon fault and Titus Canyon anticline–Corkscrew Peak syncline) are truncated at the Boundary Canyon detachment (Fig. 11 and Plate 2), a top-to-the-northwest low-angle detachment fault that bounds the Funeral Mountains metamorphic core complex (Holm and Dokka, 1991; Hoisch and Simpson, 1993; Beyene, 2011; Fridrich and Thompson, 2011; Lutz et al., 2021). The Boundary Canyon detachment separates amphibolite-grade Neoproterozoic sedimentary rocks in its footwall from zeolite-grade strata in its hanging wall (Hoisch and Simpson, 1993; Wright and Troxel, 1993; Mattinson et al., 2007; Verdel et al., 2011; Hoisch et al., 2014; Affinati et al., 2020). The metamorphic history of the footwall rocks exhumed by the Boundary Canyon detachment is complex (Hoisch and Simpson, 1993; Applegate and Hodges, 1995; Mattinson et al., 2007; Wells and Hoisch, 2008; Affinati et al., 2020), but the timing of metamorphic core complex development is well constrained to the middle to late Miocene by a variety of low-temperature thermochronometric studies (e.g., Holm and Dokka, 1991; Lutz et al., 2021).

Where the Boundary Canyon detachment truncates the Titus Canyon fault along the eastern margin of the northern Funeral Mountains (near Indian Butte, Fig. 3), exposures of the Titus Canyon Formation are incomplete and primarily consist of the Variegated member of the Titus Canyon Formation (Plate 2). Near the Boundary Canyon detachment, the base of the Titus Canyon Formation is commonly faulted and juxtaposed against upper Neoproterozoic siliciclastic strata in the footwall of the detachment, recording disarticulation of the Titus Canyon Formation and associated Eocene structures during Miocene displacement on the Boundary Canyon detachment (Plate 2; Wright and Troxel, 1993; Gutenkunst, 2006).

Evidence for Miocene reactivation of the Eocene–Oligocene structures that bound the Titus Canyon basin is equivocal. Thick sequences of middle Miocene strata and ignimbrites from the Southwest Nevada volcanic field are exposed to the east of the Fall Canyon fault but are conspicuously absent to

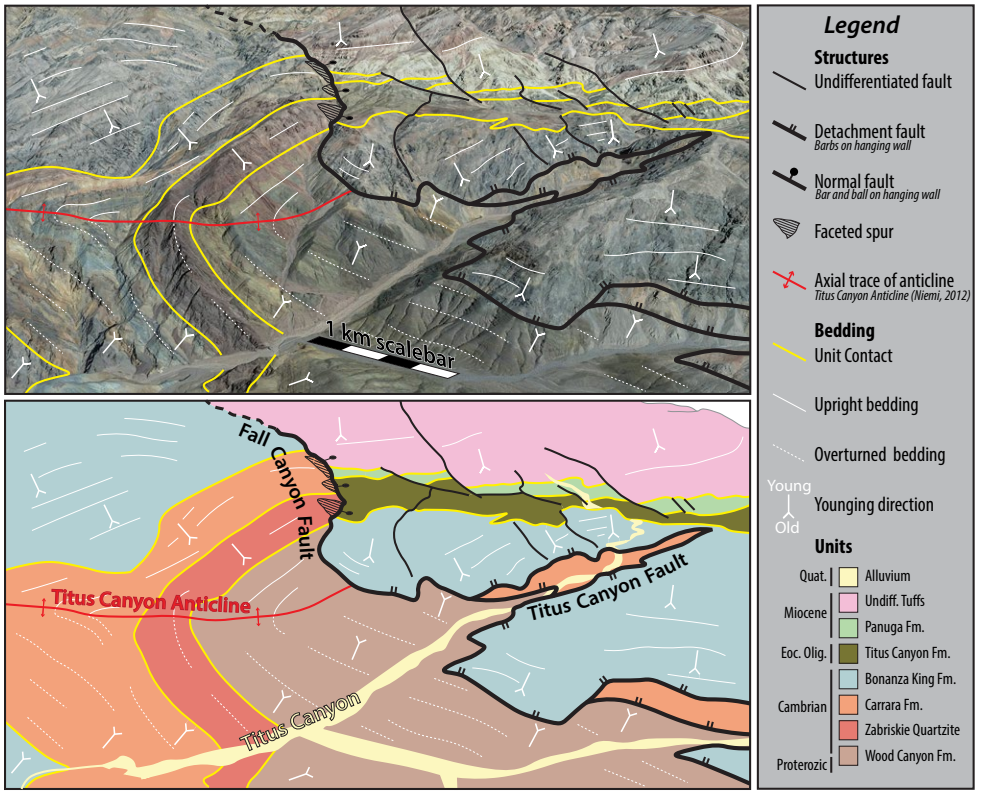

Figure 12. Annotated oblique view of the upper reaches of Titus Canyon (Fig. 3) showing key structural relationships between the Titus Canyon anticline, Titus Canyon fault, Fall Canyon fault, and variably upright and overturned strata. View is toward the north and centered on 36.8404°N, 117.1006°W (location marked on Fig. 3). Several key relationships are visible: (1) The Titus Canyon fault smoothly steepens and links into the Fall Canyon fault. (2) The Titus Canyon fault emplaces upright strata of the Bonanza King Formation onto overturned strata in the limb of the Titus Canyon anticline. (3) The Titus Canyon fault cuts across the axial trace of the Titus Canyon anticline, and neither the strata in the hanging wall of the Titus Canyon fault, nor the fault itself, participate in the folding of the Titus Canyon anticline. Note that the axial plane of the west-vergent Titus Canyon anticline is subhorizontal, and thus the axial trace of the fold can appear to trend east-west where it intersects with the steep topography of Titus Canyon. Imagery is © 2021 Google Earth and Maxar Technologies.

the west of this structure, throughout the western central Basin and Range (Niemi, 2012). Despite the thickness of these Miocene volcanic and sedimentary units, there is no clear evidence of thickening or growth fault relationships between them and the Fall Canyon fault. Moreover, we observed no unambiguous exposures that would clarify the nature of the contact between the Miocene units and the Fall Canyon fault as being structural rather than, for example, a depositional contact along a buttress unconformity. Given a lack of conclusive evidence for post-Oligocene activity on the Fall Canyon and Titus Canyon fault, we infer that the relationship observed between the Miocene ignimbrites and the Fall Canyon fault represents a buttress unconformity, but we acknowledge the challenge of preserving Oligocene structural relief into the middle Miocene.

Implications of Titus Canyon Basin Structures for Regional Palinspastic Reconstructions of Basin and Range Extension

Palinspastic restorations are key to understanding the magnitude and mechanisms of large-scale intracontinental extension (e.g., Wernicke et al., 1988; Snow and Wernicke, 2000; McQuarrie and Wernicke, 2005), and they form the basis for geodynamic models constructed to understand the internal and external forces that drive lithospheric deformation (e.g., Bahadori and Holt, 2019). In the central Basin and Range, geologic markers that constrain such reconstructions fall into two broad categories: (1) late Paleozoic to Mesozoic contractional structures formed during convergence on the North American plate boundary (e.g., Burchfiel and Davis, 1975; Giallorenzo et al., 2018), and proximal sedimentary deposits of late Cenozoic age that have been tectonically dismembered by extension (e.g., Salyards and Shoemaker, 1987; Topping, 1993; Niemi et al., 2001). The structural markers are commonly used to define the magnitude of Basin and Range extension but have limited utility for understanding timing or rates of extension, while syn-extensional sedimentary deposits can provide compelling information on the timing of deformation but generally less precise constraints on extensional magnitudes.

The Titus Canyon Formation and bounding structures are thus of significant interest for refining palinspastic reconstructions because both closely pre-date the onset of large-magnitude extension in the Basin and Range. In this context, the structural relationship between the Fall Canyon–Titus Canyon fault system and the Titus Canyon anticline–Corkscrew Peak syncline is of particular significance. The TCA-CPS is a west-vergent fold pair, a rare type of contractional structure in the Death Valley region, which is dominated by east-directed thrust faults (e.g., Snow and Wernicke, 1989). As such, the TCA-CPS has been correlated with west-vergent folds in other mountain ranges surrounding Death Valley

as a diagnostic structural marker (e.g., Wernicke et al., 1988; Snow and Wernicke, 1989), a correlation predicated on the assumption that the TCA-CPS, as well as the other west-vergent folds, are extensionally disrupted fragments of a single, originally contiguous geologic structure.

The age of west-vergent folding in the Death Valley region is constrained only in the Cottonwood Mountains, where crosscutting dikes and growth strata bracket the timing of folding to Late Permian to early Triassic age (Snow et al., 1991; Stevens and Stone, 2005). Consequently, the question of whether all west-vergent folds throughout the Death Valley region are of this age, and thus correlative, is debated (e.g., Serpa and Pavlis, 1996; Renik and Christie-Blick, 2013; Lutz et al., 2021). In particular, the TCA-CPS has been the subject of debate with respect to the timing of its formation, with similarities to structures in the Cottonwood Mountains supporting a Permo-Triassic age (Snow and Wernicke, 2000; Niemi, 2012). Alternatively, the close association of the TCA-CPS to the late Miocene Boundary Canyon detachment has been used to argue for a model of syn-extensional folding synchronous with unroofing of the Funeral Mountains metamorphic core complex (Reynolds, 1974; Lutz et al., 2021).

Age constraints on the Fall Canyon fault–Titus Canyon fault, and crosscutting relationships between that structure and the TCA-CPS, do not provide absolute age constraints on the timing of TCA-CPS folding, but do provide relative timing on the development of these structures. The normal fault emplacement of upright Paleozoic strata and Titus Canyon Formation onto overturned Neoproterozoic strata of the Corkscrew Peak syncline (Fig. 12) requires that the TCA-CPS was developed prior to displacement on the Fall Canyon–Titus Canyon fault. The coarsening and thickening of the Titus Canyon Formation into the Fall Canyon fault in western Titus Canyon therefore imply that the TCA-CPS formed prior to the Eocene. This age constraint for folding of the TCA-CPS does not resolve all outstanding questions of structural correlations between west-vergent folds in the Death Valley region but does support the inference that the TCA-CPS is a pre-Cenozoic contractional structure associated with late Paleozoic or Mesozoic shortening of the Cordilleran margin.

TECTONIC AND TOPOGRAPHIC IMPLICATIONS FOR THE EVOLUTION AND COLLAPSE OF THE SEVIER OROGENIC BELT

A variety of geodynamic mechanisms have been invoked as proximate causes for the onset of Eocene extension within the proto-Basin and Range, including flexural and isostatic dynamics ahead of the delaminating Farallon slab (e.g., Smith et al., 2017; Cassel et al., 2018), changing plate boundary stresses (e.g., Atwater, 1970; Schellart et al., 2010), and gravitational collapse (Humphreys, 1995; Sonder and Jones, 1999). In northern Nevada, the close temporal association between Farallon slab removal and the onset of extension has been presumed to reflect a causal relationship between the two (e.g., Cassel et al., 2018). However, farther to the north, the earlier removal of the Farallon slab has been linked to an early Eocene phase of volcanism and extensional deformation that preceded a late Eocene phase of deformation, potentially related to a change in plate boundary stresses (e.g., Janecke, 1992). The southerly location of the Titus Canyon Basin may potentially record the opposite scenario, in which a late Eocene change in plate boundary stresses preceded the removal of the Farallon slab by 15 Ma, providing a unique and important constraint on the evolution of internal and external forces driving Basin and Range extension.

Stratigraphic Record of Crustal Extension along the Axis of the Sevier Orogenic Belt

In the central and northern Basin and Range, Late Cretaceous to Paleocene syn-convergent extension (e.g., Hodges and Walker, 1992; Wells et al., 2008; Druschke et al., 2009; Long et al., 2015) left a relatively sparse stratigraphic record in the hinterland of the Sevier orogen, primarily consisting of the Sheep Pass Formation (ca. 70–43 Ma) in central Nevada (Fig. 13, Druschke et al., 2009, 2011). Despite a sparse surficial record of syn-convergent extension, thermochronometric and isotopic data sets from several metamorphic core complexes record cooling during the late Cretaceous to early Cenozoic that may be attributable to early extensional exhumation, including in the Raft River–Albion metamorphic core complex (Wells et al., 2012), the Funeral Mountain metamorphic core complex (Applegate et al., 1992; Hoisch and Simpson, 1993; Applegate and Hodges, 1995), the Eureka Culmination (Long et al., 2015), and the Pequop Mountains (Camilleri, 1996). Syn-convergent extension has been attributed to collapse driven by gravitational potential energy gradients produced by a lithosphere over-thickened by Sevier deformation (e.g., Vandervoort and Schmitt, 1990; Hodges and Walker, 1992; DeCelles, 2004; Platt, 2007; Druschke et al., 2009).

Compared to earlier deposition, the Eocene stratigraphic record of extensional tectonism is more widespread and better constrained temporally (Fig. 13). This stratigraphic record preserves a north-to-south sweep in the onset of Eocene basin deposition, with the earliest deposits preserved in the Challis volcanic field of southern Idaho, where a basal conglomerate records deposition prior to the eruption of overlying volcanic units that have been dated with $^{40}Ar/^{39}Ar$ at ca. 49.5 Ma (Fig. 13; Moye et al., 1988; Sanford, 2005). In northernmost Nevada, the Elko Formation (Elko Basin) and the Dead Horse Formation (Copper Basin) contain a large number of tuffs that have enabled robust $^{40}Ar/^{39}Ar$ geochronology that indicates deposition spanned ca. 46–38 Ma, with the exception of one earlier local pulse of deposition in the vicinity of Coal Mine Canyon at ca. 49 Ma (Rahl et al., 2002; Haynes, 2003; McGrew et al., 2007; Henry, 2008; Henry et al., 2015; Mulch et al., 2015; Lund Snee et al., 2016; Smith et al., 2017). The syn-convergent Sheep Pass Formation in central Nevada is overlain by Eocene strata, including the Stinking Springs Conglomerate and Kinsey Canyon Formation with depositional ages that range from ca. 37–35 Ma (Fig. 13; Druschke et al., 2009). Eocene deposition in the Sheep Pass Basin, in particular, overlaps with Redbed member deposition in the Titus Canyon basin.

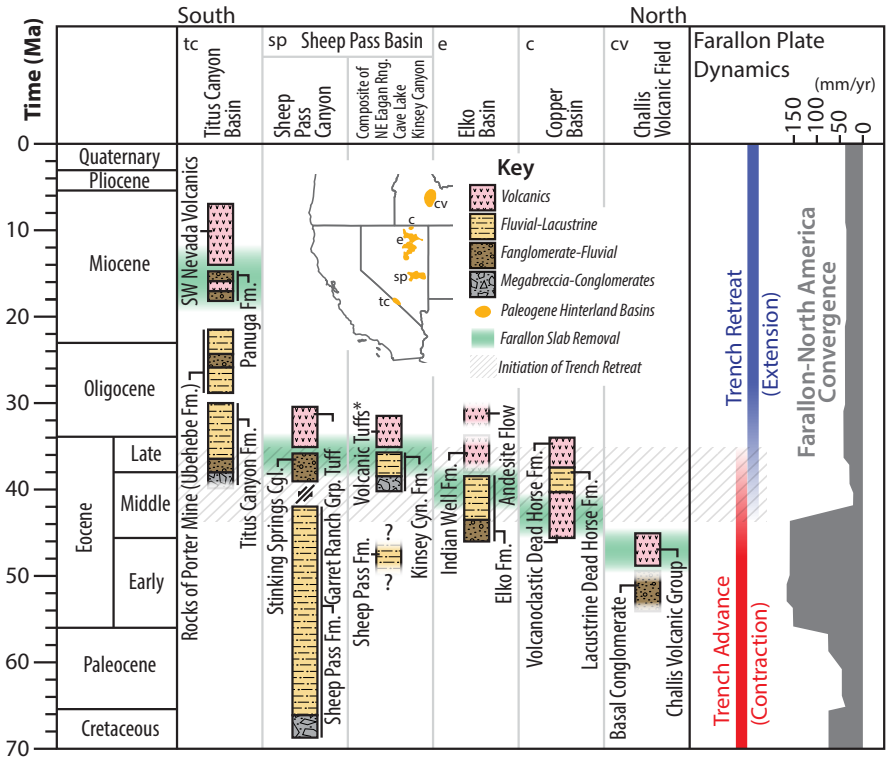

Figure 13. Comparison of the timing of deposition in major hinterland basins of the Sevier orogenic belt. Hinterland basins are arranged approximately from south to north (left to right). Figure is adapted from Figure 10 in Druschke et al. (2009), with additional data for the Challis volcanic field from Sanford (2005) and Moye et al. (1988); Elko Basin from Haynes (2003), Lund Snee et al. (2016), and Smith et al. (2017); Copper Basin from McGrew et al. (2007) and Rahl et al. (2002); and Miocene rocks of the Titus Canyon Basin from Niemi (2012). Farallon plate dynamics are from Jurdy (1984) and Schellart et al. (2010). Timing of Farallon slab removal from Dickinson (2009), Konstantinou et al. (2012), and Smith et al. (2017). Note that some basins contain Miocene and younger deposits not shown here for visual simplicity, and the Elko Basin may contain some older deposits not shown here because their exact ages are unknown (e.g., Lund Snee et al., 2016). *Late Eocene sedimentary sections in the Sheep Pass basin are overlain by tuffs of latest Eocene to earliest Oligocene age, including the Charcoal Ovens tuff and Kalamazoo tuff.

Each basin displays a broadly similar depositional pattern, with early deposition dominated by coarse basal deposits and fluvial strata that transition up section into lacustrine strata capped by volcanic or volcanic-rich units (Fig. 13). In the northern Basin and Range, the close temporal connection between clastic basin deposition and overlying volcanic deposition, combined with the southward sweep of basin initiation, has been taken to reflect subsidence and volcanism arising from the southward-propagating removal of the Farallon slab (e.g., Humphreys, 1995). In such a model, north to south delamination of the Farallon flat slab produced a south-directed, time-transgressive sweep of volcanism (Fig. 14; Humphreys, 1995; McQuarrie and Oskin, 2010), core complex exhumation (Fig. 14; e.g., MacCready and Snoke, 1997; Methner et al., 2015; Lee et al., 2017), and hinterland basin deposition (Fig. 14; Smith et al., 2017; Cassel et al., 2018; Lund Snee, 2020).

The southerly location of the Titus Canyon basin with respect to the time-transgressive removal of the Farallon slab, however, yields a markedly different pattern (Fig. 13). Eocene basin initiation and clastic deposition occurred in the Titus Canyon basin coeval with Eocene basin formation in northern Nevada, but the detaching Farallon slab, and associated volcanism, did not reach the central Basin and Range until the middle Miocene, coincident with widespread ignimbrite production in the Southwest Nevada volcanic field (Sawyer et al., 1994) and the exhumation of the Funeral Mountains metamorphic core complex (Holm and Dokka, 1991; Hoisch and Simpson, 1993; Lutz et al., 2021).

In the northern Basin and Range, Eocene hinterland basin development could reasonably represent a dynamic response to the southward removal of the Farallon slab (Smith et al., 2017; Cassel et al., 2018; Lund Snee, 2020), but the 15 m.y. gap between Eocene basin formation and volcanism and metamorphic core complex formation in the central Basin and Range would appear to be inconsistent with a singular driving force at the latitude of Titus Canyon. Throughout the Paleogene, ongoing subduction resulted in the fragmentation of the Farallon slab (e.g., Schellart et al., 2010). Between ca. 48 and 30 Ma, the trench-parallel length of the Farallon slab decreased by 75% and the Farallon–North America convergence rate rapidly slowed (Fig. 13; Jurdy, 1984; Gordon and Jurdy, 1986; Schellart et al., 2010). From the Eocene to Miocene, the Farallon slab steepened or foundered, from north to south across the northern Basin and Range (Fig. 13; Humphreys, 1995; McQuarrie and Oskin, 2010). The slowdown in Farallon–North America plate convergence rate was less time transgressive than Farallon detachment, consisting of a rapid transition from trench advance to trench retreat along the full length of the Farallon plate boundary at ca. 40 Ma (Fig. 13; Schellart et al., 2010).

In the northern Basin and Range, the transition from trench advance to trench retreat along the Farallon–North America plate boundary is

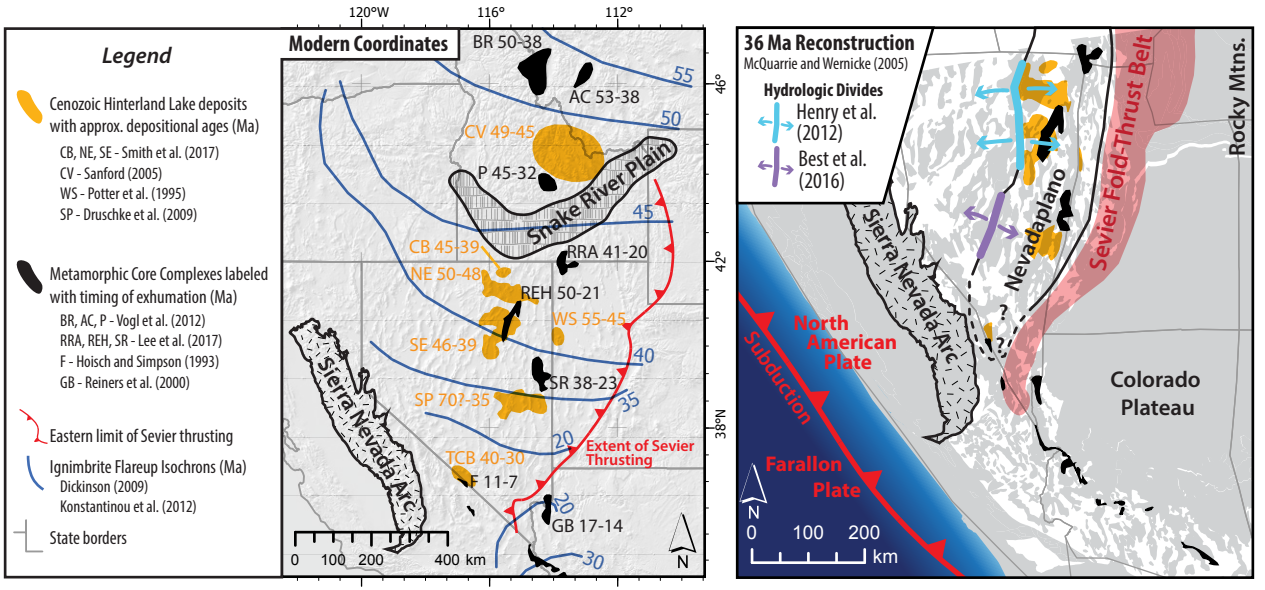

Figure 14. Geologic data in modern coordinates (left) and retrodeformed (right) to their approximate 36 Ma positions and sizes according to the tectonic reconstruction of McQuarrie and Wernicke (2005). Left: Hillshade base map with overlaid metamorphic core complexes, hinterland basins, and isochron contours of the north to south sweep of ignimbrite volcanism associated with delamination of the Farallon slab. Right: 36 Ma reconstruction of range positions from McQuarrie and Wernicke (2005) overlain with the estimated position of the Paleogene hydrologic divide, and the possible extent of the Nevadaplano assuming it contains the major hinterland basins, lies east of the hypothesized Cordilleran hydrologic divide (Henry et al., 2012; Best et al., 2016), and west of the Sevier fold-thrust belt (Yonkee and Weil, 2015). Abbreviations: BR—Bitterroot Core Complex; AC—Anaconda Core Complex; P—Pioneer Core Complex; RRA—Raft River–Albion Core Complex; REH—Ruby–East Humboldt Core Complex; SR—Snake Range Core Complex; F—Funeral Mountains core complex; GB—Gold Butte Core Complex; CV—Challis volcanic field; CB—Copper Basin; NE—Northern Elko Basin; SE—Southern Elko Basin; WS—White Sage Basin; SP—Sheep Pass Basin; TCB—Titus Canyon Basin.

temporally indistinguishable from the passage of the detaching Farallon slab (Fig. 13). However, these two events are separated by ~25 m.y. at the latitude of the Titus Canyon basin. Extensional basin formation and deposition of the Titus Canyon Formation is approximately coeval with the transition from trench advance to trench retreat along the plate margin, while the subsequent onset of local volcanism and metamorphic core complex formation is contemporaneous with the removal of the Farallon slab at that latitude (Fig. 13). We infer that the complex history of extensional tectonism, deposition, and basin formation in the central Basin and Range results from multiple discrete episodes of deformation. In the Eocene, extensional basin formation was driven by stress changes along the plate boundary, coupled with localized gravitational collapse of possibly over-thickened lithosphere (e.g., Vandervoort and Schmitt, 1990; Hodges and Walker, 1992; Platt, 2007; Druschke et al., 2009; Wells et al., 2012; Bahadori et al., 2018). These early extensional basins were overprinted by middle Miocene volcanism and core complex formation that accompanied extension driven by lithospheric weakening and heating during removal of the Farallon slab (e.g., Armstrong and Ward, 1991; Axen et al., 1993; Humphreys et al., 2003). Such a model is compatible with early clastic basin formation and subsequent volcanism and core complex formation in the northern Basin and Range, but the temporal overlap between these two geodynamic processes precludes their effects from being assessed separately in that region.

Spatial Extent of an Early Eocene Nevadaplano

Thickened crust within the Sevier orogenic belt is hypothesized to have supported a high-elevation, low-relief orogenic plateau called the Nevadaplano (Ernst, 2009). The spatial extent and elevation of this plateau are the subjects of considerable debate (e.g., Chamberlain et al., 2012; Long, 2012; Lechler et al., 2013; Snell et al., 2014; Miller et al., 2022) and are of particular interest in relating the distribution and magnitude of Basin and Range extension to the pre-extensional distribution of topography and crustal thickness (e.g., Bahadori et al., 2018). Approaches that directly constrain pre-extensional topography of the Nevadaplano are limited by the

small number of deposits of appropriate age and composition for paleoelevation analysis, the thermal resetting of paleoaltimetric proxies such as carbonate clumped isotopes (Lechler et al., 2013), and the relatively large elevation uncertainties associated with paleofloral data and stable isotopic proxies (e.g., Chamberlain et al., 2012; Snell et al., 2014). The low spatial and temporal density of paleoelevation, paleotopographic, and paleocrustal thickness estimates has resulted in a number of competing models for the topographic profile of the Sevier orogenic belt (Cecil et al., 2010; Cassel et al., 2014; Bahadori and Holt, 2019). Among the most pronounced discrepancies in these models is the recognition of a paleotopographic divide, based on ignimbrite sheet distributions (Henry et al., 2012; Best et al., 2016), that lies ~150 km west (in pre-extensional coordinates) of the belt of core complexes and presumed greatest pre-extensional crustal thickness (Fig. 14; Bahadori and Holt, 2019).

The distribution of Eocene hinterland extensional basin deposits, including the Titus Canyon Formation, sheds some light on the potential paleotopography in the hinterland of the Sevier orogenic belt. All Eocene basins lie east of the paleotopographic divide and west of the inferred axis of thick crust produced by Sevier shortening (Fig. 14). In particular, the large areal extents of the lacustrine-dominated Elko Formation and the Sheep Pass Formation imply basin development across a region of relatively low-relief topography. An interpretation of low-relief paleotopography in this region is supported by the general lack of structural relief across the inferred Nevadaplano (Gans and Miller, 1983; Miller and Gans, 1989; DeCelles and Coogan, 2006; Van Buer et al., 2009; Konstantinou et al., 2012; Long, 2012, 2018), and the local relief on the base of ignimbrite sheets, as well as their long outflow distances and broad aprons (Henry et al., 2012). Together, these observations suggest the existence of a low-relief, and perhaps at times internally drained, portion of the Nevadaplano that can be extended along the belt of Eocene basins, from the Copper Basin in northern Nevada to the Titus Canyon basin in eastern California (Fig. 14). The extent of large paleo-lakes and lacustrine basins has been invoked as a proxy for low-relief topography on elevated plateau surfaces (Zhenhan et al., 2008), and the presence of such basins along the axis of the Sevier orogenic belt in Eocene time should be considered in paleotopographic reconstructions of western U.S. topography at that time (e.g., Bahadori and Holt, 2019).

CONCLUSIONS

In this study, we redefine the internal stratigraphy of the Eocene–Oligocene Titus Canyon Formation and clarify its correlation to regionally similar units through a combination of detailed stratigraphic descriptions and geochronology. A combination of mammalian biostratigraphy, new detrital zircon U-Pb maximum depositional age constraints, and relocated $^{40}Ar/^{39}Ar$ ages indicate that the Titus Canyon basin spans ca. 40–30 Ma and may record the earliest hinterland sedimentation in the central Basin and Range following the Mesozoic Sevier orogeny. The stratigraphy and structural position of the Titus Canyon Formation in the hanging wall of the linked Fall Canyon and Titus Canyon faults support previous interpretations of the formation as an extensional basin deposit. A change in detrital zircon provenance from an entirely Mesozoic Sierran arc source to a dominantly Paleozoic and Neoproterozoic miogeoclinal source may record progressive extensional unroofing of deeper miogeoclinal formations that contain greater concentrations of zircons, which along with the basin subsidence itself, supports continued extensional tectonism throughout the deposition of the formation. The phase of low-magnitude extension recorded by the Titus Canyon Formation predates large-magnitude exhumation of the nearby Funeral Mountains metamorphic core complex and suggests that extensional deformation in the central Basin and Range may have initiated because of changes in plate boundary forces and was later over-printed by deformation associated with removal of the Farallon slab.

ACKNOWLEDGMENTS

This work was supported by the U. S. Geological Survey National Cooperative Geologic Mapping Program under USGS award number G19AC00138, with matching support from the University of Michigan. The views and conclusions contained in this document are those of the authors and should not be interpreted as necessarily representing the official policies, either expressed or implied, of the U.S. Government. Additional support came from National Science Foundation grant EAR-1151247 to NAN, a Geological Society of America Graduate Student Research Grant to NM, and a University of Michigan Department of Earth and Environmental Sciences Turner Award to NM. Fieldwork in Death Valley National Park was conducted under permit DEVA-2017- SCI-0037, issued to Torrey Nyborg. John Stark (DVNP) provided access to National Park Service GIS data. We thank Bruce Lander for providing the impetus to revisit the Titus Canyon Formation, and for many stimulating conversations with both him and Torrey Nyborg in the field. Tom Kelly, Brandt Nyborg, and John Sifling are thanked for participating in field expeditions. Thank you to Ken Ridgway for granting permission to publish $^{40}Ar/^{39}Ar$ data produced under U.S. Nuclear Regulatory Commission Contract NRC-02-07-006. This manuscript was improved by constructive criticism from Marin Clark, Michael Wells, Jens-Erik Lund Snee, Ryan Leary, and Jeff Lee. We acknowledge the Indigenous peoples who are the original inhabitants of the lands this work examines—the Newe Segobia (Western Shoshone) and Nuwuvi (Southern Paiute) tribes. We thank Mel for breakfast.

REFERENCES CITED

Abbey, A.L., Niemi, N.A., Geissman, J.W., Winkelstern, I.Z., and Heizler, M., 2018, Early Cenozoic exhumation and paleotopography in the Arkansas River valley, southern Rocky Mountains, Colorado: Lithosphere, v. 10, p. 239–266, https://doi.org/10.1130/L673.1.

Affinati, S.C., Hoisch, T.D., Wells, M.L., and Vervoort, J.D., 2020, Pressure-temperature-time paths from the Funeral Mountains, California, reveal Jurassic retroarc underthrusting during early Sevier orogenesis: Geological Society of America Bulletin, v. 132, p. 1047–1065, https://doi.org/10.1130/B35095.1.

Allen, P.A., and Allen, J.R., 2013, Basin Analysis: Principles and Application to Petroleum Play Assessment: Hoboken, New Jersey, Wiley-Blackwell, 549 p.

Applegate, J.D.R., and Hodges, K.V., 1995, Mesozoic and Cenozoic extension recorded by metamorphic rocks in the Funeral Mountains, California: Geological Society of America Bulletin, v. 107, p. 1063–1076, https://doi.org/10.1130/0016-7606(1995)107<1063:MACERB>2.3.CO;2.

Applegate, J.D.R., Walker, J.D., and Hodges, K.V., 1992, Late Cretaceous extensional unroofing in the Funeral Mountains metamorphic core complex, California: Geology, v. 20, p. 519–522, https://doi.org/10.1130/0091-7613(1992)020<0519:LCEUIT>2.3.CO;2.

Armstrong, R.L., and Ward, P., 1991, Evolving geographic patterns of Cenozoic magmatism in the North American Cordillera: The temporal and spatial association of magmatism and metamorphic core complexes: Journal of Geophysical Research, v. 96, p. 13,201–13,224, https://doi.org/10.1029/91JB00412.

Atwater, T., 1970, Implications of plate tectonics for the Cenozoic tectonic evolution of western North America: Geological Society of America Bulletin, v. 81, p. 3513–3536, https://doi.org/10.1130/0016-7606(1970)81[3513:IOPTFT]2.0.CO;2.

Axen, G.J., Taylor, W.J., and Bartley, J.M., 1993, Space-time patterns and tectonic controls of Tertiary extension and magmatism in the Great Basin of the western United States: Geological Society of America Bulletin, v. 105, p. 56–76, https://doi.org/10.1130/0016-7606(1993)105<0056:STPATC>2.3.CO;2.

Bahadori, A., and Holt, W.E., 2019, Geodynamic evolution of southwestern North America since the Late Eocene: Nature Communications, v. 10, p. 5213, https://doi.org/10.1038/s41467-019-12950-8.

Bahadori, A., Holt, W.E., and Rasbury, E.T., 2018, Reconstruction modeling of crustal thickness and paleotopography of western North America since 36 Ma: Geosphere, v. 14, p. 1207–1231, https://doi.org/10.1130/GES01604.1.

Berry, M., Wijk, J., Cadol, D., Emry, E., and Garcia-Castellanos, D., 2019, Endorheic-Exorheic Transitions of the Rio Grande and East African Rifts: Geochemistry, Geophysics, Geosystems, v. 20, p. 3705–3729, https://doi.org/10.1029/2018GC008176.

Best, M.G., Barr, D.L., Christiansen, E.H., Gromme, S., Deino, A.L., and Tingey, D.G., 2009, The Great Basin Altiplano during the middle Cenozoic ignimbrite flareup: Insights from volcanic rocks: International Geology Review, v. 51, p. 589–633, https://doi.org/10.1080/00206810902867690.

Best, M.G., Christiansen, E.H., and Gromme, S., 2013, The 36–18 Ma southern Great Basin, USA, ignimbrite province and flareup: Swarms of subduction-related supervolcanoes: Geosphere, v. 9, p. 260–274, https://doi.org/10.1130/GES00870.1.

Best, M.G., Christiansen, E.H., de Silva, S., and Lipman, P.W., 2016, Slab-rollback ignimbrite flareups in the southern Great Basin and other Cenozoic American arcs: A distinct style of arc volcanism: Geosphere, v. 12, p. 1097–1135, https://doi.org/10.1130/GES01285.1.

Beyene, M.A., 2011, Mesozoic burial, Mesozoic and Cenozoic exhumation of the Funeral Mountains core complex, Death Valley, southeastern California [Ph.D. thesis]: Reno, University of Nevada, 363 p.

Bindeman, I.N., Schmitt, A.K., and Valley, J.W., 2006, U-Pb zircon geochronology of silicic tuffs from the Timber Mountain/Oasis Valley caldera complex, Nevada: Rapid generation of large volume magmas by shallow-level remelting: Contributions to Mineralogy and Petrology, v. 152, p. 649–665, https://doi.org/10.1007/s00410-006-0124-1.

Blatt, H., 1967, Provenance determinations and recycling of sediments: Journal of Sedimentary Research, v. 37, p. 1031–1044, https://doi.org/10.1306/74D71825-2B21-11D7-8648000102C1865D.

Burchfiel, B.C., and Davis, G.A., 1975, Nature and controls of Cordilleran orogenesis, western United States: Extensions of an earlier synthesis: American Journal of Science, v. 275-A, p. 363–396.

Camilleri, P.A., 1996, Evidence for Late Cretaceous–Early Tertiary(?) extension in the Pequop Mountains, Nevada: Implications for the nature of the early Tertiary unconformity, *in* Taylor, W.J., and Langrock, H., eds., Cenozoic Structure and Stratigraphy of Central Nevada, Reno, Nevada Petroleum Society Inc., 1996 Field Conference Volume, p. 19–28.

Camilleri, P.A., and Chamberlain, K.R., 1997, Mesozoic tectonics and metamorphism in the Pequop Mountains and Wood Hills region, northeast Nevada: Implications for the architecture and evolution of the Sevier orogen: Geological Society of America Bulletin, v. 109, p. 74–94, https://doi.org/10.1130/0016-7606(1997)109<0074:MTAMIT>2.3.CO;2.

Canada, A.S., Cassel, E.J., McGrew, A.J., Smith, M.E., Stockli, D.F., Foland, K.A., Jicha, B.R., and Singer, B.S., 2019, Eocene exhumation and extensional basin formation in the Copper Mountains, Nevada, USA: Geosphere, v. 15, p. 1577–1597, https://doi.org/10.1130/GES02101.1.

Canada, A.S., Cassel, E.J., Stockli, D.F., Smith, M.E., Jicha, B.R., and Singer, B.S., 2020, Accelerating exhumation in the Eocene North American Cordilleran hinterland: Implications from detrital zircon (U-Th)/(He-Pb) double dating: Geological Society of America Bulletin, v. 132, p. 198–214, https://doi.org/10.1130/B35160.1.

Carr, M.D., Sawyer, D.A., Nimz, K., Maldonado, F., and Swadley, W.C., 1996, Digital bedrock geologic map database of the Beatty 30 × 60-minute quadrangle, Nevada and California: U.S. Geological Survey Open-File Report 96-291, 16 p., 2 over-size sheets, scale 1:100,000, https://doi.org/10.3133/ofr96291.

Carroll, A.R., and Bohacs, K.M., 1999, Stratigraphic classification of ancient lakes: Balancing tectonic and climatic controls: Geology, v. 27, p. 99–102, https://doi.org/10.1130/0091-7613(1999)027<0099:SCOALB>2.3.CO;2.

Cashman, P.H., and Sturmer, D.M., 2021, Paleogeographic reconstruction of Mississippian to Middle Pennsylvanian basins in Nevada, southwestern Laurentia: Palaeogeography, Palaeoclimatology, Palaeoecology, v. 584, https://doi.org/10.1016/j.palaeo.2021.110666.

Cassel, E.J., Breecker, D.O., Henry, C.D., Larson, T.E., and Stockli, D.F., 2014, Profile of a paleo-orogen: High topography across the present-day Basin and Range from 40 to 23 Ma: Geology, v. 42, p. 1007–1010, https://doi.org/10.1130/G35924.1.

Cassel, E.J., Smith, M.E., and Jicha, B.R., 2018, The impact of slab rollback on earth's surface: Uplift and extension in the hinterland of the North American Cordillera: Geophysical Research Letters, v. 45, p. 10,966–11,004, https://doi.org/10.1029/2018GL079887.

Cecil, M.R., Ducea, M.N., Reiners, P., Gehrels, G., Mulch, A., Allen, C., and Campbell, I., 2010, Provenance of Eocene river sediments from the central northern Sierra Nevada and implications for paleotopography: Tectonics, v. 29, TC6010, https://doi.org/10.1029/2010TC002717.

Cecil, M.R., Ferrer, M.A., Riggs, N.R., Marsaglia, K., Kylander-Clark, A., Ducea, M.N., and Stone, P., 2019, Early arc development recorded in Permian–Triassic plutons of the northern Mojave Desert region, California, USA: Geological Society of America Bulletin, v. 131, p. 749–765, https://doi.org/10.1130/B31963.1.

Çemen, I., and Wright, L.A., 1990, Effect of Cenozoic extension on Mesozoic thrust surfaces, *in* Wernicke, B.P., ed., Basin and Range Extensional Tectonics near the Latitude of Las Vegas, Nevada: Geological Society of America Memoir 176, p. 305–316, https://doi.org/10.1130/MEM176-p305.

Çemen, I., Drake, R., and Wright, L.A., 1982, Stratigraphy and chronology of the Tertiary sedimentary and volcanic units at the southeastern end of the Funeral Mountains, Death Valley region, California, *in* Cooper, J.D., Troxel, B.W., and Wright, L.A., eds., Geology of Selected Areas in the San Bernardino Mountains, Western Mojave Desert, and Southern Great Basin, California, Shoshone, California, Death Valley Publishing Co., p. 77–87.

Çemen, I., Wright, L.A., Drake, R.E., and Johnson, F.C., 1985, Cenozoic sedimentation and sequence of deformational events at the southeastern end of the Furnace Creek strike slip fault zone, Death Valley region California, *in* Biddle, K.T., and Christie-Blick, N., eds., Strike-Slip Deformation and Basin Formation: Society of Economic Paleontologists and Mineralogists, Special Publication 37, p. 127–141, https://doi.org/10.2110/pec.85.37.0127.

Çemen, I., Wright, L.A., and Prave, A.R., 1999, Stratigraphy and tectonic implications of the latest Oligocene and early Miocene sedimentary succession, southernmost Funeral Mountains, Death Valley region, California, *in* Wright, L.A., and Troxel, B.W., eds., Cenozoic Basins of the Death Valley Region: Geological Society of America Special Paper 333, p. 65–86, https://doi.org/10.1130/0-8137-2333-7.65.

Chamberlain, C.P., Mix, H.T., Mulch, A., Hren, M.T., Kent-Corson, M.L., Davis, S.J., Horton, T.W., and Graham, S.A., 2012, The Cenozoic climatic and topographic evolution of the western North American Cordillera: American Journal of Science, v. 312, p. 213–262, https://doi.org/10.2475/02.2012.05.

Chapman, J.B., Ducea, M.N., DeCelles, P.G., and Profeta, L., 2015, Tracking changes in crustal thickness during orogenic evolution with Sr/Y: An example from the North American Cordillera: Geology, v. 43, p. 919–922, https://doi.org/10.1130/G36996.1.

Chen, J.H., and Moore, J.G., 1982, Uranium-lead isotopic ages from the Sierra Nevada batholith, California: Journal of Geophysical Research. Solid Earth, v. 87, p. 4761–4784, https://doi.org/10.1029/JB087iB06p04761.

Coleman, D.S., and Glazner, A.F., 1998, The Sierra Crest magmatic event: Rapid formation of juvenile crust during the Late Cretaceous in California, *in* Ernst, W.G., ed., Integrated Earth and Environmental Evolution of the Southwestern United States: Columbia, Maryland, Bellwether Publishing, p. 253–272.

Coleman, D.S., Briggs, S., Glazner, A.F., and Northrup, C.J., 2003, Timing of plutonism and deformation in the White Mountains of eastern California: Geological Society of America Bulletin, v. 115, p. 48–57, https://doi.org/10.1130/0016-7606(2003)115<0048:TOPADI>2.0.CO;2.

Colgan, J.P., and Henry, C.D., 2009, Rapid middle Miocene collapse of the Mesozoic orogenic plateau in north-central Nevada: International Geology Review, v. 51, p. 920–961, https://doi.org/10.1080/00206810903056731.

Coney, P.J., 1978, Mesozoic-Cenozoic Cordilleran plate tectonics, *in* Smith, R.B., and Eaton, G.P., eds., Cenozoic Tectonics and Regional Geophysics of the Western Cordillera: Geological Society of America Memoir 152, p. 33–50, https://doi.org/10.1130/MEM152-p33.

Coney, P.J., and Harms, T.A., 1984, Cordilleran metamorphic core complexes: Cenozoic extensional relics of Mesozoic compression: Geology, v. 12, p. 550–554, https://doi.org/10.1130/0091-7613(1984)12<550:CMCCCE>2.0.CO;2.

Cornwall, H.R., and Kleinhampl, F.J., 1964, Geology of Bullfrog Quadrangle and ore deposits related to Bullfrog Hills Caldera, Nye County, Nevada and Inyo County, California: U.S. Geological Survey Professional Paper Professional Paper 454-J, 29 p.

Coutts, D.S., Matthews, W.A., and Hubbard, S.M., 2019, Assessment of widely used methods to derive depositional ages from detrital zircon populations: Geoscience Frontiers, v. 10, p. 1421–1435, https://doi.org/10.1016/j.gsf.2018.11.002.

DeCelles, P.G., 2004, Late Jurassic to Eocene evolution of the cordilleran thrust belt and foreland basin system, western

U.S.A.: American Journal of Science, v. 304, p. 105–168, https://doi.org/10.2475/ajs.304.2.105.
DeCelles, P.G., and Coogan, J.C., 2006, Regional structure and kinematic history of the Sevier fold-and-thrust belt, central Utah: Geological Society of America Bulletin, v. 118, p. 841–864, https://doi.org/10.1130/B25759.1.
Dickinson, W.R., 2002, The Basin and Range Province as a composite extensional domain: International Geology Review, v. 44, p. 1–38, https://doi.org/10.2747/0020-6814.44.1.1.
Dickinson, W.R., 2009, Anatomy and global context of the North American Cordillera, *in* Kay, S.M., Ramos, V.A., and Dickinson, W.R., eds., Backbone of the Americas: Shallow Subduction, Plateau Uplift, and Ridge and Terrane Collision: Geological Society of America Memoir 204, p. 1–29, https://doi.org/10.1130/2009.1204(01).
Dickinson, W.R., and Gehrels, G.E., 2009, Use of U-Pb ages of detrital zircons to infer maximum depositional ages of strata: A test against a Colorado Plateau Mesozoic database: Earth and Planetary Science Letters, v. 288, p. 115–125, https://doi.org/10.1016/j.epsl.2009.09.013.
Druschke, P., Hanson, A.D., and Wells, M.L., 2009, Structural, stratigraphic, and geochronologic evidence for extension predating Palaeogene volcanism in the Sevier hinterland, east-central Nevada: International Geology Review, v. 51, p. 743–775, https://doi.org/10.1080/00206810902917941.
Druschke, P., Hanson, A.D., Wells, M.L., Gehrels, G.E., and Stockli, D., 2011, Paleogeographic isolation of the Cretaceous to Eocene Sevier hinterland, east-central Nevada: Insights from U-Pb and (U-Th)/He detrital zircon ages of hinterland strata: Geological Society of America Bulletin, v. 123, p. 1141–1160, https://doi.org/10.1130/B30029.1.
Dubiel, R.F., Potter, C.J., Good, S.C., and Snee, L.W., 1996, Reconstructing an Eocene extensional basin: The White Sage Formation, eastern Great Basin, *in* Beratan, K.K., ed., Reconstructing the History of Basin and Range Extension Using Sedimentology and Stratigraphy: Geological Society of America Special Paper 303, p. 1–14, https://doi.org/10.1130/0-8137-2303-5.1.
Ducea, M.N., 2001, The California arc: Thick granitic batholiths, eclogitic residues, lithospheric-scale thrusting, and magmatic flare-ups: GSA Today, v. 11, no. 11, p. 4–10, https://doi.org/10.1130/1052-5173(2001)011<0004:TCATGB>2.0.CO;2.
Ernst, W.G., 2009, Rise and fall of the Nevadaplano: International Geology Review, v. 51, p. 583–588, https://doi.org/10.1080/00206810903063315.
Evans, S.L., Styron, R.H., van Soest, M.C., Hodges, K.V., and Hanson, A.D., 2015, Zircon and apatite (U-Th)/He evidence for Paleogene and Neogene extension in the Southern Snake Range, Nevada, USA: Tectonics, v. 34, p. 2142–2164, https://doi.org/10.1002/2015TC003913.
Fan, M., Ayyash, S.A., Tripati, A., Passey, B.H., and Griffith, E.M., 2018, Terrestrial cooling and changes in hydroclimate in the continental interior of the United States across the Eocene-Oligocene boundary: Geological Society of America Bulletin, v. 130, p. 1073–1084, https://doi.org/10.1130/B31732.1.
Foster, D.A., and Raza, A., 2002, Low-temperature thermochronological record of exhumation of the Bitterroot metamorphic core complex, northern Cordilleran Orogen: Tectonophysics, v. 349, p. 23–36, https://doi.org/10.1016/S0040-1951(02)00044-6.
Fridrich, C.J., and Thompson, R.A., 2011, Cenozoic tectonic reorganizations of the Death Valley region, southeast California and southwest Nevada: U.S. Geological Survey Professional Paper Professional Paper 1783, 47 p.
Fridrich, C.J., Thompson, R.A., Slate, J.L., Berry, M.E., and Machette, M.N., 2012, Geologic map of the southern Funeral Mountains including nearby groundwater discharge sites in Death Valley National Park, California and Nevada: U.S. Geological Survey Scientific Investigations Map 3151, scale 1:50,000.
Galbraith, R.F., and Laslett, G.M., 1993, Statistical models for mixed fission track ages: Nuclear Tracks and Radiation Measurements, v. 21, p. 459–470, https://doi.org/10.1016/1359-0189(93)90185-C.
Gans, P.B., and Miller, E.L., 1983, Style of mid-Tertiary extension in east-central Nevada, *in* Gurgel, K.D., ed., Geologic Excursions in the Overthrust Belt and Metamorphic Core Complexes of the Intermountain Region, Salt Lake City, Utah: Utah Geological and Mineral Survey, Special Studies 59, p. 107–139.
Gawthorpe, R.L., and Leeder, M.R., 2000, Tectono-sedimentary evolution of active extensional basins: Basin Research, v. 12, p. 195–218, https://doi.org/10.1111/j.1365-2117.2000.00121.x.
Gehrels, G.E., Dickinson, W.R., Ross, G.M., Stewart, J.H., and Howell, D.G., 1995, Detrital zircon reference for Cambrian to Triassic miogeoclinal strata of western North America: Geology, v. 23, p. 831–834, https://doi.org/10.1130/0091-7613(1995)023<0831:DZRFCT>2.3.CO;2.
Gehrels, G.E., Valencia, V.A., and Ruiz, J., 2008, Enhanced precision, accuracy, efficiency, and spatial resolution of U-Pb ages by laser ablation–multicollector–inductively coupled plasma–mass spectrometry: Geochemistry, Geophysics, Geosystems, v. 9, Q03017, https://doi.org/10.1029/2007GC001805.
Geurts, A.H., Whittaker, A.C., Gawthorpe, R.L., and Cowie, P.A., 2020, Transient landscape and stratigraphic responses to drainage integration in the actively extending central Italian Apennines: Geomorphology, v. 353, https://doi.org/10.1016/j.geomorph.2019.107013.
Ghosh, A., Holt, W.E., and Bahadori, A., 2019, Role of large-scale tectonic forces in intraplate earthquakes of central and eastern North America: Geochemistry, Geophysics, Geosystems, v. 20, p. 2134–2156, https://doi.org/10.1029/2018GC008060.
Giallorenzo, M.A., Wells, M.L., Yonkee, W.A., Stockli, D.F., and Wernicke, B.P., 2018, Timing of exhumation, Wheeler Pass thrust sheet, southern Nevada and California: Late Jurassic to middle Cretaceous evolution of the southern Sevier fold-and-thrust belt: Geological Society of America Bulletin, v. 130, p. 558–579, https://doi.org/10.1130/B31777.1.
Goldstrand, P.M., 1992, Evolution of Late Cretaceous and early Tertiary basins of southwest Utah based on clastic petrology: Journal of Sedimentary Research, v. 62, p. 495–507, https://doi.org/10.1306/D4267933-2B26-11D7-8648000102C1865D.
Gordon, R.G., and Jurdy, D.M., 1986, Cenozoic global plate motions: Journal of Geophysical Research. Solid Earth, v. 91, p. 12,389–12,406, https://doi.org/10.1029/JB091iB12p12389.
Gutenkunst, M., 2006, Stratigraphic and geochronologic analysis of Eocene-Miocene synextensional strata in the Grapevine and Funeral mountains of southwestern Nevada and southeastern California: Implications for regional correlation of "pre-basin and range" stratigraphy [M.S. thesis]: West Lafayette, Indiana, Purdue University, 265 p.
Haynes, S.R., 2003, Development of the Eocene Elko Basin, Northeastern Nevada: Implications for Paleogeography and Regional Tectonism [M.S. thesis]: Vancouver, University of British Columbia, 159 p.
Henry, C.D., 2008, Ash-flow tuffs and paleovalleys in northeastern Nevada: Implications for Eocene paleogeography and extension in the Sevier hinterland, northern Great Basin: Geosphere, v. 4, p. 1, https://doi.org/10.1130/GES00122.1.
Henry, C.D., and John, D.A., 2013, Magmatism, ash-flow tuffs, and calderas of the ignimbrite flareup in the western Nevada volcanic field, Great Basin, USA: Geosphere, v. 9, p. 951–1008, https://doi.org/10.1130/GES00867.1.
Henry, C.D., Hinz, N.H., Faulds, J.E., Colgan, J.P., John, D.A., Brooks, E.R., Cassel, E.J., Garside, L.J., Davis, D.A., and Castor, S.B., 2012, Eocene–Early Miocene paleotopography of the Sierra Nevada–Great Basin–Nevadaplano based on widespread ash-flow tuffs and paleovalleys: Geosphere, v. 8, p. 1–27, https://doi.org/10.1130/GES00727.1.
Henry, C.D., Jackson, M.R., Mathewson, D.C., Koehler, S.R., and Moore, S.C., 2015, Eocene igneous geology and relation to mineralization: Railroad District, southern Carlin Trend, Nevada, *in* Pennell, W.M., and Garside, L.J., eds., New Concepts and Discoveries: Geological Society of Nevada, p. 939–965.
Hodges, K.V., and Walker, J.D., 1992, Extension in the Cretaceous Sevier orogen, North American Cordillera: Geological Society of America Bulletin, v. 104, p. 560–569, https://doi.org/10.1130/0016-7606(1992)104<0560:EITCSO>2.3.CO;2.
Hoisch, T.D., and Simpson, C., 1993, Rise and tilt of metamorphic rocks in the lower plate of a detachment fault in the Funeral Mountains, Death Valley, California: Journal of Geophysical Research. Solid Earth, v. 98, p. 6805–6827, https://doi.org/10.1029/92JB02411.
Hoisch, T.D., Wells, M.L., Beyene, M.A., Styger, S., and Vervoort, J.D., 2014, Jurassic Barrovian metamorphism in a western U.S. Cordilleran metamorphic core complex, Funeral Mountains, California: Geology, v. 42, p. 399–402, https://doi.org/10.1130/G35352.1.
Holm, D.K., and Dokka, R.K., 1991, Major Late Miocene cooling of the middle crust associated with extensional orogenesis in the Funeral Mountains, California: Geophysical Research Letters, v. 18, p. 1775–1778, https://doi.org/10.1029/91GL02079.
Horton, B.K., and Schmitt, J.G., 1998, Development and exhumation of a Neogene sedimentary basin during extension, east-central Nevada: Geological Society of America Bulletin, v. 110, p. 163–172, https://doi.org/10.1130/0016-7606(1998)110<0163:DAEOAN>2.3.CO;2.
Humphreys, E., Hessler, E., Dueker, K., Farmer, G.L., Erslev, E., and Atwater, T., 2003, How Laramide-age hydration of North American lithosphere by the Farallon slab controlled subsequent activity in the western United States: International Geology Review, v. 45, p. 575–595, https://doi.org/10.2747/0020-6814.45.7.575.
Humphreys, E.D., 1995, Post-Laramide removal of the Farallon slab, western United States: Geology, v. 23, p. 987–990, https://doi.org/10.1130/0091-7613(1995)023<0987:PLROTF>2.3.CO;2.
Janecke, S.U., 1992, Kinematics and timing of three superposed extensional systems, east central Idaho: Evidence for an Eocene tectonic transition: Tectonics, v. 11, p. 1121–1138, https://doi.org/10.1029/92TC00334.
Jennings, C.W., Strand, R.G., and Rogers, T.H., 1977, Geologic map of California: California Division of Mines and Geology, scale 1:750,000.

Jones, C.H., Unruh, J.R., and Sonder, L.J., 1996, The role of gravitational potential energy in active deformation in the southwestern United States: Nature, v. 381, p. 37–41, https://doi.org/10.1038/381037a0.

Jones, C.H., Sonder, L.J., and Unruh, J.R., 1998, Lithospheric gravitational potential energy and past orogenesis: Implications for conditions of initial Basin and Range and Laramide deformation: Geology, v. 26, p. 639–642, https://doi.org/10.1130/0091-7613(1998)026<0639:LGPEAP>2.3.CO;2.

Jurdy, D.M., 1984, The subduction of the Farallon plate beneath North America as derived from relative plate motions: Tectonics, v. 3, p. 107–113, https://doi.org/10.1029/TC003i002p00107.

Konstantinou, A., Strickland, A., Miller, E.L., and Wooden, J.P., 2012, Multistage Cenozoic extension of the Albion–Raft River–Grouse Creek metamorphic core complex: Geochronologic and stratigraphic constraints: Geosphere, v. 8, p. 1429–1466, https://doi.org/10.1130/GES00778.1.

Lander, E.B., 2019, Early Late Duchesnean (Late Middle Eocene) Titus Canyon Fauna, Titus Canyon Formation, Death Valley National Park, Inyo County, southeastern California, *in* Miller, D.M., ed., Exploring Ends of Eras in the Eastern Mojave Desert, 2019 Desert Symposium Field Guide and Proceedings, p. 141–152.

Lechler, A.R., and Niemi, N.A., 2011, Sedimentologic and isotopic constraints on the Paleogene paleogeography and paleotopography of the southern Sierra Nevada, California: Geology, v. 39, p. 379–382, https://doi.org/10.1130/G31535.1.

Lechler, A.R., Niemi, N.A., Hren, M.T., and Lohmann, K.C., 2013, Paleoelevation estimates for the northern and central proto-Basin and Range from carbonate clumped isotope thermometry: Tectonics, v. 32, p. 295–316, https://doi.org/10.1002/tect.20016.

Lee, J., 1995, Rapid uplift and rotation of mylonitic rocks from beneath a detachment fault: Insights from potassium feldspar $^{40}Ar/^{39}Ar$ thermochronology, northern Snake Range, Nevada: Tectonics, v. 14, p. 54–77, https://doi.org/10.1029/94TC01508.

Lee, J., Blackburn, T., and Johnston, S., 2017, Timing of mid-crustal ductile extension in the northern Snake Range metamorphic core complex, Nevada: Evidence from U/Pb zircon ages: Geosphere, v. 13, p. 439–459, https://doi.org/10.1130/GES01429.1.

Lee, J.K.W., Williams, I.S., and Ellis, D.J., 1997, Pb, U and Th diffusion in natural zircon: Nature, v. 390, p. 159–162, https://doi.org/10.1038/36554.

Levandowski, W., Zellman, M., and Briggs, R., 2017, Gravitational body forces focus North American intraplate earthquakes: Nature Communications, v. 8, https://doi.org/10.1038/ncomms14314.

Liu, Z., Pagani, M., Zinniker, D., DeConto, R., Huber, M., Brinkhuis, H., Shah, S.R., Leckie, R.M., and Pearson, A., 2009, Global cooling during the Eocene–Oligocene climate transition: Science, v. 323, p. 1187–1190, https://doi.org/10.1126/science.1166368.

Long, S.P., 2012, Magnitudes and spatial patterns of erosional exhumation in the Sevier hinterland, eastern Nevada and western Utah, USA: Insights from a Paleogene paleogeologic map: Geosphere, v. 8, p. 881–901, https://doi.org/10.1130/GES00783.1.

Long, S.P., 2018, Geometry and magnitude of extension in the Basin and Range Province (39°N), Utah, Nevada, and California, USA: Constraints from a province-scale cross section: Geological Society of America Bulletin, v. 131, p. 99–119, https://doi.org/10.1130/B31974.1.

Long, S.P., Thomson, S.N., Reiners, P.W., and Di Fiori, R.V., 2015, Synorogenic extension localized by upper-crustal thickening: An example from the Late Cretaceous Nevadaplano: Geology, v. 43, p. 351–354, https://doi.org/10.1130/G36431.1.

Lund Snee, J.E., 2020, State of stress in North America: Seismicity, tectonics, and unconventional energy development [Ph.D. thesis]: Stanford, California, Stanford University, 273 p.

Lund Snee, J.E., and Miller, E.L., 2022, Magmatism, migrating topography, and the transition from Sevier shortening to Basin and Range extension, western United States, *in* Craddock, J.P., Malone, D.H., Foreman, B.Z., and Konstantinou, A., eds., Tectonic Evolution of the Sevier-Laramide Hinterland, Thrust Belt, and Foreland, and Postorogenic Slab Rollback (180–20 Ma): Geological Society of America Special Paper 555, https://doi.org/10.1130/2021.2555(13).

Lund Snee, J.E., and Zoback, M.D., 2020, Multiscale variations of the crustal stress field throughout North America: Nature Communications, v. 11, p. 1951, https://doi.org/10.1038/s41467-020-15841-5.

Lund Snee, J.E., Miller, E.L., Grove, M., Hourigan, J.K., and Konstantinou, A., 2016, Cenozoic paleogeographic evolution of the Elko Basin and surrounding region, northeast Nevada: Geosphere, v. 12, p. 464–500, https://doi.org/10.1130/GES01198.1.

Lutz, B.M., Ketcham, R.A., Axen, G.J., Beyene, M.A., Wells, M.L., van Wijk, J.W., Stockli, D.F., and Ross, J.I., 2021, Thermokinematic modeling of detachment-dominated extension, northeastern Death Valley area, USA: Implications for mid-crustal thermal-rheological evolution: Tectonophysics, v. 808, https://doi.org/10.1016/j.tecto.2021.228755.

MacCready, T., and Snoke, A.W., 1997, Mid-crustal flow during Tertiary extension in the Ruby Mountains core complex, Nevada: Geological Society of America Bulletin, v. 109, p. 1576–1594, https://doi.org/10.1130/0016-7606(1997)109<1576:MCFDTE>2.3.CO;2.

Maldonado, F., Spengler, R.W., Hanna, W.F., and Dixon, G.L., 1988, Index of granitic rock masses in the State of Nevada: U.S. Geological Survey Bulletin 1831, 86 p.

Mason, M.A., 1988, Mammalian Paleontology and stratigraphy of the Early to Middle Tertiary Sespe and Titus Canyon Formations, Southern California [Ph.D. thesis]: Berkeley, University of California, Berkeley, 257 p.

Mattinson, C.G., Colgan, J.P., Metcalf, J.R., Miller, E.L., and Wooden, J.L., 2007, Late Cretaceous to Paleocene metamorphism and magmatism in the Funeral Mountains metamorphic core complex, Death Valley, California, *in* Cloos, M., Carlson, W.D., Gilbert, M.C., Liou, J.G., and Sorenson, S.S., eds., Convergent Margin Terranes and Associated Regions: A Volume in Honor of W.G. Ernst: Geological Society of America Special Paper 419, p. 205–223, https://doi.org/10.1130/2006.2419(11).

McAllister, J.F., 1952, Rocks and structure of the Quartz Spring area, northern Panamint Range, California: U.S. Geological Survey Open-File Report 51–73, 143 p.

McAllister, J.F., 1971, Preliminary geologic map of the Funeral Mountains in the Ryan quadrangle, Death Valley region, Inyo County, California: United States: U.S. Geological Survey Open-File Report 71-187, https://doi.org/10.3133/ofr71187.

McGrew, A.J., Foland, K.A., and Stockli, D., 2007, Evolution of Cenozoic volcanism and extension in the Copper Mountains, northeastern Nevada: Geological Society of America Abstracts with Programs, v. 39, no. 6, p. 226.

McQuarrie, N., and Oskin, M., 2010, Palinspastic restoration of NAVDat and implications for the origin of magmatism in southwestern North America: Journal of Geophysical Research, v. 115, B10401, https://doi.org/10.1029/2009JB006435.

McQuarrie, N., and Wernicke, B.P., 2005, An animated tectonic reconstruction of southwestern North America since 36 Ma: Geosphere, v. 1, p. 147–172, https://doi.org/10.1130/GES00016.1.

Mercer, C.M., and Hodges, K.V., 2016, ArAR—A software tool to promote the robust comparison of K-Ar and $^{40}Ar/^{39}Ar$ dates published using different decay, isotopic, and monitor-age parameters: Chemical Geology, v. 440, p. 148–163, https://doi.org/10.1016/j.chemgeo.2016.06.020.

Methner, K., Mulch, A., Teyssier, C., Wells, M.L., Cosca, M.A., Gottardi, R., Gébelin, A., and Chamberlain, C.P., 2015, Eocene and Miocene extension, meteoric fluid infiltration, and core complex formation in the Great Basin (Raft River Mountains, Utah): Tectonics, v. 34, p. 680–693, https://doi.org/10.1002/2014TC003766.

Miller, E.L., and Gans, P.B., 1989, Cretaceous crustal structure and metamorphism in the hinterland of the Sevier thrust belt, western U.S. Cordillera: Geology, v. 17, p. 59–62, https://doi.org/10.1130/0091-7613(1989)017<0059:CCSAMI>2.3.CO;2.

Miller, E.L., Raftrey, M.E., and Lund Snee, J.E., 2022, Downhill from Austin and Ely to Las Vegas: U-Pb detrital zircon suites from the Eocene–Oligocene Titus Canyon Formation and associated strata, Death Valley, California, *in* Craddock, J.P., Malone, D.H., Foreman, B.Z., and Konstantinou, A., eds., Tectonic Evolution of the Sevier-Laramide Hinterland, Thrust Belt, and Foreland, and Postorogenic Slab Rollback (180–20 Ma): Geological Society of America Special Paper 555, https://doi.org/10.1130/2021.2555(14).

Molnar, P., England, P.C., and Jones, C.H., 2015, Mantle dynamics, isostasy, and the support of high terrain: Journal of Geophysical Research. Solid Earth, v. 120, p. 1932–1957, https://doi.org/10.1002/2014JB011724.

Moye, F.J., Hackett, W.R., Blakley, J.D., and Snider, L.G., 1988, Regional geologic setting and volcanic stratigraphy of the Challis Volcanic Field, central Idaho, *in* Link, P.K., and Hackett, W.R., eds., Guidebook to the Geology of Central and Southern Idaho, Idaho Geological Survey Bulletin 27, p. 87–97.

Mulch, A., Chamberlain, C.P., Cosca, M.A., Teyssier, C., Methner, K., Hren, M.T., and Graham, S.A., 2015, Rapid change in high-elevation precipitation patterns of western North America during the Middle Eocene Climatic Optimum (MECO): American Journal of Science, v. 315, p. 317–336, https://doi.org/10.2475/04.2015.02.

Murray, D.A., 2002, Oligocene to Lower Miocene Stratigraphy and extensional basin development, southwestern Nevada and southeastern California [M.S. thesis]: West Lafayette, Indiana, Purdue University, 179 p.

Niemi, N.A., 2002, Extensional tectonics in the Basin and Range province and the geology of the Grapevine Mountains, Death Valley region, California and Nevada [Ph.D. thesis]: California Institute of Technology, 344 p.

Niemi, N.A., 2012, Geologic map of the central Grapevine Mountains, Inyo County, California, and Esmeralda and

Nye Counties, Nevada: Geological Society of America Digital Map and Chart 12, https://doi.org/10.1130/2012.DMCH012.

Niemi, N.A., and Clark, M.K., 2018, Long-term exhumation rates exceed paleoseismic slip rates in the central Santa Monica Mountains, Los Angeles County, California: Geology, v. 46, p. 63–66, https://doi.org/10.1130/G39388.1.

Niemi, N.A., Wernicke, B.P., Brady, R.J., Saleeby, J.B., and Dunne, G.C., 2001, Distribution and provenance of the middle Miocene Eagle Mountain Formation, and implications for regional kinematic analysis of the Basin and Range province: Geological Society of America Bulletin, v. 113, p. 419–442, https://doi.org/10.1130/0016-7606(2001)113<0419:DAPOTM>2.0.CO;2.

Nyborg, T., Nyborg, B., Fairfield, H., and Jansen, B., 2017, Fossil fishes of Death Valley National Park, California: Reconstructing the origins and geographical distribution of the indigenous ichthyofauna of southeastern California: Geological Society of America Abstracts with Programs, v. 49, no. 6, https://doi.org/10.1130/abs/2017AM-302235.

Platt, J.P., 2007, From orogenic hinterlands to Mediterranean-style back-arc basins: A comparative analysis: Journal of the Geological Society of London, v. 164, p. 297–311, https://doi.org/10.1144/0016-76492006-093.

Poole, F.G., and Sandberg, C.A., 1977, Mississippian paleogeography and tectonics of the western United States, *in* Stewart, J.H., Stevens, C.H., and Fritsche, A.E. eds., Paleozoic Paleogeography of the Western United States, Pacific Section, Society of Economic Paleontologists and Mineralogists, Pacific Coast Paleogeography Symposium 1, p. 67–86.

Potter, C.J., Dubiel, R.F., Snee, L.W., and Good, S.C., 1995, Eocene extension of early Eocene lacustrine strata in a complexly deformed Sevier-Laramide hinterland, northwest Utah and northeast Nevada: Geology, v. 23, p. 181–184, https://doi.org/10.1130/0091-7613(1995)023<0181:EEOEEL>2.3.CO;2.

Rahl, J.M., McGrew, A.J., and Foland, K.A., 2002, Transition from contraction to extension in the northeastern Basin and Range: New evidence from the Copper Mountains, Nevada: The Journal of Geology, v. 110, p. 179–194, https://doi.org/10.1086/338413.

Reiners, P.W., Brady, R., Farley, K.A., Fryxell, J.E., Wernicke, B., and Lux, D., 2000, Helium and argon thermochronometry of the Gold Butte block, south Virgin Mountains, Nevada: Earth and Planetary Science Letters, v. 178, p. 315–326, https://doi.org/10.1016/S0012-821X(00)00080-7.

Renik, B., and Christie-Blick, N., 2013, A new hypothesis for the amount and distribution of dextral displacement along the Fish Lake Valley–northern Death Valley–Furnace Creek fault zone, California-Nevada: Tectonics, v. 32, p. 123–145, https://doi.org/10.1029/2012TC003170.

Renne, P.R., Mundil, R., Balco, G., Min, K., and Ludwig, K.R., 2010, Joint determination of ^{40}K decay constants and ^{40}Ar*/^{40}K for the Fish Canyon sanidine standard, and improved accuracy for ^{40}Ar/^{39}Ar geochronology: Geochimica et Cosmochimica Acta, v. 74, p. 5349–5367, https://doi.org/10.1016/j.gca.2010.06.017.

Renne, P.R., Balco, G., Ludwig, K.R., Mundil, R., Balco, G., Ludwig, K.R., Mundil, R., and Min, K., 2011, Response to the comment by W.H. Schwarz et al. on "Joint determination of ^{40}K decay constants and ^{40}Ar*/^{40}K for the Fish Canyon sanidine standard, and improved accuracy for ^{40}Ar/^{39}Ar geochronology" by P.R. Renne et al. (2010): Geochimica et Cosmochimica Acta, v. 75, p. 5097–5100, https://doi.org/10.1016/j.gca.2011.06.021.

Repasch, M., Karlstrom, K., Heizler, M., and Pecha, M., 2017, Birth and evolution of the Rio Grande fluvial system in the past 8 Ma: Progressive downward integration and the influence of tectonics, volcanism, and climate: Earth-Science Reviews, v. 168, p. 113–164, https://doi.org/10.1016/j.earscirev.2017.03.003.

Reynolds, M.W., 1969, Stratigraphy and structural geology of the Titus and Titanothere Canyons area, Death Valley, California [Ph.D. thesis]: University of California, Berkeley, 310 p.

Reynolds, M.W., 1974, Geology of the Grapevine Mountains, Death Valley, California: A summary, *in* Guidebook, Death Valley Region, California and Nevada, Geological Society of America Cordilleran Section Fieldtrip 1, Shoshone, California, Death Valley Publishing Company, p. 92–99.

Ridgway, K., Stamatakos, J., Gutenkunst, M., and Dubreuilh, P., 2011, Stratigraphic analysis and regional correlation of Oligocene and Early Miocene strata in the Yucca Mountain area: U.S. Nuclear Regulatory Commission Contract NRC-02-07-006, 60 p.

Salyards, S.L., and Shoemaker, E.M., 1987, Landslide and debris-flow deposits in the Thumb Member of the Miocene Horse Spring Formation on the east side of Frenchman Mountain, Nevada: A measure of basin-range extension, *in* Hill, M., ed., Geological Society of America Centennial Field Guide Volume 1—Cordilleran Section: Boulder, Colorado, Decade of North American Geology, p. 49–51, https://doi.org/10.1130/0-8137-5401-1.49.

Sanford, R.F., 2005, Geology and stratigraphy of the Challis Volcanic Group and related rocks, Little Wood River area, south-central Idaho, with a section on Geochronology by Lawrence W. Snee: U.S. Geological Survey Bulletin 2064–II, 22 p., https://doi.org/10.3133/b2064II.

Satarugsa, P., and Johnson, R.A., 2000, Cenozoic tectonic evolution of the Ruby Mountains metamorphic core complex and adjacent valleys, northeastern Nevada: Rocky Mountain Geology, v. 35, p. 205–230, https://doi.org/10.2113/35.2.205.

Sawyer, D.A., Fleck, R.J., Lanphere, M.A., Warren, R.G., Broxton, D.E., and Hudson, M.R., 1994, Episodic caldera volcanism in the Miocene southwestern Nevada volcanic field: Revised stratigraphic framework, ^{40}Ar/^{39}Ar geochronology, and implications for magmatism and extension: Geological Society of America Bulletin, v. 106, p. 1304–1318, https://doi.org/10.1130/0016-7606(1994)106<1304:ECVITM>2.3.CO;2.

Saylor, B.Z., 1991, The Titus Canyon Formation: Evidence for early Oligocene extension in the Death Valley area, California [M.S. thesis]: Cambridge, Massachusetts Institute of Technology, 65 p.

Saylor, B.Z., and Hodges, K.V., 1994, ^{40}Ar/^{39}Ar age constraints on the depositional history of the Oligocene Titus Canyon Formation, Death Valley, California: Geological Society of America Abstracts with Programs, v. 26, p. 88.

Schellart, W.P., Stegman, D.R., Farrington, R.J., Freeman, J., and Moresi, L., 2010, Cenozoic tectonics of western North America controlled by evolving width of Farallon slab: Science, v. 329, p. 316–319, https://doi.org/10.1126/science.1190366.

Serpa, L., and Pavlis, T.L., 1996, Three-dimensional model of the late Cenozoic history of the Death Valley region, southeastern California: Tectonics, v. 15, p. 1113–1128, https://doi.org/10.1029/96TC01633.

Smith, M.E., Cassel, E.J., Jicha, B.R., Singer, B.S., and Canada, A.S., 2017, Hinterland drainage closure and lake formation in response to middle Eocene Farallon slab removal, Nevada, U.S.A: Earth and Planetary Science Letters, v. 479, p. 156–169, https://doi.org/10.1016/j.epsl.2017.09.023.

Snell, K.E., Koch, P.L., Druschke, P., Foreman, B.Z., and Eiler, J.M., 2014, High elevation of the "Nevadaplano" during the Late Cretaceous: Earth and Planetary Science Letters, v. 386, p. 52–63, https://doi.org/10.1016/j.epsl.2013.10.046.

Snow, J.K., 1990, Cordilleran orogenesis, extensional tectonics, and geology of the Cottonwood Mountains area, Death Valley region, California and Nevada [Ph.D. thesis]: Cambridge, Massachusetts, Harvard University, 533 p.

Snow, J.K., 1993, Tertiary strata of the Ubehebe basin and northern Cottonwood Mountains, Death Valley region, California, *in* Sherrod, D.R., and Nelson, J.E., eds., Tertiary Stratigraphy of Highly Extended Terranes, California, Arizona, and Nevada: U.S. Geological Survey Bulletin, v. 2053, p. 7–11, https://doi.org/10.3133/b2053.

Snow, J.K., and Lux, D.R., 1999, Tectono-sequence stratigraphy of Tertiary rocks in the Cottonwood Mountains and northern Death Valley area, California and Nevada, *in* Wright, L.A., and Troxel, B.W., eds., Cenozoic Basins of the Death Valley Region: Geological Society of America Special Paper 333, p. 17–64, https://doi.org/10.1130/0-8137-2333-7.17.

Snow, J.K., and Wernicke, B., 1989, Uniqueness of geological correlations: An example from the Death Valley extended terrain: Geological Society of America Bulletin, v. 101, p. 1351–1362, https://doi.org/10.1130/0016-7606(1989)101<1351:UOGCAE>2.3.CO;2.

Snow, J.K., and Wernicke, B.P., 2000, Cenozoic tectonism in the central basin and range: Magnitude, rate, and distribution of upper crustal strain: American Journal of Science, v. 300, p. 659–719, https://doi.org/10.2475/ajs.300.9.659.

Snow, J.K., and White, C., 1990, Listric normal faulting and synorogenic sedimentation, northern Cottonwood Mountains, Death Valley region, California, *in* Wernicke, B.P., ed., Basin and Range Extensional Tectonics near the Latitude of Las Vegas, Nevada: Geological Society of America Memoir 176, p. 413–446, https://doi.org/10.1130/MEM176-p413.

Snow, J.K., Asmerom, Y., and Lux, D.R., 1991, Permian-Triassic plutonism and tectonics, Death Valley region, California and Nevada: Geology, v. 19, p. 629–632, https://doi.org/10.1130/0091-7613(1991)019<0629:PTPATD>2.3.CO;2.

Snyder, N.P., and Hodges, K.V., 2000, Depositional and tectonic evolution of a supradetachment basin: ^{40}Ar/^{39}Ar geochronology of the Nova Formation, Panamint Range, California: Basin Research, v. 12, p. 19–30, https://doi.org/10.1046/j.1365-2117.2000.00108.x.

Sonder, L.J., and Jones, C.H., 1999, Western United States extension: How the west was widened: Annual Review of Earth and Planetary Sciences, v. 27, p. 417–462, https://doi.org/10.1146/annurev.earth.27.1.417.

Sonder, L.J., England, P.C., Wernicke, B.P., and Christiansen, R.L., 1987, A physical model for Cenozoic extension of western North America, *in* Coward, M.P., Dewey, J.F., and Hancock, P.L., eds., Continental Extensional Tectonics: Geological Society of London, Special Publications 28, p. 187–201, https://doi.org/10.1144/GSL.SP.1987.028.01.14.

Spell, T.L., and McDougall, I., 2003, Characterization and calibration of $^{40}Ar/^{39}Ar$ dating standards: Chemical Geology, v. 198, p. 189–211, https://doi.org/10.1016/S0009-2541(03)00005-6.

Stevens, C.H., and Stone, P., 2005, Interpretation of the Last Chance thrust, Death Valley region, California, as an Early Permian décollement in a previously undeformed shale basin: Earth-Science Reviews, v. 73, p. 79–101, https://doi.org/10.1016/j.earscirev.2005.04.005.

Stewart, J.H., 1970, Upper Precambrian and lower Cambrian strata in the southern Great Basin, California and Nevada: U.S. Geological Survey Professional Paper Professional Paper 620, 206 p., https://doi.org/10.3133/pp620.

Stock, C., 1936, Titanotheres from the Titus Canyon Formation, California: Proceedings of the National Academy of Sciences of the United States of America, v. 22, p. 656–661, https://doi.org/10.1073/pnas.22.11.656.

Stock, C., and Bode, F.D., 1935, Occurrence of Lower Oligocene mammal-bearing beds near Death Valley, California: Proceedings of the National Academy of Sciences of the United States of America, v. 21, p. 571–579, https://doi.org/10.1073/pnas.21.10.571.

Sullivan, W.A., and Snoke, A.W., 2007, Comparative anatomy of core-complex development in the northeastern Great Basin, U.S.A.: Rocky Mountain Geology, v. 42, p. 1–29, https://doi.org/10.2113/gsrocky.42.1.1.

Thomas, W.A., 2011, Detrital-zircon geochronology and sedimentary provenance: Lithosphere, v. 3, p. 304–308, https://doi.org/10.1130/RF.L001.1.

Topping, D.J., 1993, Paleogeographic reconstruction of the Death Valley extended region: Evidence from Miocene large rock-avalanche deposits in the Amargosa Chaos Basin, California: Geological Society of America Bulletin, v. 105, p. 1190–1213, https://doi.org/10.1130/0016-7606(1993)105<1190:PROTDV>2.3.CO;2.

Trexler, J.H., Jr., and Cashman, P.H., 1997, A southern Antler foredeep submarine fan: The Mississippian Eleana Formation, Nevada Test Site: Journal of Sedimentary Research, v. 67, p. 1044–1059, https://doi.org/10.1306/D42686C1-2B26-11D7-8648000102C1865D.

Van Buer, N.J., Miller, E.L., and Dumitru, T.A., 2009, Early Tertiary paleogeologic map of the northern Sierra Nevada batholith and the northwestern Basin and Range: Geology, v. 37, p. 371–374, https://doi.org/10.1130/G25448A.1.

Vandervoort, D.S., and Schmitt, J.G., 1990, Cretaceous to early Tertiary paleogeography in the hinterland of the Sevier thrust belt, east-central Nevada: Geology, v. 18, p. 567–570, https://doi.org/10.1130/0091-7613(1990)018<0567:CTETPI>2.3.CO;2.

Verdel, C., Niemi, N., and van der Pluijm, B.A., 2011, Variations in the illite to muscovite transition related to metamorphic conditions and detrital muscovite content: Insight from the Paleozoic passive margin of the southwestern United States: The Journal of Geology, v. 119, p. 419–437, https://doi.org/10.1086/660086.

Vermeesch, P., 2018, IsoplotR: A free and open toolbox for geochronology: Geoscience Frontiers, v. 9, p. 1479–1493, https://doi.org/10.1016/j.gsf.2018.04.001.

Vermeesch, P., 2021, Maximum depositional age estimation revisited: Geoscience Frontiers, v. 12, p. 843–850, https://doi.org/10.1016/j.gsf.2020.08.008.

Vogl, J.J., Foster, D.A., Fanning, C.M., Kent, K.A., Rodgers, D.W., and Diedesch, T., 2012, Timing of extension in the Pioneer metamorphic core complex with implications for the spatial-temporal pattern of Cenozoic extension and exhumation in the northern U.S. Cordillera: Tectonics, v. 31, TC1008, https://doi.org/10.1029/2011TC002981.

Wagner, F.H., and Johnson, R.A., 2006, Coupled basin evolution and late-stage metamorphic core complex exhumation in the southern Basin and Range Province, southeastern Arizona: Tectonophysics, v. 420, p. 141–160, https://doi.org/10.1016/j.tecto.2006.01.012.

Wells, M.L., and Hoisch, T.D., 2008, The role of mantle delamination in widespread Late Cretaceous extension and magmatism in the Cordilleran orogen, western United States: Geological Society of America Bulletin, v. 120, p. 515–530, https://doi.org/10.1130/B26006.1.

Wells, M.L., Dallmeyer, R.D., and Allmendinger, R.W., 1990, Late Cretaceous extension in the hinterland of the Sevier thrust belt, northwestern Utah and southern Idaho: Geology, v. 18, p. 929–933, https://doi.org/10.1130/0091-7613(1990)018<0929:LCEITH>2.3.CO;2.

Wells, M.L., Spell, T.L., Hoisch, T.D., Arriola, T., and Zanetti, K.A., 2008, Laser-probe $^{40}Ar/^{39}Ar$ dating of strain fringes: Mid-Cretaceous synconvergent orogen-parallel extension in the interior of the Sevier orogen: Tectonics, v. 27, TC3012, https://doi.org/10.1029/2007TC002153.

Wells, M.L., Hoisch, T.D., Cruz-Uribe, A.M., and Vervoort, J.D., 2012, Geodynamics of synconvergent extension and tectonic mode switching: Constraints from the Sevier-Laramide orogen: Tectonics, v. 31, TC1002, https://doi.org/10.1029/2011TC002913.

Wernicke, B., Axen, G.J., and Snow, J.K., 1988, Basin and Range extensional tectonics at the latitude of Las Vegas, Nevada: Geological Society of America Bulletin, v. 100, p. 1738–1757, https://doi.org/10.1130/0016-7606(1988)100<1738:BARETA>2.3.CO;2.

Wright, L.A., and Troxel, B.W., 1993, Geologic map of the central and northern Funeral Mountains and adjacent areas, Death Valley region, southern California: U.S. Geological Survey Miscellaneous Investigations Series Map I-2305, scale 1:48,000.

Yonkee, W.A., and Weil, A.B., 2015, Tectonic evolution of the Sevier and Laramide belts within the North American Cordillera orogenic system: Earth-Science Reviews, v. 150, p. 531–593, https://doi.org/10.1016/j.earscirev.2015.08.001.

Zhenhan, W., Barosh, P.J., Zhonghai, W., Daogong, H., Xun, Z., and Peisheng, Y., 2008, Vast early Miocene lakes of the central Tibetan Plateau: Geological Society of America Bulletin, v. 120, p. 1326–1337, https://doi.org/10.1130/B26043.1.

Zhou, Q., and Liu, L., 2019, Topographic evolution of the western United States since the early Miocene: Earth and Planetary Science Letters, v. 514, p. 1–12, https://doi.org/10.1016/j.epsl.2019.02.029.